Ultrafast phenomena in photoexcited semiconductors

REVIEWS OF MODERN PHYSICS, VOLUME 74, JULY 2002

Theory of ultrafast phenomena in photoexcited semiconductors

Fausto Rossi

Istituto Nazionale per la Fisica della Materia (INFM) and Dipartimento di Fisica, Politecnico di Torino, Corso Duca degli Abruzzi 24, 10129 Torino, Italy

Tilmann Kuhn

Institut für Festkörpertheorie, Westfälische Wilhelms-Universität, Wilhelm-Klemm-Str. 10, D-48149 Münster, Germany

(Published 30 August 2002)

The authors review the physics of ultrafast dynamics in semiconductors and their heterostructures, including both the observed experimental phenomena and the theoretical description of the processes. These are probed by ultrafast optical excitation, generating nonequilibrium states that can be monitored by time-resolved spectroscopy. Light pulses create coherent superpositions of states, and the dynamics of the associated phase relationships can be directly investigated by means of many-pulse experiments. The commonly used experimental techniques are briefly reviewed. A variety of different phenomena can be described within a common theoretical framework based on the density-matrix formalism. The important interactions of the carriers included in the theoretical description are the phonon interactions, the interactions with classical and quantum light fields, and the Coulomb interaction among the carriers themselves. These interactions give rise to a strong interplay between phase coherence and relaxation, which strongly affects the nonequilibrium dynamics. Based on the general theory, the authors review the physical phenomena in various semiconductor structures including superlattices, quantum wells, quantum wires, and bulk media. Particular results which have played a central role in understanding the microscopic origins of the relaxation processes are discussed in detail.

CONTENTS

I. INTRODUCTION

The magic word *faster* has always been one of the major challenges in the development of semiconductor microelectronics and optoelectronics (Capasso, 1990; Shah, 1992). For many years this has basically been a

concern for device and chip designers; however, today semiconductor technology has reached a level where the characteristic time scales of the underlying physical processes may determine the speed limits. Investigation of these ultrafast dynamics has thus become a strategic field both in basic research and from a technological point of view. Recent developments in ultrafast laser physics and technology now allow us to study the very initial interaction processes of nonequilibrium carriers in a semiconductor (Phillips, 1994; Shah, 1999), which are directly related to the microscopic details of the coupling mechanisms. Therefore time-resolved laser spectroscopy has become an essential tool in modern semiconductor physics.

Linear optical spectroscopy of semiconductors has provided invaluable information on electronic band structures, phonons, plasmons, single-particle spectra, and defects. These are impressive contributions, but information on the details of interaction processes among the elementary excitations is often much more difficult to obtain. In many cases it enters only in a strongly averaged way, e.g., in terms of momentum or phase relaxation times determining the spectral linewidth. Here, ultrafast optical spectroscopy can do much more. Indeed, an optical excitation has the ability to generate nonequilibrium carrier and exciton distributions, and time-resolved spectroscopy provides the best means for determining the temporal evolution of such distribution functions. Furthermore, by means of ultrafast pulses, coherent superpositions of states can be generated and the dynamics of such phase-related quantities can be analyzed. When these unique strengths are combined with spatial imaging techniques and/or specific low-dimensional structures, optical spectroscopy becomes a powerful tool for investigating a wide variety of phenomena related to relaxation and transport dynamics in semiconductors (Shah, 1999). It is this wide range that makes ultrafast optical spectroscopy a preferred technique for obtaining fundamental new information about the nonequilibrium, nonlinear, and transport properties of semiconductors.

Generally speaking, the optical excitation of a semiconductor creates both interband excitations, i.e., a coherent interband polarization, and intraband excitations, i.e., electron and hole distributions as well as intraband polarizations. The time evolution of these quantities is governed by a nontrivial interplay between phase coherence and energy relaxation. Indeed, scattering processes tend to destroy the coherence, leading to a dephasing of interband and intraband polarizations. Furthermore, they lead to a relaxation of the distribution functions towards the respective equilibrium distributions. Typical time scales for scattering processes in semiconductors are in the range of picoseconds or femtoseconds and the resulting dynamics are generally termed *ultrafast*. It is the aim of an ultrafast optical experiment to provide information on the details of this temporal evolution, which, in turn, gives insight into the fundamental processes governing microscopic carrier dynamics. Before going into detail let us start with a brief historical overview and a description of typical experimental techniques.

A. Nonequilibrium carrier dynamics in photoexcited semiconductors

The investigation of nonequilibrium carrier dynamics in optically excited semiconductors started in the late 1960s with the analysis of the energy relaxation process (Shah and Leite, 1969) by using cw excitation. The measurement of the carrier temperature as a function of the cw laser intensity—obtained from the luminescence spectrum—gave insight into the power loss from the carriers to the lattice, i.e., in carrier-phonon scattering processes. In subsequent years, these investigations were extended to different materials and excitation conditions. While band-to-band luminescence spectra gave only a combination of electron and hole temperatures, direct information on the electron distribution function was obtained by studying band-to-acceptor luminescence spectra of doped semiconductors (Ulbrich, 1977).

However, as stressed before, only by using a pulsed excitation can one directly investigate dynamical processes. Here, the pulse duration limits the temporal resolution and therefore restricts the phenomena that can be studied. The typical time scales for most of the processes discussed in the present review range from a few femtoseconds to a few picoseconds. Therefore the application of time-resolved nonlinear optical spectroscopy to the study of dynamical processes in semiconductors is closely related to the ability to produce laser pulses on these time scales. Such laser sources became available for semiconductor studies in the late 1970s (Shank *et al.*, 1979). Since then, a great number of phenomena have been studied, first mainly focusing on incoherent dynamics, i.e., the nonequilibrium dynamics of distribution functions, and subsequently analyzing more and more coherent phenomena, i.e., the dynamics of optically created interband and intraband polarizations.

A typical scenario for the dynamics of distribution functions is plotted schematically in Fig. 1: The laser pulse with a given photon energy and a certain spectral width determined by its duration creates electron-hole pairs in a more or less localized region in $\mathbf{k}$ space. This initial distribution then relaxes due to the presence of scattering processes. In polar semiconductors on ultrafast time scales, there are typically two mechanisms of particular importance: Due to the polar coupling to longitudinal optical (LO) phonons, the carriers may lose their initial kinetic energy to the lattice. Since optical phonons in the relevant region close to the center of the Brillouin zone have a negligible dispersion, this leads to the buildup of replicas of the initial distribution shifted downwards by multiples of the phonon energy [Fig. 1(c)]. The scattering among the electrons themselves due to the Coulomb interaction, on the other hand, conserves the total kinetic energy; however, it leads to a spreading in $\mathbf{k}$ space [Fig. 1(d)] and eventually, to a Fermi-Dirac distribution in which the temperature is de-

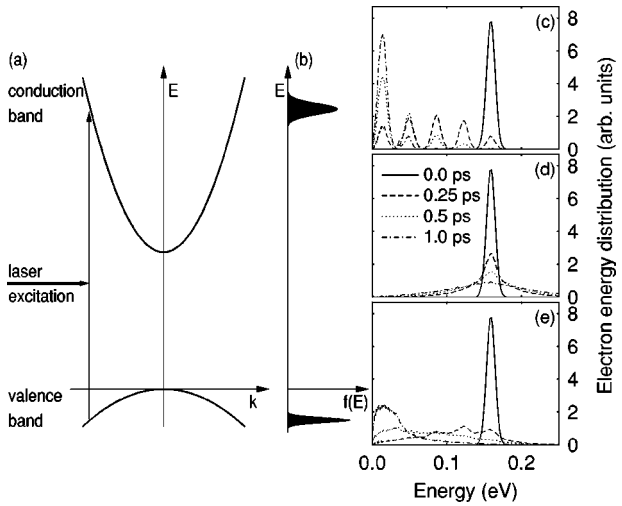

FIG. 1. The dynamics of distribution functions: (a) excitation by a short laser pulse with a certain excess energy above the band gap; (b) the resulting distribution of electrons and holes as well as the subsequent relaxation of the electron distribution due to (c) electron-phonon scattering, (d) electron-electron scattering, and (e) both types of scattering processes.

termined by the initial excess energy. If, as is always the case in a real semiconductor, both mechanisms are present, both energy relaxation and thermalization towards a Fermi-Dirac distribution occur simultaneously [Fig. 1(e)]; the respective time scales, however, are strongly dependent on the excitation conditions, in particular on the carrier density.

These thermalization and relaxation processes have been studied in great detail over the past two decades, both experimentally and theoretically, in bulk semiconductor materials as well as in a variety of heterostructures. The most commonly used experimental techniques for these studies have been luminescence, in which the photons created by the radiative recombination of electrons and holes are detected, and pump-probe measurements, in which the change in the absorption (or reflection) of a probe beam caused by the prior excitation of electron-hole pairs by the pump beam is observed. Since it is impossible to cite all the work, we mention only some of the phenomena that have turned out to be important under certain excitation conditions. In the case of sufficiently high excitation densities, it has been found that the distribution function of LO phonons is driven substantially out of equilibrium and that this "hot-phonon effect" may drastically reduce the cooling process (van Driel, 1979; Pötz and Kocevar, 1983; Kocevar, 1985; Lugli *et al.*, 1989). The dynamics of the nonequilibrium phonons have been studied directly by Raman measurements (von der Linde, Kuhl, and Klingenberg, 1980; Ryan and Tatham, 1992). If the excitation energy is above the threshold for transitions to satellite valleys in the conduction band, intervalley transitions due to carrier-phonon interaction are a very effective scattering process mainly because of the high density of states in these valleys (Shah *et al.*, 1987; Oberli, Shah, and Damen, 1989).

Starting in the mid-1980s, the field of coherent excitations in semiconductors became an increasingly active research area. Even if essentially carrier relaxation processes were monitored in the measurements mentioned above, it turned out that features related to coherence were present in these signals, as will be discussed in more detail in Sec. III. Under certain conditions, however, coherent aspects may be dominant. In the case of pump-probe spectra, this holds most prominently if the pump pulse is nonresonant with optical transitions, i.e., if it is tuned into the band-gap region where it does not create real populations. Here it gives rise to shifts and splittings of the exciton line, which is known as the optical or ac Stark effect. This effect has been extensively investigated since the mid-1980s (Mysyrowicz *et al.*, 1986; Schmitt-Rink and Chemla, 1986; Balslev and Stahl, 1988; Schmitt-Rink, Chemla, and Haug, 1988; Combescot and Combescot, 1989; Joffre *et al.*, 1989).

Besides pump-probe and luminescence measurements, there are other techniques that rely completely on the phase coherence in the carrier system, thus providing direct information on the dynamics of coherent interband and intraband polarizations. The most prominent of these techniques are four-wave-mixing (FWM) experiments and the detection of coherently emitted radiation in the terahertz range.

Many physical systems exhibit inhomogeneous broadening. In the case of a semiconductor in the excitonic region, this is typically due to some disorder in the sample, while in the band-to-band continuum region the **k** dependence of transition energies may also be interpreted as such broadening. Then, coherent polarization rapidly decays due to destructive interference of the different frequency components, and thus it is difficult to extract information on the true loss of phase coherence due to dephasing processes. In the case of magnetic resonance, the spin-echo technique was introduced in 1950 (Hahn, 1950), to eliminate the decay due to inhomogeneous broadening and thus to make possible the measurement of dephasing times (so-called T_2 times). In the 1960s, due to the availability of laser sources, echo experiments were brought into the optical regime and photon echoes were first observed in ruby (Kurnit, Abella, and Hartmann, 1964; Abella, Kurnit, and Hartmann, 1966). Since dephasing times are much shorter in semiconductors, very short pulses are required for such techniques. In 1985 photon echoes from delocalized excitons in semiconductors were observed by using 7-ps pulses (Schultheis, Sturge, and Hegarty, 1985), and a few years later photon echoes from band-to-band transitions were measured with 6-fs pulses (Becker *et al.*, 1988). These photon echoes were typically studied by means of degenerate four-wave-mixing experiments, which will be described in the next section. In such experiments an exciton phase coherence time of 7 ps was obtained in GaAs at low temperatures (Schultheis *et al.*, 1986); in addition, the dephasing time T_2 of an electron-hole plasma was shown to depend on the carrier density n according to $T_2 \sim n^{-0.3}$ (Becker *et al.*, 1988). Not only do such experiments provide information on the decay of

the coherence, they also are useful in the study of other coherent phenomena, e.g., quantum beats due to quantum-mechanical superpositions of states, which exhibit a splitting caused by a variety of physical phenomena.[1]

If such superpositions are excited between states with different spatial localizations, they are the source of electromagnetic radiation with a frequency given by the energy splitting. Often this frequency is in the terahertz range; in this regime the electric-field strength may be directly measured, in contrast to the optical regime, where typically only intensities can be measured. Such a terahertz emission was first observed from asymmetric double-quantum-well structures (Roskos *et al.*, 1992), which opened up the field of terahertz spectroscopy in semiconductors (Planken *et al.*, 1992; Waschke *et al.*, 1993; Nuss *et al.*, 1994; Dekorsy, Auer, *et al.*, 1995; Leitenstorfer *et al.*, 1999).

Another direct approach to coherent phenomena is the technique of coherent control by two temporally separated, phase-locked pulses (Planken *et al.*, 1993; Heberle, Baumberg, and Köhler, 1995). If the optical polarization created by the first pulse is still present in the sample, this polarization can constructively or destructively interfere with the second pulse, leading to dynamics in the system that strongly depend on the relative phases of the two pulses. These dynamics can then be probed by the reflection or transmission change, i.e., a pump-probe technique, or by the four-wave-mixing signal induced by a third pulse. It should be noted that there is a second type of coherent-control experiment in which superposition of a one-photon and a two- or three-photon excitation by two simultaneous pulses is used to control the final state in the case of degeneracy (Dupont *et al.*, 1995; Atanasov *et al.*, 1996). An overview of different applications of coherent control can be found in Pötz and Schroeder (1999). Generally, coherent control makes use of the full time dependence of the electric-field vector of the light pulse, including intensity, phase, and polarization. Pulses of arbitrary shape within a wide range of parameters can be created by using a liquid-crystal-display spatial light modulator (Weiner *et al.*, 1990). Then the inverse problem can be formulated: Which pulse shape produces the desired dynamics in the sample? This question of constructing an optimal interaction Hamiltonian has been addressed mainly in the context of coherent control of chemical reactions (Shapiro and Brumer, 1986; Warren, Rabitz, and Dahleh, 1993; Shapiro and Brumer, 1997); it has been shown that efficiencies (for example, of multiphoton ionization processes) can indeed be substantially increased by using an evolutionary algorithm (Assion *et al.*, 1996; Baumert *et al.*, 1997).

Coherences do not only exist in the electronic subsystem of the semiconductor. In spatially inhomogeneous systems or in systems with sufficiently low symmetry, optical excitation may also generate coherent phonons, i.e., phonons with a nonvanishing expectation value of the lattice displacement, in contrast to incoherent phonons, for which only the mean-square displacement is nonzero. The excitation of coherent phonons in semiconductors was first observed by optically exciting the surface field of n-doped GaAs (Cho, Kütt, and Kurz, 1990). Here the differential reflectivity change exhibited clear modulations with the phonon frequency. If the generated phonons are infrared active, they will also directly emit electromagnetic radiation with a frequency in the terahertz range, which can be detected in the way described above (Dekorsy, Auer, *et al.*, 1995). Coherent phonons have been observed in many materials and in different types of heterostructures; a recent review on this topic is that of Dekorsy, Cho, and Kurz (2000). Particularly interesting are situations in which the phonons couple to other types of elementary excitations with which they are nearly resonant. In addition to the generation of coherent phonons, the coupling of such phonons to plasmons (Cho *et al.*, 1996), to Bloch oscillations in superlattices (Dekorsy, Kim, Cho, Köhler, and Kurz, 1996), or to intersubband plasmon modes in quantum wells (Dekorsy, Kim, Cho, Kurz, *et al.*, 1996) has been studied.

The enormous progress in the experimental study of ultrafast phenomena has been paralleled by an increasingly refined theoretical understanding. In fact, this progress has often been possible only because of the strong collaboration between theory and experiment. While the first studies on energy relaxation were modeled by simple rate equations for the mean carrier energy, detailed understanding of carrier relaxation and thermalization processes required a modeling of the distribution functions of the carriers involved. Their temporal evolution is governed by the Boltzmann transport equation, which, in general, can only be solved numerically. Monte Carlo simulations have proven to be a technique well suited for this purpose (Jacoboni and Reggiani, 1983; Jacoboni and Lugli, 1989). Additionally, modeling coherent phenomena requires taking into account the interband (or intraband/intersubband) polarization. On the mean-field level the dynamics are described by the semiconductor Bloch equations (Huhn and Stahl, 1984; Lindberg and Koch, 1988a), a generalization of the well-known optical Bloch equations (Allen and Eberly, 1987). Scattering processes that give rise to relaxation and dephasing can be introduced in a Boltzmann-like (semiclassical) way (Binder *et al.*, 1992; Kuhn and Rossi, 1992b). Such a density-matrix approach has recently been generalized to describe quantum systems with open boundaries (Rossi, di Carlo, and Lugli, 1998).

On very short time scales even the description of scattering processes in terms of rates obtained from Fermi's golden rule is no longer sufficient. Quantum-kinetic theories that overcome this limitation have been developed based on different approaches, in particular nonequilibrium Green's functions (Haug and Jauho, 1996;

[1]See, for example, Göbel *et al.* (1990); Leo, Damen, *et al.* (1990); Schoenlein *et al.* (1993); Bányai *et al.* (1995); Mayer *et al.* (1995); Joschko *et al.* (1997).

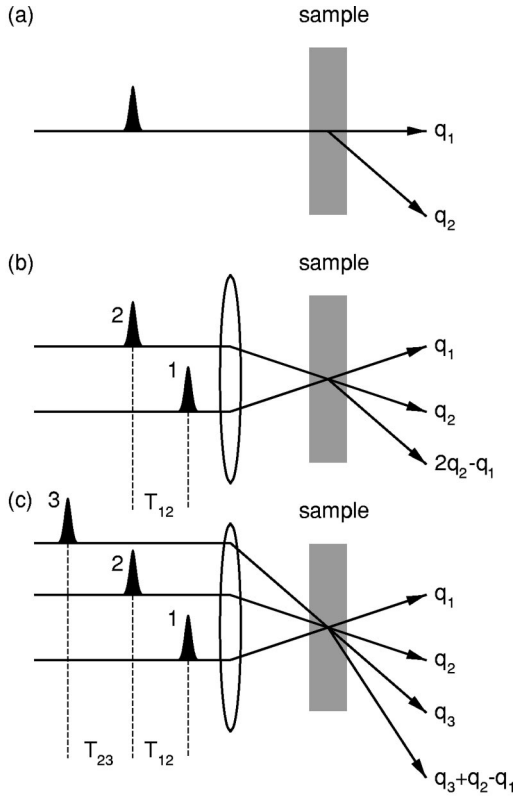

FIG. 2. Schematic representation of typical experimental setups for the study of ultrafast phenomena in semiconductors: (a) single-pulse excitation in which the secondary emission (resonant Rayleigh scattering or luminescence) is detected in a direction different from that of incidence; (b) pump-probe experiments or four-wave mixing in the two-pulse self-diffraction geometry; (c) three-pulse four-wave-mixing experiments.

Haug, 2001) and density matrices (Bonitz, 1998; Kuhn, 1998). These theories have been shown to describe the dynamics on a femtosecond time scale with very high accuracy. A more detailed discussion of theoretical approaches will be given in Sec. II.

B. Experimental techniques

As already mentioned above, essentially two different classes of experiments have been used for the study of carrier relaxation processes: luminescence and pump-probe measurements. In both cases a pump pulse is used to generate electron-hole pairs and bring the semiconductor into a state far from thermal equilibrium. In a luminescence experiment the radiation emitted in a direction different from that of the incident pulse due to recombination processes is analyzed spectrally and/or temporally. This is shown schematically in Fig. 2(a). Depending on the temporal resolution, different techniques have to be used: Temporal resolution in the range of 10 ps can be achieved by direct techniques by using either fast photodiodes or a streak camera that provides spectral and temporal information simultaneously. Higher time resolution is obtained by gating the luminescence signal with a second delayed laser pulse. Both the signal and the delayed pulse are focused on a nonlinear crystal, which creates a sum-frequency signal only in the presence of such a gating laser pulse. In this upconversion technique the temporal resolution is limited only by the laser-pulse duration; thus resolution in the 10-fs range is possible. In an intrinsic semiconductor the luminescence is due to the recombination of an electron in the conduction band with a hole in the valence band. In a fully incoherent picture, according to Fermi's golden rule, the signal is essentially proportional to the product of the distribution functions of electrons and holes. This complicates the interpretation of experimental results. An alternative is the use of doped semiconductors, e.g., p-doped samples, in which the band-to-acceptor luminescence directly monitors the distribution function of electrons.

In a pump-probe experiment the semiconductor is excited by a pump pulse traveling in a direction $\mathbf{q}_1$ [pulse 1 in Fig. 2(b)], and the dynamics of the carriers induced by this excitation are studied by looking at some property related to a delayed probe pulse in a direction $\mathbf{q}_2$. The most commonly used technique is transmission or reflection spectroscopy, in which the change in the transmission or reflection of the probe pulse—induced by the pump—is measured as a function of the time delay between the two pulses.[2] By using a broadband probe pulse, one therefore obtains differential transmission/reflection spectra. In a purely incoherent free-carrier picture the absorption is changed due to phase-space filling, and these signals provide information on the sum of the electron and hole populations in the optically coupled states. Again, the interpretation of the results is facilitated if the spectra are determined by a single distribution function. This can be achieved by exploiting optical transitions for the probe in a different spectral range, e.g., by pumping the heavy and light hole-to-conduction-band transitions and probing the splitoff to the conduction-band transition. A variation of the pump-probe technique is electro-optic sampling, in which the difference between two polarization components of the transmitted/reflected signal is analyzed, providing information, for example, on the birefringence induced by the optically excited dynamics. Instead of the change in the transmitted/reflected signal, the change in the Raman-scattering signal generated by the probe pulse can also be measured. The dynamics of photoexcited phonons as well as electronic excitations can be studied using this technique.

It is clear that the interpretation of luminescence and pump-probe experiments in terms of a fully incoherent free-carrier picture is valid only under limited conditions. In intrinsic semiconductors at sufficiently low carrier densities, absorption and luminescence spectra in the region close to the band gap are strongly dominated by excitonic effects. Even high up in the band, pump-induced changes in the Coulomb enhancement may significantly influence pump-probe spectra. Furthermore,

[2]In Fig. 2 only the transmission case is plotted.

on time scales comparable to or shorter than the characteristic dephasing times, the signals may be considerably modified by coherence effects. Therefore a detailed analysis of luminescence and pump-probe spectra in the ultrafast regime also provides information on coherent phenomena in the semiconductor. In Sec. III we shall discuss several examples in which such phase-related effects play a dominant role.

The most popular technique that provides direct information on coherence in semiconductors is four-wave-mixing spectroscopy. It can be performed in both a two-pulse and a three-pulse configuration, as shown schematically in Figs. 2(b) and (c).[3] For clarity let us start with the three-pulse configuration by assuming that the time delay T_{12} between the two laser pulses 1 and 2 with wave vectors $\mathbf{q}_1$ and $\mathbf{q}_2$ is zero. In this case these pulses create an interference pattern with wave vector $\pm(\mathbf{q}_2-\mathbf{q}_1)$ on the sample, which translates into a density grating when the light is absorbed. This density grating results in a refractive index grating, which may diffract a third pulse with incident wave vector $\mathbf{q}_3$ into various diffraction orders $\mathbf{q}_3+n(\mathbf{q}_2-\mathbf{q}_1)$, where n is an integer. In four-wave-mixing the first diffracted order $(n=1)$ is measured; here, three interacting incident waves interact, giving rise to a fourth emitted wave, which explains the name of the technique. Access to the coherent polarization in the sample is now obtained if pulses 1 and 2 are temporally separated. In this case there is no longer a direct interference pattern on the sample. However, as long as the microscopic interband polarization created by pulse 1 is still at least partly present when pulse 2 arrives, the interaction of a pulse with wave vector $\mathbf{q}_2$ with the interband polarization in the direction of $\mathbf{q}_1$ again results in a transient grating which can diffract pulse 3. Thus, by varying T_{12}, one obtains information on the dynamics and the lifetime of the polarization, i.e., on the dephasing time. It should be noted that a microscopic interband polarization may still be present even if, in the case of a continuous spectrum due to destructive interference of different microscopic components, there is no longer macroscopic polarization in the sample. This is exactly why four-wave-mixing spectroscopy can distinguish between homogeneous and inhomogeneous broadening. In the more often used two-pulse setup, pulse 2 simultaneously creates the grating and is diffracted by this grating; hence the name *self-diffraction geometry*. Besides analyzing the signal in a time-integrated way, one can also spectrally disperse it in a monochromator or temporally resolve it by means of an upconversion technique, as discussed in the case of luminescence, which provides additional information on the dynamics of the interband polarization.

Both pump-probe and four-wave-mixing experiments can be used to study coherent-control phenomena. In this case pulse 1 is replaced by a pair of phase-locked pulses with variable delay traveling in the same direction $\mathbf{q}_1$. The carrier dynamics induced by these pulses then depend on the relative phase between these two pulses and can be analyzed by the second pulse traveling in direction $\mathbf{q}_2$. In general, measuring the transmitted signal in direction $\mathbf{q}_2$ (or the corresponding reflected direction) and the four-wave-mixing signal in direction $2\mathbf{q}_2-\mathbf{q}_1$ yields complementary information on the dynamics of distribution functions and polarizations.

If the optically excited interband polarizations couple electronic states with different spatial localizations, the dynamics are associated with a time-dependent dipole moment, which, according to classical electrodynamics, acts as a source of electromagnetic radiation. Often this radiation is in the terahertz spectral range. In a typical terahertz-emission experiment a short laser pulse excites the system in a superposition of states, thus creating an intraband polarization. The intraband polarization oscillates according to the energy splitting of the corresponding states and emits a pulse of electromagnetic radiation with the corresponding frequency. This radiation is then collimated and transmitted to an optically gated photoconductive antenna, which measures the electric field of the radiation. Thus the general setup is the same as Fig. 2(a), except that the emitted signal in direction $\mathbf{q}_2$ is in the terahertz range. For a more detailed discussion of experimental techniques, we refer the reader to the book by Shah (1999).

C. Aim and outline of the paper

Ultrafast spectroscopy of semiconductors has been an extremely active field of research and has led to many new insights into phenomena of fundamental importance in semiconductor physics and technology. Such rapid development has been accompanied by a growing theoretical understanding of the basic processes governing the ultrafast nonequilibrium dynamics of photoexcited carriers. However, theoretical activity in the field has often been focused on specific problems within different perspectives.

The aim of this paper is to provide a cohesive discussion of ultrafast phenomena in semiconductors. More specifically, our primary goal is to show how a variety of apparently different phenomena can be described within the same theoretical framework based on the density-matrix formalism. Within this approach one can describe the strong interplay between coherent and incoherent (i.e., phase-breaking) phenomena that characterizes the ultrafast electro-optical response of semiconductor bulk and heterostructures.

In terms of this general theory, we shall review a variety of physical phenomena in different semiconductor structures such as bulk systems, superlattices, quantum wells, and quantum wires. The field is so active and extensive that an exhaustive treatment of all the research would be impossible. Thus we have to limit ourselves to a discussion of selected theoretical and experimental results, including recent developments, which have led to fundamental new insights into many diverse aspects of semiconductor physics. We shall concentrate on phe-

[3]Four-wave-mixing experiments can also be performed in a reflection geometry.

nomena in which carrier dynamics play the central role. Therefore phenomena like resonant Rayleigh scattering will be briefly mentioned but not discussed in detail. Furthermore, we shall restrict ourselves to the case in which the exciting light field can be treated as an external field initializing the carrier dynamics, which excludes propagation effects as well as phenomena related to microcavities. Finally, all the semiconductor structures mentioned above have in common a continuous spectrum. The increasingly active field of ultrafast dynamics in quantum dot structures has its own set of theoretical considerations, which will not be covered by this review. We shall briefly come back to this point in our concluding remarks.

The paper is organized as follows: In Sec. II we discuss the fundamentals of the density-matrix formalism applied to the analysis of the electro-optical response of semiconductor bulk and heterostructures. The contributions to the equations of motion due to various interaction mechanisms are derived and their physical meaning is explained. In the last part of the section we discuss how typical experiments are modeled within the framework presented earlier. A selection of fundamental results, both experimental and theoretical, is presented in Sec. III. Finally, in Sec. IV we summarize and draw some conclusions.

II. THEORETICAL BACKGROUND

A. Physical system

In order to study the optical and transport properties of semiconductor bulk and heterostructures, let us consider a gas of carriers in a crystal under the action of an applied electromagnetic field. The carriers will experience mutual interaction as well as interaction with the phonon modes of the crystal. This physical system can be described by the following Hamiltonian:

$$\mathbf{H}=\mathbf{H}_c+\mathbf{H}_p+\mathbf{H}_{cc}+\mathbf{H}_{cp}+\mathbf{H}_{pp}. \tag{1}$$

The first term describes the noninteracting-carrier system in the presence of the external electromagnetic field, while the second one refers to the free-phonon system. The last three terms describe many-body contributions: carrier-carrier, carrier-phonon, and phonon-phonon interactions, respectively.

In order to discuss their explicit form, let us introduce the usual second-quantization field operators $\mathbf{\Psi}^\dagger(\mathbf{r})$ and $\mathbf{\Psi}(\mathbf{r})$. They describe, respectively, the creation and the destruction of an electron in $\mathbf{r}$. In terms of the above field operators, the carrier Hamiltonian $\mathbf{H}_c$ can be written as

$$\mathbf{H}_c=\int d\mathbf{r}\mathbf{\Psi}^\dagger(\mathbf{r}) \times\left[\frac{\left[-i\hbar\nabla_{\mathbf{r}}+\frac{e}{c}\mathbf{A}(\mathbf{r},t)\right]^2}{2m_0}-e\varphi(\mathbf{r},t)+V^c(\mathbf{r})\right]\mathbf{\Psi}(\mathbf{r}). \tag{2}$$

Here, $V^c(\mathbf{r})$ denotes an effective single-particle potential due to the perfect crystal plus the valence electrons, m_0 is the free-electron mass, and $-e$ is the charge of the electron. $\mathbf{A}(\mathbf{r},t)$ and $\varphi(\mathbf{r},t)$ denote, respectively, the vector and scalar potentials corresponding to the external electromagnetic field:

$$\mathbf{E}(\mathbf{r},t)=-\frac{1}{c}\frac{\partial}{\partial t}\mathbf{A}(\mathbf{r},t)-\nabla_{\mathbf{r}}\varphi(\mathbf{r},t),$$
$$\mathbf{B}(\mathbf{r},t)=\nabla_{\mathbf{r}}\times\mathbf{A}(\mathbf{r},t). \tag{3}$$

The above equation reflects the well-known gauge freedom: there is an infinite number of possible combinations of $\mathbf{A}$ and φ which give rise to the same electromagnetic fields $\mathbf{E}$ and $\mathbf{B}$. This gauge invariance will be crucial in understanding the relationship between Bloch oscillations and Wannier-Stark localization, and will be discussed in more detail in Sec. III.F.1.

Since we are interested in the electro-optical properties as well as in the ultrafast dynamics of photoexcited carriers, the electromagnetic field acting on the crystal—and the corresponding electromagnetic potentials—will be regarded as the sum of two different contributions: one part which will be treated dynamically in the equations of motion (term 1) and an additional static (electric and/or magnetic) field (term 2) which will be included in the evaluation of single-particle basis states. Term 1 contains the time-dependent laser field responsible for the intraband as well as interband electronic excitations, but it may also contain additional static or dynamic electric fields not included in the definition of the basis states. However, we assume that all these contributions to term 1 are spatially sufficiently slowly varying (on the atomic scale) that they are well described by the scalar potential

$$\varphi_1(\mathbf{r},t)=-\mathbf{E}_1(\mathbf{r},t)\cdot\mathbf{r}. \tag{4}$$

With this particular choice of the electromagnetic potentials, the Hamiltonian in Eq. (2) can be rewritten as $\mathbf{H}_c=\mathbf{H}_c^0+\mathbf{H}_{cf}$, where

$$\mathbf{H}_c^0=\int d\mathbf{r}\mathbf{\Psi}^\dagger(\mathbf{r}) \times\left[\frac{\left[-i\hbar\nabla_{\mathbf{r}}+\frac{e}{c}\mathbf{A}_2(\mathbf{r},t)\right]^2}{2m_0}-e\varphi_2(\mathbf{r},t)+V^c(\mathbf{r})\right]\mathbf{\Psi}(\mathbf{r}) \tag{5}$$

describes the carrier system in the crystal under the action of the static field 2 only,[4] while

$$\mathbf{H}_{cf}=-e\int d\mathbf{r}\mathbf{\Psi}^\dagger(\mathbf{r})\varphi_1(\mathbf{r},t)\mathbf{\Psi}(\mathbf{r}) \tag{6}$$

describes the carrier-field interaction.

In analogy to the carrier system, when $b_{\mathbf{q}}^\dagger$ and $b_{\mathbf{q}}$ denote the creation and destruction operators for a phonon with wave vector $\mathbf{q}$, the free-phonon Hamiltonian takes the form

[4]It should be noted that, depending on the gauge, the potentials may be time dependent even for static fields.

$$\mathbf{H}_p = \sum_{\mathbf{q}} \hbar \omega_{\mathbf{q}} b_{\mathbf{q}}^\dagger b_{\mathbf{q}}, \tag{7}$$

where $\omega_{\mathbf{q}}$ is the phonon dispersion. For simplicity, here we restrict ourselves to a single branch of bulk phonons; the generalization to several branches as well as to other types of modes, e.g., confined phonons, is obvious.

Let us now discuss the explicit form of the many-body contributions. The carrier-carrier interaction is described by the two-body Hamiltonian

$$\mathbf{H}_{cc} = \frac{1}{2} \int d\mathbf{r} \int d\mathbf{r}' \boldsymbol{\Psi}^\dagger(\mathbf{r}) \boldsymbol{\Psi}^\dagger(\mathbf{r}') V_{cc}(\mathbf{r}-\mathbf{r}') \boldsymbol{\Psi}(\mathbf{r}') \boldsymbol{\Psi}(\mathbf{r}), \tag{8}$$

where V_{cc} denotes the Coulomb potential screened by the valence electrons as well as by those phonon degrees of freedom that are not taken into account dynamically. The coupling between carriers and phonons is described by the Hamiltonian

$$\mathbf{H}_{cp} = \int d\mathbf{r} \boldsymbol{\Psi}^\dagger(\mathbf{r}) V_{cp}(\mathbf{r}) \boldsymbol{\Psi}(\mathbf{r}), \tag{9}$$

where

$$V_{cp} = \sum_{\mathbf{q}} [\tilde{g}_{\mathbf{q}} b_{\mathbf{q}} e^{i\mathbf{q}\cdot\mathbf{r}} + \tilde{g}_{\mathbf{q}}^* b_{\mathbf{q}}^\dagger e^{-i\mathbf{q}\cdot\mathbf{r}}] \tag{10}$$

is the potential induced by the lattice vibrations, linearized in the displacements of the nuclei. Here, the explicit form of the coupling function $\tilde{g}_{\mathbf{q}}$ depends on the particular phonon branch (acoustic, optical, etc.) as well as on the coupling mechanism considered (deformation potential, polar coupling, etc.).

Finally, let us briefly comment on the phonon-phonon contribution $\mathbf{H}_{pp}$: The free-phonon Hamiltonian $\mathbf{H}_p$ in Eq. (7), which describes a system of noninteracting phonons, by definition accounts only for the harmonic part of the lattice potential. However, nonharmonic contributions of the interatomic potential can play an important role in determining the lattice dynamics in highly excited systems (Kash and Tsang, 1989), since they are responsible for the decay of optical phonons into phonons of lower frequency. In our second-quantization picture, these nonharmonic contributions can be described in terms of a phonon-phonon interaction which, in general, induces transitions between free-phonon states. Here, we shall not discuss the explicit form of the phonon-phonon Hamiltonian $\mathbf{H}_{pp}$ responsible for such a decay. For the results discussed in this review, it is not important either because the phonon system remains sufficiently close to thermal equilibrium or because the characteristic time scale of this decay (about 7 ps for the decay of LO phonons in bulk GaAs; von der Linde *et al.*, 1980; Kash *et al.*, 1985; Shah, 1992) is considerably longer than the femtosecond time scales typically studied in ultrafast experiments.

It is well known that the coordinate representation used so far is not the most convenient one for describing the electron dynamics within a crystalline semiconductor. In general, it is more convenient to employ the representation given by the eigenstates of a suitably chosen noninteracting-carrier Hamiltonian, since it automatically accounts for some of the symmetries of the system.

In this spirit, let us denote with $\{\phi_n(\mathbf{r},t)\}$ the set of eigenfunctions of the noninteracting-carrier Hamiltonian in Eq. (5) and with $\epsilon_n(t)$ the corresponding energy levels. Since the Hamiltonian is, in general, a function of time, the basis functions ϕ_n and the energies ϵ_n may be time dependent. Here, the label n denotes, in general, a set of discrete and/or continuous quantum numbers. In the absence of the static field 2, the above wave functions will correspond to the well-known Bloch states of the crystal, and the index n will reduce to the wave vector $\mathbf{k}$ plus the band (or subband) index ν. In the presence of a homogeneous magnetic field, the eigenfunctions ϕ_n, after performing an effective mass approximation, may instead correspond to Landau states. Finally, in a constant and homogeneous electric field, depending on the gauge chosen, there exist two equivalent representations: the accelerated Bloch states and the Wannier-Stark picture. We shall come back to this point in Sec. III.F.1 when discussing the relationship between Bloch oscillations and Wannier-Stark localization.

Let us now reconsider the system Hamiltonian introduced so far in terms of ϕ_n. As a starting point, we shall expand the second-quantization field operators in terms of the new wave functions:

$$\boldsymbol{\Psi}(\mathbf{r}) = \sum_n \phi_n(\mathbf{r},t) a_n, \quad \boldsymbol{\Psi}^\dagger(\mathbf{r}) = \sum_n \phi_n^*(\mathbf{r},t) a_n^\dagger. \tag{11}$$

The above expansion defines the new set of second-quantization operators $a_n^\dagger$ and a_n; they describe, respectively, the creation and destruction of an electron in state n.

In the case of a semiconductor structure (the only one considered here), the energy spectrum ϵ_n of the noninteracting-carrier Hamiltonian (5) is always characterized by two well-separated energy regions: the valence and the conduction band. Also, in the presence of an applied electromagnetic field, the effective lattice potential V^c gives rise to a large energy gap. Therefore we are dealing with two energetically well-separated regions, which suggests the introduction of the usual electron-hole picture. This corresponds to a separation of the set of states $\{\phi_n\}$ into conduction states $\{\phi_i^e\}$ and valence states $\{\phi_j^h\}$. Thus the creation operator $a_n^\dagger$ introduced in Eq. (11) will also be divided into electron creation and hole destruction operators $c_i^\dagger$ and $d_j^\dagger$, while the destruction operators a_n will be divided into electron destruction and hole creation operators c_i and $d_j^\dagger$. In terms of the new electron-hole picture, the expansion (11) is given by

$$\boldsymbol{\Psi}(\mathbf{r}) = \sum_i \phi_i^e(\mathbf{r},t) c_i + \sum_j \phi_j^{h*}(\mathbf{r},t) d_j^\dagger,$$

$$\boldsymbol{\Psi}^\dagger(\mathbf{r}) = \sum_i \phi_i^{e*}(\mathbf{r},t) c_i^\dagger + \sum_j \phi_j^h(\mathbf{r},t) d_j. \tag{12}$$

If we now insert the above expansion into Eq. (5), the noninteracting-carrier Hamiltonian takes the form

$$\mathbf{H}_c^0(t)=\sum_i \epsilon_i^e(t)c_i^\dagger c_i+\sum_j \epsilon_j^h(t)d_j^\dagger d_j$$
$$=\mathbf{H}_e^0(t)+\mathbf{H}_h^0(t). \quad (13)$$

As already pointed out, the above Hamiltonian is in general time dependent. We shall discuss this feature in the following section, where we shall derive our set of kinetic equations.

Let us now write the carrier-field interaction Hamiltonian [Eq. (6)] in terms of our electron-hole representation:

$$\mathbf{H}_{cf}=\sum_{i,i'} \mathcal{E}_{ii'}^{e(cf)}c_i^\dagger c_{i'}+\sum_{j,j'} \mathcal{E}_{jj'}^{h(cf)}d_j^\dagger d_{j'}$$
$$+\sum_{i,j} [\mathcal{U}_{ij}^{(cf)}c_i^\dagger d_j^\dagger+\mathcal{U}_{ij}^{(cf)*}d_j c_i]. \quad (14)$$

Here, $\mathcal{E}_{ll'}^{e,h(cf)}$ denote the electron and hole intraband and $\mathcal{U}_{ij}^{(cf)}$ the interband matrix elements of the scalar potential $\varphi_1(\mathbf{r},t)$:

$$\mathcal{E}_{ll'}^{e,h(cf)}=\pm e\int d\mathbf{r}\phi_l^{e,h*}(\mathbf{r},t)\mathbf{E}_1(\mathbf{r},t)\cdot\mathbf{r}\phi_{l'}^{e,h}(\mathbf{r},t), \quad (15a)$$

$$\mathcal{U}_{ij}^{(cf)}=e\int d\mathbf{r}\phi_i^{e*}(\mathbf{r},t)\mathbf{E}_1(\mathbf{r},t)\cdot\mathbf{r}\phi_j^{h*}(\mathbf{r},t) \quad (15b)$$

where the upper (positive) sign refers to electrons and the lower (negative) sign to holes. Equations (7), (13), and (14) define the single-particle Hamiltonian $\mathbf{H}_{sp}=\mathbf{H}_p+\mathbf{H}_c^0+\mathbf{H}_{cf}$.

Similarly, the carrier-carrier Hamiltonian (8) can be rewritten as

$$\mathbf{H}_{cc}=\frac{1}{2}\sum_{i_1i_2i_3i_4} V_{i_1i_2i_3i_4}^{ee}c_{i_1}^\dagger c_{i_2}^\dagger c_{i_3}c_{i_4}$$
$$+\frac{1}{2}\sum_{j_1j_2j_3j_4} V_{j_1j_2j_3j_4}^{hh}d_{j_1}^\dagger d_{j_2}^\dagger d_{j_3}d_{j_4}$$
$$-\sum_{i_1i_2j_1j_2} V_{i_1j_1j_2i_2}^{eh}c_{i_1}^\dagger d_{j_1}^\dagger d_{j_2}c_{i_2}, \quad (16)$$

where $V_{l_1l_2l_3l_4}^{ee/hh/eh}$ are the Coulomb matrix elements of the two-body Coulomb potential in our ϕ representation. The first two terms describe the repulsive electron-electron and hole-hole interaction, while the third describes the attractive electron-hole interaction. The effective single-particle contributions that appear due to the reordering of the operators are assumed to be included in $\mathbf{H}_c^0(t)$. Here, we restrict ourselves to the monopole-monopole contributions, which means that we neglect terms that do not conserve the number of electron-hole pairs, i.e., impact-ionization and Auger recombination processes (Quade *et al.*, 1994), as well as the interband exchange interaction. The former assumption is typically well satisfied in the range of energies and densities considered here; the latter is justified if the longitudinal-transverse splitting of the exciton is much smaller than its binding energy (Egri, 1985).

Finally, we rewrite the carrier-phonon interaction Hamiltonian introduced in Eq. (9):

$$\mathbf{H}_{cp}=\sum_{ii',\mathbf{q}} [g_{\mathbf{q}}^{ii'}c_i^\dagger b_{\mathbf{q}}c_{i'}+g_{\mathbf{q}}^{ii'*}c_{i'}^\dagger b_{\mathbf{q}}^\dagger c_i]$$
$$-\sum_{jj',\mathbf{q}} [g_{\mathbf{q}}^{jj'}d_j^\dagger b_{\mathbf{q}}d_{j'}+g_{\mathbf{q}}^{jj'*}d_{j'}^\dagger b_{\mathbf{q}}^\dagger d_j], \quad (17)$$

where

$$g_{\mathbf{q}}^{ll'}=\tilde{g}_{\mathbf{q}}\int d\mathbf{r}\phi_l^*(\mathbf{r},t)e^{i\mathbf{q}\cdot\mathbf{r}}\phi_{l'}(\mathbf{r},t). \quad (18)$$

In Eq. (17) we can clearly recognize four different contributions corresponding to phonon absorption and emission by electrons and holes. The interband terms have been neglected because of their strong off-resonance nature.

B. Kinetic description

Many experimentally observable quantities like current densities, phonon populations, photon numbers, or electronic polarizations which act as sources for emitted electromagnetic radiation are single-particle quantities. They can be expressed in terms of single-particle density matrices like the intraband electron and hole density matrices $f_{ii'}^e=\langle c_i^\dagger c_{i'}\rangle$ and $f_{jj'}^h=\langle d_j^\dagger d_{j'}\rangle$, the corresponding interband density matrix $p_{ji}=\langle d_j c_i\rangle$, or the phonon occupation number $n_{\mathbf{q}}=\langle b_{\mathbf{q}}^\dagger b_{\mathbf{q}}\rangle$. The diagonal elements of these density matrices describe the occupation probabilities of the respective states, while the off-diagonal elements determine the degree of quantum-mechanical superposition of the two states involved. The expectation value is taken with respect to the initial state of the system, which in most cases discussed in this review is the vacuum of electron-hole pairs and a thermal phonon distribution.

The primary goal of a kinetic theory of ultrafast processes is to calculate the temporal evolution of the quantities introduced above, which constitute the kinetic variables of the system. However, due to the many-body nature of the problem, an exact solution is generally not possible, except for some simple model systems (Zimmermann and Wauer, 1994; Meden *et al.*, 1995; Axt, Herbst, and Kuhn, 1999; Castella and Zimmermann, 1999). Such exact calculations provide valuable information on specific features of certain experiments, but for a full understanding realistic semiconductor models have to be considered, which then can only be treated approximately.

Different techniques for the theoretical treatment of the dynamics of many-body systems have been developed in the past. Among the most commonly used methods are the nonequilibrium Green's-function technique and the density-matrix formalism. The former, introduced in the 1960s by Kadanoff and Baym (1962) and Keldysh (1965), is an extension of the well-known equilibrium or zero-temperature Green's-function theory to nonequilibrium systems. The basic ingredient is a

contour-ordered Green's function for which, as in the equilibrium case, a Dyson equation can be formulated. This contour-ordered function can be separated into four types of two-time Green's functions. The central approximation in this formalism is the identification of the self-energy by selecting a specific subset of the infinitely many diagrams, to define the interaction processes taken into account. Since in most cases the quantities that are directly related to experimental observables depend on one time only, the question arises whether the theory can be reduced to single-time variables. Kadanoff and Baym (1962) showed that the Boltzmann equation can be recovered if the two-time Green's function $G^<$ is written as a product of its time-diagonal part—i.e., the single-particle density matrix—and a spectral function of noninteracting carriers. This ansatz was extended by Lipavský, Špička, and Velický (1986) to the so-called generalized Kadanoff-Baym ansatz, which correctly treats causality. Under nonequilibrium conditions, however, this is only an approximation. An introduction to the theory of nonequilibrium Green's functions with applications to many problems in transport and optics of semiconductors can be found in the book by Haug and Jauho (1996). A recent review is that of Haug (2001).

In the density-matrix formalism, one starts directly with the equations of motion for the single-particle density matrices. Due to the many-body nature of the problem, the resulting set of equations of motion is not closed; instead, it constitutes the starting point of an infinite hierarchy of higher-order density matrices. Aside from differences related to the quantum statistics of the quasiparticles involved, this is equivalent to the Bogoliubov-Born-Green-Kirkwood-Yvon (BBGKY) hierarchy in classical gas dynamics (Bogoliubov, 1967; McQuarrie, 1976). The central approximation to obtain a tractable problem in this formalism is the truncation of the hierarchy. This can be based on different physical pictures. In this review we shall use the argument that correlations involving an increasing number of particles will become less and less important. On the classical level this corresponds to the derivation of the Vlasov equation (mean field) and the Boltzmann equation (two-particle correlations) from the BBGKY hierarchy. An alternative scheme was introduced by Axt and Stahl (1994a): the so-called "dynamics-controlled truncation." Here, the basic idea is an expansion in powers of the exciting laser field, as is done in nonlinear optics when nonlinear susceptibilities are introduced. It turns out that for the usual case of a pair-conserving many-body Hamiltonian and a system in which the initial state is given by the vacuum of electron-hole pairs, the hierarchy can be rigorously truncated to any order in the driving field. This approach is particularly useful when higher-order Coulomb correlations like biexcitons and correlated two-exciton states are important. Furthermore, it allows a unified treatment of semiconductors and molecular structures. For a detailed discussion of this formalism, the reader is referred to the review article by Axt and Mukamel (1998).

The standard procedure for deriving the set of kinetic equations, i.e., the equations of motion for the relevant kinetic variables, is to derive the equations of motion for the electron and hole operators introduced in Eq. (12):

$$c_i = \int d\mathbf{r}\, \phi_i^{e*}(\mathbf{r},t)\boldsymbol{\Psi}(\mathbf{r}),$$

$$d_j = \int d\mathbf{r}\, \phi_j^{h*}(\mathbf{r},t)\boldsymbol{\Psi}^\dagger(\mathbf{r}). \tag{19}$$

By applying the Heisenberg equation of motion for the field operator $\boldsymbol{\Psi}$, one can easily obtain the following equations of motion:

$$\frac{d}{dt}c_i = \frac{1}{i\hbar}[c_i,\mathbf{H}] + \frac{1}{i\hbar}\sum_{i'} Z^e_{ii'}c_{i'}, \tag{20a}$$

$$\frac{d}{dt}d_j = \frac{1}{i\hbar}[d_j,\mathbf{H}] + \frac{1}{i\hbar}\sum_{j'} Z^h_{jj'}d_{j'}, \tag{20b}$$

where

$$Z^e_{ii'} = i\hbar\int d\mathbf{r}\left(\frac{\partial}{\partial t}\phi_i^{e*}(\mathbf{r},t)\right)\phi^e_{i'}(\mathbf{r},t),$$

$$Z^h_{jj'} = i\hbar\int d\mathbf{r}\left(\frac{\partial}{\partial t}\phi_j^{h}(\mathbf{r},t)\right)\phi^{h*}_{j'}(\mathbf{r},t). \tag{21}$$

Here we neglect minor contributions due to coupling between valence and conduction bands. Compared to the more conventional Heisenberg equations of motion, they contain an extra term, the last one. It accounts for the possible time dependence of our ϕ representation, which will induce transitions between different states according to the matrix elements $Z^{e,h}$.

By combining the above equations of motion with the definitions of the kinetic variables, we can schematically write the resulting set of kinetic equations as

$$\frac{d}{dt}F = \frac{d}{dt}F\big|^{\mathbf{H}} + \frac{d}{dt}F\big|^{\phi}, \tag{22}$$

where F denotes the generic kinetic variable. They exhibit the same structure as the equations of motion [Eq. (20)] for the electron and hole creation and destruction operators: a first term induced by the system Hamiltonian $\mathbf{H}$ (which does not account for the time variation of the basis states) and a second term induced by the time dependence of the basis functions ϕ.

The explicit form of this second term is given by

$$\frac{d}{dt}f^e_{i_1i_2}\big|^{\phi} = \frac{1}{i\hbar}\sum_{i_3}[Z^e_{i_2i_3}f^e_{i_1i_3} - Z^e_{i_3i_1}f^e_{i_3i_2}], \tag{23a}$$

$$\frac{d}{dt}f^h_{j_1j_2}\big|^{\phi} = \frac{1}{i\hbar}\sum_{j_3}[Z^h_{j_2j_3}f^h_{j_1j_3} - Z^h_{j_3j_1}f^h_{j_3j_2}], \tag{23b}$$

$$\frac{d}{dt}p_{j_1i_1}\big|^{\phi} = \frac{1}{i\hbar}\left[\sum_{j_2} Z^h_{j_1j_2}p_{j_2i_1} + \sum_{i_2} Z^e_{i_1i_2}p_{j_1i_2}\right]. \tag{23c}$$

As we shall see, these contributions play a central role in the description of Zener tunneling in superlattices within the vector-potential representation.

The first term—which is the only one present if a time-independent basis is considered—is the sum of different contributions corresponding to the various parts of the Hamiltonian. In the remainder of this section we shall discuss the time evolution induced by the different contributions to the total Hamiltonian.

C. Single-particle dynamics

The time evolution induced by the single-particle Hamiltonian is easily obtained from the Heisenberg equations of motion in Eq. (20), resulting in a closed set of kinetic equations for the single-particle density matrices. The intraband contributions have the same structure as those in Eq. (23); therefore the time dependence of the basis states can be directly included, which is again related to the gauge invariance of our formulation as discussed in Rossi (1998). The resulting equations of motion are

$$\frac{d}{dt}f^e_{i_1i_2}|^{(sp)}=\frac{1}{i\hbar}\sum_{i_3}\left[\mathcal{E}^{e(sp)}_{i_2i_3}f^e_{i_1i_3}-\mathcal{E}^{e(sp)}_{i_3i_1}f^e_{i_3i_2}\right]+\frac{1}{i\hbar}\sum_{j_1}\left[\mathcal{U}^{(sp)}_{i_2j_1}p^*_{j_1i_1}-\mathcal{U}^{(sp)*}_{i_1j_1}p_{j_1i_2}\right], \tag{24a}$$

$$\frac{d}{dt}p_{j_1i_1}|^{(sp)}=\frac{1}{i\hbar}\left[\sum_{j_2}\mathcal{E}^{h(sp)}_{j_1j_2}p_{j_2i_1}+\sum_{i_2}\mathcal{E}^{e(sp)}_{i_1i_2}p_{j_1i_2}\right]+\frac{1}{i\hbar}\left[\mathcal{U}^{(sp)}_{i_1j_1}-\sum_{i_2}\mathcal{U}^{(sp)}_{i_2j_1}f^e_{i_2i_1}-\sum_{j_2}\mathcal{U}^{(sp)}_{i_1j_2}f^h_{j_2j_1}\right], \tag{24b}$$

where the effective electron and hole single-particle energies (intraband energies) are $\mathcal{E}^{e,h(sp)}_{ll'}=\epsilon^{e,h}_l\delta_{ll'}+\mathcal{E}^{e,h(cf)}_{ll'}+Z^{e,h}_{ll'}$ and the effective field (interband energy) is $\mathcal{U}^{(sp)}_{ij}=\mathcal{U}^{(cf)}_{ij}$. The equations for the hole density matrix $f^h_{jj'}$ typically have the same structure as those for the electron density matrix. Therefore, in general, we shall give explicitly only the equations for f^e and p.

It should be noted that Eqs. (24) are nothing more than a multilevel generalization of the optical Bloch equations. Indeed, by restricting ourselves to the case of a single electron state i and a single hole state j, and by identifying the elements of the density matrix ρ of a two-level system with our variables according to $\rho_{22}=f^e_{ii}$, $\rho_{11}=1-f^h_{jj}$, and $\rho_{12}=p_{ji}$, we recover the well-known optical Bloch equations for a two-level system (Allen and Eberly, 1987).

For the derivation of the equations of motion, no specific time dependence of the electric field has been assumed. The importance of the different contributions, however, is strongly determined by the frequency of the electromagnetic excitation. For a static or low-frequency field the intraband terms—describing carrier transport phenomena—are usually the most important ones. Indeed, in this case the interband terms are strongly off-resonant; they give rise to Zener tunneling, which requires very high fields to become relevant. If, in contrast, the frequency of the field is of the order of the band gap, the creation of a coherent interband polarization—and the resulting generation of electron-hole pairs—is the dominant process.

1. Semiclassical generation rate

Many transport and relaxation phenomena in optically excited semiconductors, in particular if the relevant time scales are not too short, can be described quite well on a purely incoherent or semiclassical level, where distribution functions are the only dynamical variables. Therefore one of the purposes of a quantum-kinetic theory is to derive the semiclassical theory as a limiting case and to study the approximations involved in such a derivation. The general procedure employed to obtain the semiclassical limit is the same for all types of interactions. As we shall see, it consists of an adiabatic elimination of variables involving quantum-mechanical correlations by means of a Markov approximation, assuming that the system was initially uncorrelated. In this section we discuss this approach for the case of interaction dynamics induced by an external field.

In the semiclassical limit the system is completely determined by the distribution functions of electrons and holes. Thus all off-diagonal elements have to be eliminated. As discussed above, the dominant terms in Eq. (24) are determined by the frequency of the field. In the following we shall consider the case of a time-independent single-particle basis ϕ_n and an optical (interband) excitation. By keeping only the nearly resonant parts in the equations of motion, i.e., performing a "rotating-wave" approximation (Haug and Koch, 1993), we get

$$\frac{d}{dt}f^e_{ii}=\sum_j g_{ji}(t),\quad \frac{d}{dt}f^h_{jj}=\sum_i g_{ji}(t), \tag{25a}$$

$$\frac{d}{dt}p_{ji}=\frac{1}{i\hbar}(\epsilon^h_j+\epsilon^e_i)p_{ji}+\frac{1}{i\hbar}\mathcal{U}^{0*}_{ij}(t)e^{-i\omega_Lt}[1-f^e_{ii}-f^h_{jj}], \tag{25b}$$

where the generation rate is

$$g_{ji}(t)=\frac{1}{i\hbar}[\mathcal{U}^0_{ij}(t)e^{-i\omega_Lt}p^*_{ji}-\mathcal{U}^0_{ij}(t)e^{i\omega_Lt}p_{ji}], \tag{26}$$

the effective field in the rotating-wave approximation is $\mathcal{U}_{ij}=\mathcal{U}^0_{ij}(t)e^{-i\omega_Lt}$, and $\mathcal{U}^0_{ij}(t)$ denotes the slowly varying part of $\mathcal{U}$. In this case the above polarization equation can be formally integrated:

$$p_{ji}(t)=\frac{1}{i\hbar}e^{-i\omega_Lt}\int_0^\infty d\tau e^{-i(\omega_{ji}-\omega_L)\tau}U^0_{ij}(t-\tau)\times[1-f^e_{ii}(t-\tau)-f^h_{jj}(t-\tau)], \tag{27}$$

where $\hbar\omega_{ji}=\epsilon^h_j+\epsilon^e_i$. In the case of a continuous spectrum, the summation over the final states eventually leads to a finite memory depth due to destructive interference of the different frequency contributions. The semiclassical limit is then obtained with two assumptions: First, within the Markov approximation one as-

sumes that the dominant time dependence is given by the exponential in Eq. (27) and therefore that the carrier distribution and field amplitude are sufficiently slowly varying that their value at time t can be taken out of the integral. Second, in order to have a well-defined initial condition, the field is adiabatically switched on according to $\mathcal{U}^0_{ij}(t)=\lim_{\eta\to 0}\tilde{\mathcal{U}}^0_{ij}(t)e^{\eta t}$. Then, the polarization is an instantaneous function of the carrier distribution and field according to

$$p_{ji}(t)=-\frac{i\pi}{\hbar}\mathcal{U}^0_{ij}(t)e^{-i\omega_L t}[1-f^e_{ii}(t)-f^h_{jj}(t)]\mathcal{D}(\omega_{ji}-\omega_L), \tag{28}$$

where we have introduced the function

$$\mathcal{D}(x)=-\frac{i}{\pi}\lim_{\eta\to 0}\frac{1}{x-i\eta}=\delta(x)-\frac{i}{\pi}\frac{\mathcal{P}}{x}. \tag{29}$$

Here $\mathcal{P}$ denotes the principal value. This leads to the semiclassical generation rate

$$g_{ji}(t)=\frac{2\pi}{\hbar^2}|\mathcal{U}^0_{ij}(t)|^2[1-f^e_{ii}(t)-f^h_{jj}(t)]\delta(\omega_{ji}-\omega_L), \tag{30}$$

i.e., Fermi's golden rule. The general procedure for obtaining a semiclassical rate, which has been performed here for the case of light-matter interaction, is the same for all coupling mechanisms: The interaction process introduces a new variable describing the correlation associated with this interaction. In the present case this is the electron-hole correlation due to the light field described by p_{ji}. This new variable is then adiabatically eliminated on the basis of a Markov approximation and the assumption of an initially uncorrelated system.

Completely neglecting the time dependence of the field amplitude has led us to a monochromatic generation rate. Any pulse with a finite duration, however, is characterized by a finite spectral width. Often this broadening is introduced by multiplying the generation rate by the spectral intensity of the pulse and integrating over the light frequency. More rigorously, this broadening can be derived from the time-integrated generation obtained from Eqs. (26) and (27) after a change of the integration variables according to

$$\begin{aligned}G_{ji}&=\int_{-\infty}^{\infty}dt\,g_{ji}(t)\\&=\frac{1}{\hbar^2}\int_{-\infty}^{\infty}dt\int_{-\infty}^{\infty}dt'\left[1-f^e_{ii}\left(t-\frac{1}{2}t'\right)-f^h_{jj}\left(t-\frac{1}{2}t'\right)\right]\\&\quad\times\mathcal{U}^{0*}_{ij}\left(t+\frac{1}{2}t'\right)\mathcal{U}^0_{ij}\left(t-\frac{1}{2}t'\right)e^{-i(\omega_{ji}-\omega_L)t'}.\end{aligned} \tag{31}$$

If we now perform the Markov approximation for the distribution functions only and identify the time of generation with the central time t, we arrive at a semiclassical generation rate of the form

$$\begin{aligned}g_{ji}(t)&=\frac{1}{\hbar^2}[1-f^e_{ii}(t)-f^h_{jj}(t)]\\&\quad\times\int_{-\infty}^{\infty}dt'\mathcal{U}^{0*}_{ij}\left(t+\frac{1}{2}t'\right)\\&\quad\times\mathcal{U}^0_{ij}\left(t-\frac{1}{2}t'\right)e^{-i(\omega_{ji}-\omega_L)t'},\end{aligned} \tag{32}$$

i.e., a rate determined by the time-dependent spectrum of the pulse. In the absence of other types of interactions and when phase-space filling effects can be neglected, this generation rate leads to the correct final distribution of electrons and holes. However, it is not strictly causal: The generation rate at time t also depends on the amplitude of the light field at later times. This is a consequence of the definition of an instantaneous spectrum which violates energy-time uncertainty. In the case of a Gaussian pulse $\mathcal{U}^0_{ij}(t)=\overline{\mathcal{U}_{ij}}\exp[-t^2/\tau_L^2]$, Eq. (32) leads to

$$\begin{aligned}g_{ji}(t)&=\frac{\sqrt{2\pi}}{\hbar^2}[1-f^e_{ii}(t)-f^h_{jj}(t)]|\overline{\mathcal{U}_{ij}}|^2\tau_L\\&\quad\times\exp\left[-2\frac{t^2}{\tau_L^2}\right]\exp\left[-\frac{1}{2}\tau_L^2(\omega_{ji}-\omega_L)^2\right],\end{aligned} \tag{33}$$

i.e., to a generation rate according to the product of the temporal and spectral shape of the pulse. In general, however, such a decomposition is not possible.

2. Homogeneous system, homogeneous excitation

The set of kinetic equations derived so far is valid in any single-particle basis and for any type of semiconductor structure. In many experimentally relevant systems, however, symmetries occur that may reduce the complexity of the problem. The most important is the homogeneous system. This can be a bulk semiconductor that is homogeneous in all three dimensions, but it also applies to low-dimensional structures like quantum wells and wires in the so-called strong-confinement limit, i.e., if only one carrier subband contributes to the dynamics. These structures are therefore homogeneous in d dimensions, where d is two or one. In such homogeneous systems Bloch functions with a $\mathbf{k}$ vector in the d dimensions can be chosen as basis states. Then, all interaction mechanisms in the Hamiltonian satisfy momentum conservation. If, in addition, the $\mathbf{k}$ dependence of the lattice-periodic part of the Bloch functions for electrons $[u^e(\mathbf{r})]$ and holes $[u^h(\mathbf{r})]$ is neglected—which corresponds to an effective-mass approximation—the Coulomb and carrier-phonon matrix elements $V_{\mathbf{q}}$ and $g_{\mathbf{q}}$ depend on the momentum transfer $\mathbf{q}$ only; moreover, the interband dipole matrix element

$$\mathbf{M}=-e\int_{\mathcal{V}_c}d\mathbf{r}u^{e*}(\mathbf{r})\mathbf{r}u^{h*}(\mathbf{r}) \tag{34}$$

is $\mathbf{k}$ independent.

If such a homogeneous system is excited by a spatially homogeneous electric field $\mathbf{E}(t)$, the effective energies and fields are given by

$$\mathcal{E}^{e,h}_{\mathbf{k}\mathbf{k}'}=\left[\epsilon^{e,h}_{\mathbf{k}}\pm ie\mathbf{E}_{\parallel}\cdot\frac{\partial}{\partial\mathbf{k}}\right]\delta_{\mathbf{k}\mathbf{k}'}, \tag{35a}$$

$$\mathcal{U}_{\mathbf{k}\mathbf{k}'}=-\mathbf{M}\cdot\mathbf{E}\delta_{\mathbf{k},-\mathbf{k}'}, \tag{35b}$$

where $\mathbf{E}_{\parallel}$ is the component of the electric field in the d-dimensional homogeneous subspace. Due to the diagonality of these matrices, only spatially homogeneous dynamical variables—i.e., electron and hole distribution functions $f^e_{\mathbf{k}}=\langle c^{\dagger}_{\mathbf{k}}c_{\mathbf{k}}\rangle$ and $f^h_{\mathbf{k}}=\langle d^{\dagger}_{\mathbf{k}}d_{\mathbf{k}}\rangle$—and diagonal interband polarizations $p_{\mathbf{k}}=\langle d_{-\mathbf{k}}c_{\mathbf{k}}\rangle$ will be generated. They satisfy the following equations of motion:

$$\frac{d}{dt}f^e_{\mathbf{k}}|^{(sp)}=\frac{e}{\hbar}\mathbf{E}_{\parallel}\cdot\frac{\partial}{\partial\mathbf{k}}f^e_{\mathbf{k}}-\frac{1}{i\hbar}\mathbf{E}\cdot(\mathbf{M}p^*_{\mathbf{k}}-\mathbf{M}^*p_{\mathbf{k}}), \tag{36a}$$

$$\frac{d}{dt}p_{\mathbf{k}}|^{(sp)}=\frac{1}{i\hbar}(\epsilon^e_{\mathbf{k}}+\epsilon^h_{-\mathbf{k}})p_{\mathbf{k}}+\frac{e}{\hbar}\mathbf{E}_{\parallel}\cdot\frac{\partial}{\partial\mathbf{k}}p_{\mathbf{k}}-\frac{1}{i\hbar}\mathbf{M}\cdot\mathbf{E}(1-f^e_{\mathbf{k}}-f^h_{-\mathbf{k}}). \tag{36b}$$

The intraband terms involving $\mathbf{E}_{\parallel}$ describe acceleration of the carriers due to the electric field. It is the same for diagonal and off-diagonal parts and it agrees with the Boltzmann drift term. The interband terms couple distribution functions and polarization. Again, as discussed above, the relevance of the various contributions depends on the frequency of the electromagnetic field. For optical fields the drift terms can usually be neglected, while for low-frequency fields the interband terms are of minor importance. If a static or low-frequency field and an optical field are applied simultaneously, the drift term in Eq. (36b) gives rise to the static or dynamical Franz-Keldysh effect in the optical absorption (Franz, 1958; Keldysh, 1958; Jauho and Johnsen, 1996).

3. Homogeneous system, inhomogeneous excitation

If the spatially homogeneous system is excited by a spatially inhomogeneous electric field, the dynamical variables become inhomogeneous, and off-diagonal density matrices have to be included. Due to the structure of the crystal Hamiltonian, a momentum representation is often still useful, but a real-space representation can also be chosen. In both cases the general equations of motion (24) with the corresponding intraband and interband energies have to be applied. An alternative approach is a mixed momentum and real-space representation, the so-called Wigner representation (Wigner, 1932). This is particularly useful for three purposes: (i) The intraband density matrix in this representation has the closest similarity to the classical distribution function; therefore it is best suited for a comparison to semiclassical kinetics described by the Boltzmann equation. (ii) For sufficiently slowly varying spatial inhomogeneities a gradient expansion can be performed. (iii) Boundary conditions that occur in systems with open boundaries—for example, due to the coupling to contacts—can be incorporated (Frensley, 1990).

The single-particle density matrices in the Wigner representation are obtained by performing a Fourier transformation with respect to the relative momentum according to

$$f^e_{\mathbf{k}}(\mathbf{r})=\sum_{\mathbf{q}}e^{i\mathbf{q}\mathbf{r}}\langle c^{\dagger}_{\mathbf{k}-(1/2)\mathbf{q}}c_{\mathbf{k}+(1/2)\mathbf{q}}\rangle, \tag{37a}$$

$$f^h_{\mathbf{k}}(\mathbf{r})=\sum_{\mathbf{q}}e^{i\mathbf{q}\mathbf{r}}\langle d^{\dagger}_{\mathbf{k}-(1/2)\mathbf{q}}d_{\mathbf{k}+(1/2)\mathbf{q}}\rangle, \tag{37b}$$

$$p_{\mathbf{k}}(\mathbf{r})=\sum_{\mathbf{q}}e^{i\mathbf{q}\mathbf{r}}\langle d_{-\mathbf{k}+(1/2)\mathbf{q}}c_{\mathbf{k}+(1/2)\mathbf{q}}\rangle. \tag{37c}$$

Here, $\mathbf{r}$ is again a vector within the d-dimensional homogeneous subspace. A lengthy but straightforward calculation allows us to derive the new set of kinetic equations in the Wigner picture; for the case of f^e the derivation can be found in Hess and Kuhn (1996). A characteristic feature is that these kinetic equations are nonlocal in space. By performing a Taylor expansion, we can formally transform the resulting equations into partial differential equations of infinite order according to

$$\frac{d}{dt}f^e_{\mathbf{k}}(\mathbf{r})=\frac{1}{i\hbar}\sum_{n,m=0}^{\infty}\frac{i^{n+m}}{2^{n+m}n!m!}\left(\frac{\partial}{\partial\mathbf{k}'}\cdot\frac{\partial}{\partial\mathbf{r}}\right)^n\left(\frac{\partial}{\partial\mathbf{r}'}\cdot\frac{\partial}{\partial\mathbf{k}}\right)^m\times\{[(-1)^n-(-1)^m]\mathcal{E}^e_{\mathbf{k}'}(\mathbf{r}')f^e_{\mathbf{k}}(\mathbf{r})+(-1)^n\mathcal{U}_{\mathbf{k}'}(\mathbf{r}')p^*_{\mathbf{k}}(\mathbf{r})-(-1)^m\mathcal{U}^*_{\mathbf{k}'}(\mathbf{r}')p_{\mathbf{k}}(\mathbf{r})\}|^{\mathbf{k}'=\mathbf{k}}_{\mathbf{r}'=\mathbf{r}}, \tag{38a}$$

$$\frac{d}{dt}p_{\mathbf{k}}(\mathbf{r})=\frac{1}{i\hbar}\mathcal{U}_{\mathbf{k}}(\mathbf{r})+\frac{1}{i\hbar}\times\sum_{n,m=0}^{\infty}\frac{i^{n+m}}{2^{n+m}n!m!}\left(\frac{\partial}{\partial\mathbf{k}'}\cdot\frac{\partial}{\partial\mathbf{r}}\right)^n\left(\frac{\partial}{\partial\mathbf{r}'}\cdot\frac{\partial}{\partial\mathbf{k}}\right)^m\times\{[(-1)^n\mathcal{E}^e_{\mathbf{k}'}(\mathbf{r}')+(-1)^m\mathcal{E}^h_{-\mathbf{k}'}(\mathbf{r}')]p_{\mathbf{k}}(\mathbf{r})-(-1)^n\mathcal{U}_{\mathbf{k}'}(\mathbf{r}')f^h_{-\mathbf{k}}(\mathbf{r})-(-1)^m\mathcal{U}_{\mathbf{k}'}(\mathbf{r}')f^e_{\mathbf{k}}(\mathbf{r})\}|^{\mathbf{k}'=\mathbf{k}}_{\mathbf{r}'=\mathbf{r}}, \tag{38b}$$

where the space-dependent energies and effective fields are

$$\mathcal{E}^{e,h}_{\mathbf{k}}(\mathbf{r})=\sum_{\mathbf{q}}e^{i\mathbf{q}\mathbf{r}}\mathcal{E}^{e,h}_{\mathbf{k}+(1/2)\mathbf{q},\mathbf{k}-(1/2)\mathbf{q}}=\epsilon^{e,h}_{\mathbf{k}}\pm e\mathbf{E}_{\parallel}(\mathbf{r},t)\cdot\mathbf{r}, \tag{39a}$$

$$\mathcal{U}_{\mathbf{k}}(\mathbf{r})=\sum_{\mathbf{q}}e^{i\mathbf{q}\mathbf{r}}\mathcal{U}_{\mathbf{k}+(1/2)\mathbf{q},\mathbf{k}-(1/2)\mathbf{q}}=-\mathbf{M}\cdot\mathbf{E}(\mathbf{r},t). \tag{39b}$$

In each order (n,m) there are spatial derivatives of the order $n+m$. If the length scales of the inhomogeneities are sufficiently large, then it can be expected that with increasing order the contributions will be of decreasing importance. Let us briefly discuss the structure of the lowest-order contributions.

The zeroth order $(n=m=0)$ is given by

$$\frac{d}{dt}f^e_{\mathbf{k}}(\mathbf{r},t)=\frac{d}{dt}f^h_{-\mathbf{k}}(\mathbf{r},t)=g_{\mathbf{k}}(\mathbf{r},t), \tag{40a}$$

$$\frac{d}{dt}p_{\mathbf{k}}(\mathbf{r},t)=\frac{1}{i\hbar}[\mathcal{E}^{e}_{\mathbf{k}}(\mathbf{r},t)+\mathcal{E}^{h}_{-\mathbf{k}}(\mathbf{r},t)]p_{\mathbf{k}}(\mathbf{r},t)+\frac{1}{i\hbar}\mathcal{U}_{\mathbf{k}}(\mathbf{r},t)\times[1-f^{e}_{\mathbf{k}}(\mathbf{r},t)-f^{h}_{-\mathbf{k}}(\mathbf{r},t)], \tag{40b}$$

where the generation rate is

$$g_{\mathbf{k}}(\mathbf{r},t)=\frac{1}{i\hbar}[\mathcal{U}_{\mathbf{k}}(\mathbf{r},t)p^{*}_{\mathbf{k}}(\mathbf{r},t)-\mathcal{U}^{*}_{\mathbf{k}}(\mathbf{r},t)p_{\mathbf{k}}(\mathbf{r},t)]. \tag{41}$$

Here, the spatial coordinate enters only as a parameter; locally, the dynamics coincide with those of the homogeneous case and there are no transport effects. As we shall see in Sec. III, in many cases this lowest-order picture is sufficient to describe pump-probe as well as four-wave-mixing experiments.

The first-order contributions ($n=1$, $m=0$ and $n=0$, $m=1$) are given by

$$\frac{d}{dt}f^{e(1)}_{\mathbf{k}}(\mathbf{r})=\frac{1}{\hbar}\left\{-\frac{\partial\mathcal{E}^{e}_{\mathbf{k}}(\mathbf{r})}{\partial\mathbf{k}}\cdot\frac{\partial f^{e}_{\mathbf{k}}(\mathbf{r})}{\partial\mathbf{r}}+\frac{\partial\mathcal{E}^{e}_{\mathbf{k}}(\mathbf{r})}{\partial\mathbf{r}}\cdot\frac{\partial f^{e}_{\mathbf{k}}(\mathbf{r})}{\partial\mathbf{k}}-\frac{\partial\mathcal{U}_{\mathbf{k}}(\mathbf{r})}{\partial\mathbf{k}}\cdot\frac{\partial p^{*}_{\mathbf{k}}(\mathbf{r})}{\partial\mathbf{r}}+\frac{\partial\mathcal{U}_{\mathbf{k}}(\mathbf{r})}{\partial\mathbf{r}}\cdot\frac{\partial p^{*}_{\mathbf{k}}(\mathbf{r})}{\partial\mathbf{k}}-\frac{\partial\mathcal{U}^{*}_{\mathbf{k}}(\mathbf{r})}{\partial\mathbf{k}}\cdot\frac{\partial p_{\mathbf{k}}(\mathbf{r})}{\partial\mathbf{r}}+\frac{\partial\mathcal{U}^{*}_{\mathbf{k}}(\mathbf{r})}{\partial\mathbf{r}}\cdot\frac{\partial p_{\mathbf{k}}(\mathbf{r})}{\partial\mathbf{k}}\right\}. \tag{42}$$

The first two terms on the right-hand side (rhs) correspond to the Boltzmann drift terms in phase space. The other terms can be interpreted as a local generation rate due to the flow of polarization into or out of the phase-space element. Thus this first-order approximation level can be regarded as a two-band generalization of the conventional Boltzmann equation.

Higher-order terms then give rise to such typically quantum-mechanical features as tunneling.

D. Carrier-phonon interaction

Having considered the equations of motion derived from the single-particle Hamiltonian, we now come to the many-body contributions. Here, the equations of motion for the kinetic variables are no longer closed; instead they give rise to an infinite hierarchy of equations.

Let us start with the case of carrier-phonon interaction. The corresponding Hamiltonian introduced in Eq. (17) leads to the following contributions to the equations of motion:

$$\frac{d}{dt}f^{e}_{i_1i_2}|^{(cp)}=\frac{1}{i\hbar}\sum_{i_3,\mathbf{q}}[g^{i_2i_3}_{\mathbf{q}}s^{e,i_1i_3}_{\mathbf{q}}+g^{*i_3i_2}_{\mathbf{q}}s^{e,i_3i_1*}_{\mathbf{q}}-g^{i_3i_1}_{\mathbf{q}}s^{e,i_3i_2}_{\mathbf{q}}-g^{*i_1i_3}_{\mathbf{q}}s^{e,i_2i_3^{*}}_{\mathbf{q}}], \tag{43a}$$

$$\frac{d}{dt}p_{j_1i_1}|^{(cp)}=\frac{1}{i\hbar}\sum_{i_2,\mathbf{q}}[g^{i_1i_2}_{\mathbf{q}}t^{(+),j_1i_2}_{\mathbf{q}}+g^{*i_2i_1}_{\mathbf{q}}t^{(-),j_1i_2}_{\mathbf{q}}]-\frac{1}{i\hbar}\sum_{j_2,\mathbf{q}}[g^{j_1j_2}_{\mathbf{q}}t^{(+),j_2i_1}_{\mathbf{q}}+g^{*j_2j_1}_{\mathbf{q}}t^{(-),j_2i_1}_{\mathbf{q}}]. \tag{43b}$$

The equation of motion for the phonon distribution function has the same structure:

$$\frac{d}{dt}n_{\mathbf{q}}|^{(cp)}=-\frac{1}{i\hbar}\sum_{i_1,i_2}[g^{i_1i_2}_{\mathbf{q}}s^{e,i_1i_2}_{\mathbf{q}}-g^{*i_1i_2}_{\mathbf{q}}s^{e,i_1i_2*}_{\mathbf{q}}]+\frac{1}{i\hbar}\sum_{j_1,j_2}[g^{j_1j_2}_{\mathbf{q}}s^{h,j_1j_2}_{\mathbf{q}}-g^{*j_1j_2}_{\mathbf{q}}s^{h,j_1j_2*}_{\mathbf{q}}]. \tag{44}$$

Here, new variables, the so-called phonon-assisted density matrices, have been introduced (Zimmermann, 1990):

$$s^{e,i_1i_2}_{\mathbf{q}}=\langle c^{\dagger}_{i_1}b_{\mathbf{q}}c_{i_2}\rangle,\quad s^{h,j_1j_2}_{\mathbf{q}}=\langle d^{\dagger}_{j_1}b_{\mathbf{q}}d_{j_2}\rangle, \tag{45a}$$

$$t^{(+),j_1i_1}_{\mathbf{q}}=\langle d_{j_1}b_{\mathbf{q}}c_{i_1}\rangle,\quad t^{(-),j_1i_1}_{\mathbf{q}}=\langle d_{j_1}b^{\dagger}_{\mathbf{q}}c_{i_1}\rangle. \tag{45b}$$

These variables describe correlations between carriers and phonons. The quantity $s^{e,i_1i_2}_{\mathbf{q}}$, for example, relates an initial state with one electron in the electronic one-particle state i_2 and a phonon with wave vector $\mathbf{q}$ to a final state with only an electron in i_1. Thus its temporal evolution contains information on an electronic transition from i_2 to i_1 by phonon absorption as well as the reverse process by phonon emission. The equations of motion for the above phonon-assisted density matrices involve expectation values of four operators, and therefore an infinite hierarchy of equations shows up. To obtain a solution, this hierarchy has to be truncated at some level. As has been discussed in Sec. II.B, truncation schemes based on different ideas have been proposed in the literature. Here we shall use a correlation expansion based on the assumption that correlations involving an increasing number of carriers or phonons are of decreasing importance.

1. First order: Coherent phonons

The lowest order in the hierarchy is obtained by neglecting all correlations between carriers and phonons. This corresponds to a factorization according to

$$s^{e,i_1i_2}_{\mathbf{q}}\approx\langle c^{\dagger}_{i_1}c_{i_2}\rangle\langle b_{\mathbf{q}}\rangle=f^{e}_{i_1i_2}B_{\mathbf{q}}, \tag{46}$$

where we have introduced the coherent-phonon amplitude $B_{\mathbf{q}}=\langle b_{\mathbf{q}}\rangle$. It is easy to see that a nonvanishing coherent-phonon amplitude is equivalent to a nonvanishing Fourier component of the lattice polarization and thus to a displacement of the ions (Scholz, Pfeifer, and Kurz, 1993; Kuznetsov and Stanton, 1994). This is in contrast to the usual phonon occupation number, which is determined by the ionic mean-square displacement only.

On this approximation level the contributions of carrier-phonon interaction to the equations of motion of the single-particle density matrices can be expressed in terms of nondiagonal energy renormalizations according to

$$\frac{d}{dt}f^{e}_{i_1i_2}|^{(cp,1)}=\frac{1}{i\hbar}\sum_{i_3}[\mathcal{E}^{e(cp,1)}_{i_2i_3}f^{e}_{i_1i_3}-\mathcal{E}^{e(cp,1)}_{i_3i_1}f^{e}_{i_3i_2}], \tag{47a}$$

$$\frac{d}{dt}p_{j_1i_1}|^{(cp,1)}=\frac{1}{i\hbar}\left[\sum_{j_2}\mathcal{E}^{h(cp,1)}_{j_1j_2}p_{j_2i_1}+\sum_{i_2}\mathcal{E}^{e(cp,1)}_{i_1i_2}p_{j_1i_2}\right], \tag{47b}$$

where the self-energy matrices are

$$\mathcal{E}^{e(cp,1)}_{i_1i_2}=\sum_{\mathbf{q}}\left[g^{i_1i_2}_{\mathbf{q}}B_{\mathbf{q}}+g^{i_2i_1}_{\mathbf{q}}{}^{*}B^{*}_{\mathbf{q}}\right], \tag{48a}$$

$$\mathcal{E}^{h(cp,1)}_{j_1j_2}=-\sum_{\mathbf{q}}\left[g^{j_1j_2}_{\mathbf{q}}B_{\mathbf{q}}+g^{j_2j_1}_{\mathbf{q}}{}^{*}B^{*}_{\mathbf{q}}\right], \tag{48b}$$

while the equation of motion for the phonon amplitude is given by

$$\frac{d}{dt}B_{\mathbf{q}}=-i\omega_{\mathbf{q}}B_{\mathbf{q}}+\frac{1}{i\hbar}\left[\sum_{i_1,i_2}g^{*i_2i_1}_{\mathbf{q}}f^{e}_{i_1i_2}-\sum_{j_1,j_2}g^{*j_2j_1}_{\mathbf{q}}f^{h}_{j_1j_2}\right]. \tag{49}$$

2. Second order: Scattering and dephasing

The next step in the hierarchy is obtained by taking into account deviations of the phonon-assisted density matrices from the lowest-order factorization previously introduced, e.g.,

$$\delta s^{e,i_1i_2}_{\mathbf{q}}=s^{e,i_1i_2}_{\mathbf{q}}-f^{e}_{i_1i_2}B_{\mathbf{q}}. \tag{50}$$

In order to determine the equation of motion for this phonon-assisted correlation, we first derive the equation of motion for the corresponding phonon-assisted density matrix. Assuming a time-independent basis and neglecting the carrier-field part of the Hamiltonian, we obtain

$$\begin{aligned}\frac{d}{dt}s^{e,i_1i_2}_{\mathbf{q}}=&-\frac{1}{i\hbar}(\epsilon^{e}_{i_1}-\epsilon^{e}_{i_2}-\hbar\omega_{\mathbf{q}})s^{e,i_1i_2}_{\mathbf{q}}\\&-\frac{1}{i\hbar}\sum_{i_3,\mathbf{q}'}\left[g^{i_3i_1}_{\mathbf{q}'}\langle c^{\dagger}_{i_3}c_{i_2}b_{\mathbf{q}'}b_{\mathbf{q}}\rangle\right.\\&+g^{i_1i_3}_{\mathbf{q}'}{}^{*}\langle c^{\dagger}_{i_3}c_{i_2}b^{\dagger}_{\mathbf{q}'}b_{\mathbf{q}}\rangle-g^{i_2i_3}_{\mathbf{q}'}\langle c^{\dagger}_{i_1}c_{i_3}b_{\mathbf{q}}b_{\mathbf{q}'}\rangle\\&\left.-g^{i_3i_2}_{\mathbf{q}'}{}^{*}\langle c^{\dagger}_{i_1}c_{i_3}b_{\mathbf{q}}b^{\dagger}_{\mathbf{q}'}\rangle\right]\\&+\frac{1}{i\hbar}\sum_{i_3,i_4}g^{i_3i_4}_{\mathbf{q}}{}^{*}\langle c^{\dagger}_{i_1}c^{\dagger}_{i_4}c_{i_3}c_{i_2}\rangle\\&-\frac{1}{i\hbar}\sum_{j_3,j_4}g^{j_3j_4}_{\mathbf{q}}{}^{*}\langle c^{\dagger}_{i_1}d^{\dagger}_{j_4}d_{j_3}c_{i_2}\rangle.\end{aligned} \tag{51}$$

Thus the equation of motion involves expectation values of four operators: electron-phonon and electron-electron two-particle density matrices. In the spirit of the correlation expansion previously discussed, these quantities have to be decomposed into all possible lower-order factorizations, the remaining part describing two-particle correlations. Such a decomposition is given by

$$\begin{aligned}\langle c^{\dagger}_{i_3}c_{i_2}b^{\dagger}_{\mathbf{q}'}b_{\mathbf{q}}\rangle=&f^{e}_{i_3i_2}B^{*}_{\mathbf{q}'}B_{\mathbf{q}}+\delta s^{e,i_2i_3}_{\mathbf{q}'}{}^{*}B_{\mathbf{q}}+\delta s^{e,i_3i_2}_{\mathbf{q}}B^{*}_{\mathbf{q}'}\\&+f^{e}_{i_3i_2}n_{\mathbf{q}}\delta_{\mathbf{q},\mathbf{q}'}+\delta\langle c^{\dagger}_{i_3}c_{i_2}b^{\dagger}_{\mathbf{q}'}b_{\mathbf{q}}\rangle.\end{aligned} \tag{52}$$

Here, as in the following, $n_{\mathbf{q}}$ only refers to the distribution of incoherent phonons defined as $n_{\mathbf{q}}=\langle b^{t}_{\mathbf{q}}b_{\mathbf{q}}\rangle-|B_{\mathbf{q}}|^2$ and we have assumed that this distribution is space independent, i.e., diagonal in $\mathbf{q}$. A generalization to the nondiagonal case is straightforward. The equation of motion for the phonon-assisted correlation is obtained by inserting these decompositions into Eq. (51) and by subtracting the equations of motion for the second term on the rhs of Eq. (50). Then, the first and second terms on the rhs of Eq. (52) cancel, the third leads to a renormalization of the single-particle energies by the coherent-phonon contributions, the fourth leads to the scattering part, and the last describes the influence of two-particle correlations. Again, the hierarchy can be truncated by neglecting these higher-order correlations, which results in the following equation of motion:

$$\begin{aligned}\frac{d}{dt}\delta s^{e,i_1i_2}_{\mathbf{q}}=&-\frac{1}{i\hbar}\sum_{i_3,i_4}(\mathcal{E}^{e}_{i_3i_1}\delta_{i_2i_4}\\&-\mathcal{E}^{e}_{i_2i_4}\delta_{i_1i_3}-\hbar\omega_{\mathbf{q}}\delta_{i_1i_3}\delta_{i_2i_4})\delta s^{e,i_3i_4}_{\mathbf{q}}\\&+\frac{1}{i\hbar}\sum_{i_3,i_4}g^{i_4i_3}_{\mathbf{q}}{}^{*}[(n_{\mathbf{q}}+1)f^{e}_{i_1i_4}(\delta_{i_3i_2}-f^{e}_{i_3i_2})\\&-n_{\mathbf{q}}f^{e}_{i_3i_2}(\delta_{i_1i_4}-f^{e}_{i_1i_4})]\\&-\frac{1}{i\hbar}\sum_{j_1,j_2}g^{j_2j_1}_{\mathbf{q}}{}^{*}p^{*}_{j_1i_1}p_{j_2i_2},\end{aligned} \tag{53}$$

where the renormalized energies are given by

$$\mathcal{E}^{e}_{i_1i_2}=\epsilon^{e}_{i_1}\delta_{i_1i_2}+\mathcal{E}^{e(cp,1)}_{i_1i_2}. \tag{54}$$

If the time dependence is calculated with the full single-particle Hamiltonian, the energy $\epsilon^{e}_{i_1}$ is replaced by the full single-particle energy matrix, as given in Eq. (24). Furthermore, the effective field leads to a coupling of different types of phonon-assisted correlations (Schilp, Kuhn, and Mahler, 1994a). Such equations for the four types of phonon-assisted correlations, together with the equations for the single-particle density matrices, constitute the basis for the analysis of electron-phonon quantum kinetics. Results based on this theoretical approach will be reviewed and discussed in Sec. III.G.

Again, the semiclassical limit is obtained by adiabatic elimination of the phonon-assisted correlations. This can be performed following the same procedure described in Sec. II.C for the carrier-light interaction. We shall again neglect all off-diagonal energy renormalizations. This is also in the spirit of the Boltzmann theory, in which scattering processes occur between free-carrier states. We stress that when performing the Markov approximation, one must properly take into account the fast oscillations of interband and intraband polarizations induced by $\mathbf{H}_0$. Within this approximation scheme, the phonon-assisted correlation is given by

$$\delta s_{\mathbf{q}}^{e,i_1i_2} = -i\pi \sum_{i_3,i_4} \mathcal{D}(-\epsilon_{i_4}^e + \epsilon_{i_3}^e + \hbar\omega_{\mathbf{q}}) g_{\mathbf{q}}^{i_4i_3 *} \times [(n_{\mathbf{q}}+1) f_{i_1i_4}^e (\delta_{i_3i_2} - f_{i_3i_2}^e) - n_{\mathbf{q}} f_{i_3i_2}^e (\delta_{i_1i_4} - f_{i_1i_4}^e)] + i\pi \times \sum_{j_1,j_2} \mathcal{D}(\epsilon_{j_1}^h - \epsilon_{j_2}^h + \hbar\omega_{\mathbf{q}}) g_{\mathbf{q}}^{j_2j_1 *} p_{j_1i_1}^* p_{j_2i_2}. \quad (55)$$

If this phonon-assisted correlation is now inserted into the equation of motion for the single-particle density matrix, it becomes evident that the principal-value part of $\mathcal{D}$ is associated with energy renormalizations—describing the polaron corrections to the band structure—while the δ-function part is associated with irreversible scattering and dephasing processes. Typically, the dominant polaronic features are a rigid shift of the bands and a slight modification of the effective mass. In this case, these effects can be included in $\mathbf{H}_0$, since they are always present in any experiment determining the band structure. Therefore the principal-value contributions will be neglected hereafter. However, this derivation shows that in a quantum-kinetic treatment, the polaron shift is always included. This must be taken into account when comparing quantum-kinetic to semiclassical results.

The second-order carrier-phonon contributions in the Markov limit, for example, for the electron density matrix, can be written in the general form

$$\frac{d}{dt} f_{i_1i_2}^e|^{(cp,2)} = \sum_{i_3} [-\Gamma_{i_2i_3}^{e,out(cp,2)} f_{i_1i_3}^e - \Gamma_{i_1i_3}^{e,out(cp,2)*} f_{i_2i_3}^{e*} + \Gamma_{i_2i_3}^{e,in(cp,2)} (\delta_{i_1i_3} - f_{i_1i_3}^e) + \Gamma_{i_1i_3}^{e,in(cp,2)*} (\delta_{i_2i_3} - f_{i_2i_3}^{e*})] + \frac{1}{i\hbar} \sum_{j_1} [\mathcal{U}_{i_2j_1}^{e(cp,2)} p_{j_1i_1}^* - \mathcal{U}_{i_1j_1}^{e(cp,2)*} p_{j_1i_2}]. \quad (56)$$

The explicit form of the various matrices $\Gamma^{(cp,2)}$ and $\mathcal{U}^{(cp,2)}$ due to the second-order carrier-phonon interaction appearing on the rhs of Eq. (56) can be found in Kuhn (1998). In the next section the results for the special case of a homogeneous system in momentum representation will be given explicitly. In the fully semiclassical limit, where all off-diagonal elements of the intraband density matrices and all interband polarizations are neglected, the well-known Boltzmann-like scattering contributions due to phonon emission and absorption are recovered.

3. Homogeneous system

As in the case of single-particle dynamics, let us discuss the special case of a homogeneous system that is either homogeneously or inhomogeneously excited. The first-order contributions in the momentum representation are given by the self-energy matrices

$$\mathcal{E}_{\mathbf{k}\mathbf{k}'}^{e,h(cp,2)} = g_{\mathbf{k}-\mathbf{k}'}^{e,h} B_{\mathbf{k}-\mathbf{k}'} + g_{\mathbf{k}'-\mathbf{k}}^{e,h*} B_{\mathbf{k}'-\mathbf{k}}^*, \quad (57)$$

and the generation of coherent phonons is described by

$$\frac{d}{dt} B_{\mathbf{q}} = -i\omega_{\mathbf{q}} B_{\mathbf{q}} + \frac{1}{i\hbar} \sum_{\mathbf{k}} [g_{\mathbf{q}}^{e*} f_{\mathbf{k},\mathbf{k}+\mathbf{q}}^e - g_{\mathbf{q}}^{h*} f_{\mathbf{k},\mathbf{k}+\mathbf{q}}^h]. \quad (58)$$

When the system is homogeneously excited, only coherent-phonon amplitudes with $\mathbf{q}=0$ can be generated. According to Eq. (58), however, this requires different coupling matrix elements $g_{\mathbf{q}}$ for electrons and holes. Thus no coherent phonons are generated for the case of Fröhlich interaction, in which (Madelung, 1978)

$$g_{\mathbf{q}} = g_{\mathbf{q}}^e = g_{\mathbf{q}}^h = i\left[\frac{2\pi e^2 \hbar\omega_{LO}}{\mathcal{V}} \left(\frac{1}{\varepsilon_\infty} - \frac{1}{\varepsilon_s}\right)\right]^{1/2} \frac{1}{q}, \quad (59)$$

where ε_∞ is the optical dielectric constant, ε_s is the static dielectric constant, and ω_{LO} is the LO phonon frequency. This is usually the most important type of carrier-phonon interaction for ultrafast dynamics in polar semiconductors. The carrier-phonon self-energy in Wigner representation depends on $\mathbf{r}$ only. In the case of Fröhlich interaction, it can be written as $\mathcal{E}^{e,h} = \pm e\Phi(\mathbf{r},t)$, where the electrostatic potential is determined by the Poisson equation $\Delta\Phi = 4\pi\nabla\cdot\mathbf{P}(\mathbf{r},t)$, and the lattice polarization is given by

$$\mathbf{P}_{lat} = \left[\frac{\hbar\omega_{LO}}{8\pi\mathcal{V}} \left(\frac{1}{\varepsilon_\infty} - \frac{1}{\varepsilon_s}\right)\right]^{1/2} \sum_{\mathbf{q}} \frac{\mathbf{q}}{q} e^{i\mathbf{q}\mathbf{r}} (B_{\mathbf{q}} - B_{-\mathbf{q}}^*). \quad (60)$$

It is interesting to analyze the long-wavelength limit of Eq. (58): The matrix element diverges as q^{-1}. Under the condition

$$\sum_{\mathbf{k}} f_{\mathbf{k}\mathbf{k}}^e = \sum_{\mathbf{k}} f_{\mathbf{k}\mathbf{k}}^h, \quad (61)$$

i.e., the condition of charge neutrality, this divergence cancels in Eq. (49), leading to a finite value of B_0 which is equivalent to a phononic dipole moment of the structure. According to classical electrodynamics, such a dipole moment, when oscillating, acts as a source of electromagnetic radiation typically in the terahertz range.

The second-order contributions, in the case of homogeneous excitation, can be written in a slightly different way, which can be more easily interpreted on physical grounds. By introducing proper transition matrices $W^{e,h(cp)}$ and $\mathcal{W}^{e,h(cp)}$ as well as effective fields $\mathcal{U}^{e,h(cp)}$, we obtain

$$\frac{d}{dt} f_{\mathbf{k}}^e|^{(cp,2)} = -\sum_{\mathbf{q}} [W_{\mathbf{k}-\mathbf{q},\mathbf{k}}^{e(cp)} f_{\mathbf{k}}^e (1 - f_{\mathbf{k}-\mathbf{q}}^e) - W_{\mathbf{k},\mathbf{k}-\mathbf{q}}^{e(cp)} f_{\mathbf{k}-\mathbf{q}}^e (1 - f_{\mathbf{k}}^e)] + \frac{1}{i\hbar} [\mathcal{U}_{\mathbf{k}}^{e(cp,2)} p_{\mathbf{k}}^* - \mathcal{U}_{\mathbf{k}}^{e(cp,2)*} p_{\mathbf{k}}], \quad (62a)$$

$$\frac{d}{dt}p_{\mathbf{k}}|^{(cp,2)} = -\sum_{\mathbf{q}}\left[(\mathcal{W}^{e(cp)}_{\mathbf{k}-\mathbf{q},\mathbf{k}}+\mathcal{W}^{h(cp)}_{-(\mathbf{k}-\mathbf{q}),-\mathbf{k}})p_{\mathbf{k}} - \left(\frac{g^h_{\mathbf{q}}}{g^e_{\mathbf{q}}}\mathcal{W}^{e(cp)}_{\mathbf{k},\mathbf{k}-\mathbf{q}}+\frac{g^e_{\mathbf{q}}}{g^h_{\mathbf{q}}}\mathcal{W}^{h(cp)}_{-\mathbf{k},-(\mathbf{k}-\mathbf{q})}\right)p_{\mathbf{k}-\mathbf{q}}\right], \tag{62b}$$

where the transition matrices are

$$W^{e,h(cp)}_{\mathbf{k}-\mathbf{q},\mathbf{k}} = \frac{2\pi}{\hbar}\sum_{\pm}|g^{e,h}_{\mathbf{q}}|^2\delta(\epsilon^{e,h}_{\mathbf{k}-\mathbf{q}}-\epsilon^{e,h}_{\mathbf{k}}\pm\hbar\omega_{\mathbf{q}}) \times\left(n_{\mathbf{q}}+\frac{1}{2}\pm\frac{1}{2}\right), \tag{63}$$

$$\mathcal{W}^{e,h(cp)}_{\mathbf{k}-\mathbf{q},\mathbf{k}} = \frac{\pi}{\hbar}\sum_{\pm}|g^{e,h}_{\mathbf{q}}|^2\mathcal{D}(\epsilon^{e,h}_{\mathbf{k}-\mathbf{q}}-\epsilon^{e,h}_{\mathbf{k}}\pm\hbar\omega_{\mathbf{q}}) \times\left[\left(n_{\mathbf{q}}+\frac{1}{2}\mp\frac{1}{2}\right)f^{e,h}_{\mathbf{k}-\mathbf{q}} + \left(n_{\mathbf{q}}+\frac{1}{2}\pm\frac{1}{2}\right)(1-f^{e,h}_{\mathbf{k}-\mathbf{q}})\right], \tag{64}$$

and the effective field is

$$\mathcal{U}^{e,h(cp)}_{\mathbf{k}} = i\pi\sum_{\mathbf{q}}g^e_{\mathbf{q}}g^{h*}_{\mathbf{q}}\sum_{\pm}(\pm p_{\mathbf{k}-\mathbf{q}})\mathcal{D}(\epsilon^{h,e}_{\mathbf{k}}-\epsilon^{h,e}_{\mathbf{k}-\mathbf{q}}\pm\hbar\omega_{\mathbf{q}}). \tag{65}$$

Here, we have assumed $g^e_{\mathbf{q}}/g^h_{\mathbf{q}} = g^{e*}_{\mathbf{q}}/g^{h*}_{\mathbf{q}}$, which holds both for deformation-potential and polar-coupling mechanisms. In the equations of motion for the distribution functions, we thus recover the usual Boltzmann scattering term consisting of in- and out-scattering contributions due to phonon emission and absorption. If there is an interband polarization in the system, there is an additional contribution, which is quadratic in $p_{\mathbf{k}}$. The prefactor shows that this term is due to the simultaneous interaction of electrons and holes with the same phonon mode. This type of process is sometimes called *polarization scattering* (Kuznetsov, 1991). On the other hand, according to its structure, it can also be regarded as a coherent generation-recombination process, since it has the same structure as the generation rate in Eq. (26). However, (i) the effective fields $\mathcal{U}^{e,h(cp)}_{\mathbf{k}}$ are different for electrons and holes, and (ii) it conserves the number of electrons and holes.

In the equation for polarization, we also find two different types of contributions. We have a loss term proportional to p_k, due to processes involving either electron-phonon or hole-phonon interaction. The real part of the corresponding matrices is related to the Boltzmann scattering matrices by

$$\mathrm{Re}\,\mathcal{W}^{e,h(cp)}_{\mathbf{k}-\mathbf{q},\mathbf{k}} = \frac{1}{2}[W^{e,h(cp)}_{\mathbf{k}-\mathbf{q},\mathbf{k}}(1-f^{e,h}_{\mathbf{k}-\mathbf{q}})+W^{e,h(cp)}_{\mathbf{k},\mathbf{k}-\mathbf{q}}f^{e,h}_{\mathbf{k}-\mathbf{q}}]. \tag{66}$$

Thus a scattering process of a carrier both into and out of the state $\mathbf{k}$ leads to a loss of interband coherence. However, there is an additional contribution that may reduce this loss of coherence, which is again related to the simultaneous interaction of electrons and holes with the same phonon. If, as in the case of Fröhlich interaction, both matrix elements coincide, we obtain

$$\frac{d}{dt}\sum_{\mathbf{k}}p_{\mathbf{k}}|^{(cp,2)} = 0. \tag{67}$$

In this case dephasing is the net result of two opposite contributions, whose relative magnitude is dictated by the $\mathbf{k}$ dependence of both the single-particle energies and the scattering matrix elements. In particular, it depends strongly on the energy transfer in the scattering process.

When the system is inhomogeneously excited and a Wigner representation is chosen, a gradient expansion can also be performed for the second-order contributions. Here, however, only the zeroth order is usually taken, which means that all variables in Eq. (62) depend parametrically on the space coordinate $\mathbf{r}$. This is in the spirit of Boltzmann's *Stoßzahlansatz*, in which scattering processes are treated as pointlike in space and time. As for the Markov approximation, in which energy-time uncertainty is neglected, here the position-momentum uncertainty is neglected, and a scattering process between well-defined momentum states occurs at some well-defined position.

4. Third order: Collisional broadening

The correlation expansion can be continued by taking into account two-particle correlations. In this section we briefly discuss the structure of these contributions. However, to simplify the notation we shall limit ourselves to the case of a homogeneous single-band system. Its generalization to the multiband case with arbitrary basis functions is straightforward.

The equations of motion for two-particle correlations involve expectation values of five operators, the two-particle phonon-assisted density matrices. Like the phonon-assisted density matrices, these expectation values contain information not only on two-phonon emission or absorption processes, but also on virtual processes related to the emission and reabsorption of phonons. The hierarchy is truncated by a factorization into single-particle and phonon-assisted density matrices. The resulting equation of motion, for example, for the correlation appearing in Eq. (52), is of the form

$$\begin{aligned}\frac{d}{dt}&\delta\langle c^\dagger_{\mathbf{k}+\mathbf{q}-\mathbf{q}'}c_{\mathbf{k}}b^\dagger_{\mathbf{q}'}b_{\mathbf{q}}\rangle \\ &= -\frac{1}{i\hbar}(\epsilon^e_{\mathbf{k}+\mathbf{q}-\mathbf{q}'}-\epsilon^e_{\mathbf{k}})\delta\langle c^\dagger_{\mathbf{k}+\mathbf{q}-\mathbf{q}'}c_{\mathbf{k}}b^\dagger_{\mathbf{q}'}b_{\mathbf{q}}\rangle \\ &\quad -\frac{1}{i\hbar}g_{\mathbf{q}'}(1-f^e_{\mathbf{k}+\mathbf{q}-\mathbf{q}'}+n_{\mathbf{q}'})\delta s^e_{\mathbf{k}+\mathbf{q},\mathbf{q},\mathbf{k}} \\ &\quad +\frac{1}{i\hbar}g_{\mathbf{q}'}(f^e_{\mathbf{k}}+n_{\mathbf{q}})\delta s^e_{\mathbf{k}+\mathbf{q}-\mathbf{q}',\mathbf{q},\mathbf{k}-\mathbf{q}'} \\ &\quad -\frac{1}{i\hbar}g^*_{\mathbf{q}}(1-f^e_{\mathbf{k}}+n_{\mathbf{q}})\delta s^{e*}_{\mathbf{k}+\mathbf{q},\mathbf{q}',\mathbf{k}+\mathbf{q}-\mathbf{q}'} \\ &\quad +\frac{1}{i\hbar}g^*_{\mathbf{q}}(f^e_{\mathbf{k}+\mathbf{q}-\mathbf{q}'}+n_{\mathbf{q}'})\delta s^{e*}_{\mathbf{k},\mathbf{q}',\mathbf{k}-\mathbf{q}'}.\end{aligned} \tag{68}$$

For a further simplification of this contribution, we keep in mind that Eq. (51) involves a summation over $\mathbf{q}'$. Since the phonon-assisted correlation is a complex quantity, in a first approximation we can assume that all contributions involving a summation of this quantity are small due to random phases at different momenta. This allows us to neglect the last three terms in Eq. (68), which can now be formally solved according to

$$\delta\langle c^{\dagger}_{\mathbf{k}+\mathbf{q}-\mathbf{q}'}c_{\mathbf{k}}b^{\dagger}_{\mathbf{q}'}b_{\mathbf{q}}\rangle = -\frac{1}{i\hbar}g_{\mathbf{q}'}\int_0^{\infty}d\tau e^{i(\epsilon^e_{\mathbf{k}+\mathbf{q}-\mathbf{q}'}-\epsilon^e_{\mathbf{k}})\tau/\hbar} \times[1-f^e_{\mathbf{k}+\mathbf{q}-\mathbf{q}'}(t-\tau)+n_{\mathbf{q}'}(t-\tau)]\delta s^e_{\mathbf{k}+\mathbf{q},\mathbf{q},\mathbf{k}}(t-\tau). \tag{69}$$

After inserting this result in Eq. (51), we obtain a closed equation of motion for the phonon-assisted density matrix, which, however, contains a memory term. This can be eliminated by again performing a Markov approximation. As a result, the third-order contributions give rise to second-order self-energy corrections in the equations of motion for δs according to

$$\frac{d}{dt}\delta s^e_{\mathbf{k}+\mathbf{q},\mathbf{q},\mathbf{k}} = -\frac{1}{i\hbar}(\mathcal{E}^{e(cp,2)}_{\mathbf{k}+\mathbf{q}}-\mathcal{E}^{e(cp,2)*}_{\mathbf{k}})\delta s^e_{\mathbf{k}+\mathbf{q},\mathbf{q},\mathbf{k}}, \tag{70}$$

where the complex second-order carrier-phonon self-energy is

$$\mathcal{E}^{e(cp,2)}_{\mathbf{k}} = -i\pi\sum_{\mathbf{q}',\pm}|g_{\mathbf{q}'}|^2\mathcal{D}(\epsilon^e_{\mathbf{k}}-\epsilon^e_{\mathbf{k}+\mathbf{q}'}\pm\hbar\omega_{\mathbf{q}}) \times[(n_{\mathbf{q}'}+\tfrac{1}{2}\pm\tfrac{1}{2})f^e_{\mathbf{k}+\mathbf{q}'}(n_{\mathbf{q}'}+\tfrac{1}{2}\mp\tfrac{1}{2})(1-f^e_{\mathbf{k}+\mathbf{q}'})]. \tag{71}$$

Here, the real part of the self-energy describes the fact that the scattering processes occur between renormalized polaronic states, while the imaginary part describes a collisional broadening. In the Green's-function approach this collisional broadening appears in the retarded Green's function if the two-time functions are reduced to one-time functions by means of the generalized Kadanoff-Baym ansatz (Lipavský *et al.*, 1986) and if a Markov approximation for the retarded Green's function is performed (Haug, 1992; Tran Thoai and Haug, 1993). However, it turns out that this approximation leads to a strong overestimation of the role played by the two-particle correlations. In particular, the imaginary part leads to a violation of energy conservation (Schilp *et al.*, 1995) as well as to an overestimation of the broadening. It has been shown that a non-Markovian decay of the retarded Green's function—corresponding to the non-Markovian dynamics of the phonon-assisted correlation [Eq. (69)]—improves the result (Haug and Bányai, 1996). However, as has been shown for carrier-carrier scattering, it does not completely restore the conservation of the total energy (Bonitz, Semkat, and Haug, 1999). In contrast, if all third-order terms are taken into account, it can be shown analytically that the total energy is conserved.

E. Carrier-carrier interaction

Many optical properties of semiconductors are strongly influenced by Coulomb interaction. Therefore let us now discuss the contributions to the system dynamics due to the carrier-carrier interaction Hamiltonian $\mathbf{H}_{cc}$ [Eq. (16)].

The corresponding term for the electron density matrix, is

$$\frac{d}{dt}f^e_{i_1i_2}|^{(cc)} = \frac{1}{i\hbar}\sum_{i_3,i_4,i_5}[V^{ee}_{i_2i_3i_4i_5}K_{i_1,i_3,i_4,i_5} - V^{ee}_{i_5i_4i_3i_1}K_{i_5,i_4,i_3,i_2}] - \frac{1}{i\hbar}\sum_{i_3,j_1,j_2}[V^{eh}_{i_2j_1j_2i_3}N_{i_1,j_1,j_2,i_3} - V^{eh}_{i_3j_2j_1i_1}N_{i_3,i_2,j_1,i_2}]. \tag{72}$$

It involves two-particle density matrices like

$$K_{i_1,i_2,i_3,i_4} = \langle c^{\dagger}_{i_1}c^{\dagger}_{i_2}c_{i_3}c_{i_4}\rangle,$$

$$N_{i_1,j_1,j_2,i_2} = \langle c^{\dagger}_{i_1}d^{\dagger}_{j_1}d_{j_2}c_{i_2}\rangle. \tag{73}$$

Functions involving other combinations of four fermion operators appear in the equations for the hole density matrix and the interband polarization. The variable K_{i_1,i_2,i_3,i_4}, for example, is related to a transition of two electrons from the initial states i_3 and i_4 to the final states i_2 and i_1, i.e., an electron-electron scattering process, but it also contains information on the joint occupation probabilities of two states, e.g., $i_1=i_4$ and $i_2=i_3$. Again, Eq. (72) constitutes the starting point of an infinite hierarchy of equations of motion for density matrices with an increasing number of carriers. As anticipated, this is the quantum-mechanical analog of the classical BBGKY hierarchy, in which the equation of motion for an N-particle distribution function involves the $(N+1)$-particle distribution functions (Bogoliubov, 1967; Carruthers and Zachariasen, 1983).

1. First order: Excitons and renormalization

The lowest-order contribution due to carrier-carrier interaction is obtained by factorizing the two-particle density matrices into single-particle ones,

$$K_{i_1,i_2,i_3,i_4} = f^e_{i_1i_4}f^e_{i_2i_3} - f^e_{i_1i_3}f^e_{i_2i_4}. \tag{74}$$

This corresponds to the Hartree-Fock or mean-field level, in which all correlations between the carriers are neglected. The corresponding equations of motion are given by

$$\frac{d}{dt}f^e_{i_1i_2}\Big|^{(cc,1)}=\frac{1}{i\hbar}\sum_{i_3}\left[\mathcal{E}^{e(cc,1)}_{i_2i_3}f^e_{i_1i_3}-\mathcal{E}^{e(cc,1)}_{i_3i_1}f^e_{i_3i_2}\right]+\frac{1}{i\hbar}\sum_{j_1}\left[\mathcal{U}^{(cc,1)}_{i_2j_1}p^*_{j_1i_1}-\mathcal{U}^{(cc,1)*}_{i_1j_1}p_{j_1i_2}\right], \tag{75a}$$

$$\frac{d}{dt}p_{j_1i_1}\Big|^{(cc,1)}=\frac{1}{i\hbar}\left[\sum_{j_2}\mathcal{E}^{h(cc,1)}_{j_1j_2}p_{j_2i_1}+\sum_{i_2}\mathcal{E}^{e(cc,1)}_{i_1i_2}p_{j_1i_2}\right]+\frac{1}{i\hbar}\left[\mathcal{U}^{(cc,1)}_{i_1j_1}-\sum_{i_2}\mathcal{U}^{(cc,1)}_{i_2j_1}f^e_{i_2i_1}-\sum_{j_2}\mathcal{U}^{(cc,1)}_{i_1j_2}f^h_{j_2j_1}\right], \tag{75b}$$

where the self-energy matrices due to Hartree and Fock contributions are

$$\mathcal{E}^{e(cc,1)}_{i_1i_2}=-\sum_{i_3,i_4}V^{ee}_{i_1i_3i_2i_4}f^e_{i_3i_4}+\sum_{i_3,i_4}V^{ee}_{i_1i_3i_4i_2}f^e_{i_3i_4}-\sum_{j_3,j_4}V^{eh}_{i_1j_3j_4i_2}f^h_{j_3j_4}, \tag{76a}$$

$$\mathcal{E}^{h(cc,1)}_{j_1j_2}=-\sum_{j_3,j_4}V^{hh}_{j_1j_3j_2j_4}f^h_{j_3j_4}-\sum_{i_3,i_4}V^{eh}_{i_3j_1j_2i_4}f^e_{i_3i_4}+\sum_{j_3,j_4}V^{hh}_{j_1j_3j_4j_2}f^h_{j_3j_4}, \tag{76b}$$

and the internal-field matrix due to the Fock contributions of the electron-hole interaction is

$$\mathcal{U}^{(cc,1)}_{i_1j_1}=-\sum_{i_2,j_2}V^{eh}_{i_1j_1j_2i_2}p_{j_2i_2}. \tag{77}$$

Thus we again obtain the same structure of equations as in the single-particle case, but with renormalized energies and fields. Here, the self-energies describe band-gap-renormalization effects as well as induced potentials, while the internal field gives rise to excitonic effects and Coulomb enhancement. The single-particle equations including first-order carrier-carrier contributions are usually called semiconductor Bloch equations. They were derived in real-space representation by Huhn and Stahl (1984) and in momentum representation by Schmitt-Rink and Chemla (1986) and Lindberg and Koch (1988a).

2. Second order: Scattering and dephasing

As in the case of carrier-phonon interaction, the next step in the correlation hierarchy is obtained by including two-particle correlations like

$$\delta K_{i_1,i_2,i_3,i_4}=K_{i_1,i_2,i_3,i_4}-f^e_{i_1i_4}f^e_{i_2i_3}+f^e_{i_1i_3}f^e_{i_2i_4}, \tag{78}$$

which describe deviations from the corresponding factorizations. The equations of motion for these quantities involve three-particle density matrices. The hierarchy can be truncated by factorizing the three-particle density matrices into products of three single-particle density matrices, resulting in equations like

$$i\hbar\frac{d}{dt}\delta K_{i_1,i_2,i_3,i_4}=(\epsilon^e_{i_4}+\epsilon^e_{i_3}-\epsilon^e_{i_2}-\epsilon^e_{i_1})\times\delta K_{i_1,i_2,i_3,i_4}+S^{ee}+S^{eh}, \tag{79}$$

where the source terms S^{ee} and S^{eh} involve only single-particle density matrices. The intraband term

$$S^{ee}=\sum_{i_5,i_6,i_7,i_8}(V^{ee}_{i_5i_6i_7i_8}-V^{ee}_{i_6i_5i_7i_8})\times[f^e_{i_1i_8}f^e_{i_2i_7}(\delta_{i_6i_3}-f^e_{i_6i_3})(\delta_{i_5i_4}-f^e_{i_5i_4})-(\delta_{i_1i_8}-f^e_{i_1i_8})(\delta_{i_2i_7}-f^e_{i_2i_7})f^e_{i_6i_3}f^e_{i_5i_4}] \tag{80a}$$

exhibits a structure similar to carrier-carrier scattering terms in the Boltzmann equation, but in an off-diagonal generalization. The interband term

$$S^{eh}=\sum_{i_5,i_6,j_1,j_2}V^{eh}_{i_5j_1j_2i_6}[p^*_{j_1i_1}p_{j_2i_4}(\delta_{i_2i_6}f^e_{i_5i_3}-f^e_{i_2i_6}\delta_{i_5i_3})+p^*_{j_1i_2}p_{j_2i_3}(\delta_{i_1i_6}f^e_{i_5i_4}-f^e_{i_1i_6}\delta_{i_5i_4})-p^*_{j_1i_1}p_{j_2i_3}(\delta_{i_2i_6}f^e_{i_5i_4}-f^e_{i_2i_6}\delta_{i_5i_4})-p^*_{j_1i_2}p_{j_2i_4}(\delta_{i_1i_6}f^e_{i_5i_3}-f^e_{i_1i_6}\delta_{i_5i_3})] \tag{80b}$$

gives rise to polarization scattering; it modifies the scattering processes as long as there are coherent interband polarizations present. The set of equations for two-particle correlations constitutes the starting point for the study of carrier-carrier quantum kinetics in the density-matrix formalism. Some recent results on this topic will be reviewed in Sec. III.H.

The semiclassical limit is then obtained by adiabatic elimination of the two-particle correlations, exactly as in the case of the phonon-assisted correlations discussed in Sec. II.D. The result can be cast into the same form as in Eq. (56), but with different functions $\Gamma^{(cc,2)}$ and $\mathcal{U}^{(cc,2)}$ replacing $\Gamma^{(cp,2)}$ and $\mathcal{U}^{(cp,2)}$; its explicit form can again be found in Kuhn (1998). In the next section we shall explicitly discuss the carrier-carrier contributions in momentum representation.

3. Homogeneous system

In a homogeneous material the Coulomb matrix elements depend on the momentum transfer $\mathbf{q}$ only. Here we shall also assume that the three matrix elements corresponding to electron-electron, hole-hole, and electron-hole interactions are equal. This is true in bulk semiconductors, where

$$V_{\mathbf{q}}=\frac{4\pi e^2}{\mathcal{V}\varepsilon_r q^2}, \tag{81}$$

but it also holds in low-dimensional structures if the confinement wave functions for electrons and holes are the same, i.e., in the limit of infinitely high barriers. For finite barriers the matrix elements become significantly

different for q values larger than the inverse confinement length. However, since the small-wavelength behavior dominates in most of the features discussed here, the assumption of equal matrix elements is often a good approximation, even in this case. The value of ε_r depends on the treatment of the phonon dynamics: if phonon-induced correlations due to the Fröhlich interaction are taken into account dynamically, it coincides with the optical dielectric constant; otherwise, the static value has to be taken.

The first-order contribution in momentum representation is given by the intraband and interband energies,

$$\mathcal{E}^{e,h(cc,1)}_{\mathbf{k}\mathbf{k}'}=-\sum_{\mathbf{q}}\,[V_{\mathbf{q}}f^{e,h}_{\mathbf{k}'+\mathbf{q},\mathbf{k}+\mathbf{q}}\mp V_{\mathbf{k}-\mathbf{k}'}\times(f^{e}_{\mathbf{q},\mathbf{q}-\mathbf{k}'+\mathbf{k}}-f^{h}_{\mathbf{q},\mathbf{q}-\mathbf{k}'+\mathbf{k}})], \tag{82a}$$

$$\mathcal{U}^{(cc,1)}_{\mathbf{k}\mathbf{k}'}=-\sum_{\mathbf{q}}\,V_{\mathbf{q}}p_{-\mathbf{k}'-\mathbf{q},\mathbf{k}+\mathbf{q}}, \tag{82b}$$

with Fock ($\sim V_{\mathbf{q}}$) and Hartree ($\sim V_{\mathbf{k}-\mathbf{k}'}$) terms. Here the upper sign refers to electrons and the lower sign to holes. If the system is homogeneously excited, the Hartree terms cancel due to charge neutrality. The intraband Fock terms describe band-gap renormalizations, while the interband terms describe Coulomb correlations between electrons and holes. In particular, they give rise to excitonic features in optical spectra.

In a Wigner representation the first-order terms can be written as

$$\mathcal{E}^{e,h(cc,1)}_{\mathbf{k}}(\mathbf{r})=-\sum_{\mathbf{k}'}\,V_{\mathbf{k}-\mathbf{k}'}f^{e,h}_{\mathbf{k}'}(\mathbf{r})\mp e\Phi(\mathbf{r}), \tag{83a}$$

$$\mathcal{U}_{\mathbf{k}}(\mathbf{r})=-\sum_{\mathbf{k}'}\,V_{\mathbf{k}-\mathbf{k}'}p_{\mathbf{k}'}(\mathbf{r}), \tag{83b}$$

where the induced potential satisfies the Poisson equation

$$\nabla^2\Phi(\mathbf{r})=-\frac{4\pi}{\varepsilon_r}\rho(\mathbf{r})=\frac{4\pi e}{\varepsilon_r\mathcal{V}}\sum_{\mathbf{k}}\,[f^{e}_{\mathbf{k}}(\mathbf{r})-f^{h}_{\mathbf{k}}(\mathbf{r})], \tag{84}$$

$\rho(\mathbf{r})$ being the charge density.

The second-order contributions in the case of homogeneous excitation are given by

$$\frac{d}{dt}f^{e}_{\mathbf{k}}|^{(cc,2)}=-\sum_{\mathbf{q}}\,[W^{e(cc,2)}_{\mathbf{k}-\mathbf{q},\mathbf{k}}f^{e}_{\mathbf{k}}(1-f^{e}_{\mathbf{k}-\mathbf{q}})-W^{e(cc,2)}_{\mathbf{k},\mathbf{k}-\mathbf{q}}f^{e}_{\mathbf{k}-\mathbf{q}}(1-f^{e}_{\mathbf{k}})]+\frac{1}{i\hbar}[\mathcal{U}^{e(cc,2)}_{\mathbf{k}}p^{*}_{\mathbf{k}}-\mathcal{U}^{e(cc,2)*}_{\mathbf{k}}p_{\mathbf{k}}], \tag{85a}$$

$$\frac{d}{dt}p_{\mathbf{k}}|^{(cc,2)}=-\sum_{\mathbf{q}}\,[(\mathcal{W}^{e(cc,2)}_{\mathbf{k}-\mathbf{q},\mathbf{k}}+\mathcal{W}^{h(cc,2)}_{-(\mathbf{k}-\mathbf{q}),-\mathbf{k}})p_{\mathbf{k}}-(\mathcal{W}^{e(cc,2)}_{\mathbf{k},\mathbf{k}-\mathbf{q}}+\mathcal{W}^{h(cc,2)}_{-\mathbf{k},-(\mathbf{k}-\mathbf{q})})p_{\mathbf{k}-\mathbf{q}}], \tag{85b}$$

where the transition matrices are

$$W^{e,h(cc,2)}_{\mathbf{k}-\mathbf{q},\mathbf{k}}=\frac{\pi}{\hbar}|V_{\mathbf{q}}|^2\sum_{\nu'=e,h}\sum_{\mathbf{k}'}\,\mathcal{D}(\epsilon^{e,h}_{\mathbf{k}-\mathbf{q}}+\epsilon^{\nu'}_{\mathbf{k}'+\mathbf{q}}-\epsilon^{\nu'}_{\mathbf{k}'}-\epsilon^{e,h}_{\mathbf{k}})[f^{\nu'}_{\mathbf{k}'}(1-f^{\nu'}_{\mathbf{k}'+\mathbf{q}})-p^{*}_{\mathbf{k}'+\mathbf{q}}p_{\mathbf{k}'}]+\text{c.c.}, \tag{86}$$

$$\mathcal{W}^{e,h(cc,2)}_{\mathbf{k}-\mathbf{q},\mathbf{k}}=\frac{\pi}{\hbar}|V_{\mathbf{q}}|^2\sum_{\nu'=e,h}\sum_{\mathbf{k}'}\,\mathcal{D}(\epsilon^{e,h}_{\mathbf{k}-\mathbf{q}}+\epsilon^{\nu'}_{\mathbf{k}'+\mathbf{q}}-\epsilon^{\nu'}_{\mathbf{k}'}-\epsilon^{e,h}_{\mathbf{k}})[-p^{*}_{\mathbf{k}'+\mathbf{q}}p_{\mathbf{k}'}+f^{\nu'}_{\mathbf{k}'}(1-f^{\nu'}_{\mathbf{k}'+\mathbf{q}})(1-f^{e,h}_{\mathbf{k}-\mathbf{q}})+f^{e,h}_{\mathbf{k}-\mathbf{q}}f^{\nu'}_{\mathbf{k}'+\mathbf{q}}(1-f^{\nu'}_{\mathbf{k}'})], \tag{87}$$

and the effective field is

$$\mathcal{U}^{e,h(cc,2)}_{\mathbf{k}}=i\pi\sum_{\mathbf{k}',\mathbf{q}}\sum_{\nu'=e,h}\,|V_{\mathbf{q}}|^2\mathcal{D}(\epsilon^{h,e}_{\mathbf{k}}+\epsilon^{\nu'}_{\mathbf{k}'}-\epsilon^{\nu'}_{\mathbf{k}'+\mathbf{q}}-\epsilon^{h,e}_{\mathbf{k}-\mathbf{q}})[f^{\nu'}_{\mathbf{k}'+\mathbf{q}}-f^{\nu'}_{\mathbf{k}'}]p_{\mathbf{k}-\mathbf{q}}. \tag{88}$$

The structure of the equations is the same as in the case of carrier-phonon interaction, and therefore everything that has been stated above also holds in this case. The main difference is that now the transition matrices [Eq. (86)] no longer coincide with the Boltzmann transition matrices. Instead, we have additional contributions due to the interband polarization, which, in general, remove the positive-definiteness and consequently the possibility of interpreting such terms as transition rates. Only when the polarization has decayed are the Boltzmann rates recovered. For the polarization we again obtain contributions with the structure of out-scattering ($\sim p_{\mathbf{k}}$) and in-scattering ($\sim p_{\mathbf{k}-\mathbf{q}}$) terms, which, due to equal Coulomb matrix elements, satisfy the sum rule

$$\frac{d}{dt}\sum_{\mathbf{k}}\,p_{\mathbf{k}}|^{(cc,2)}=0. \tag{89}$$

This compensation between in- and out-scattering terms is essential in order to reproduce a physically reasonable density dependence of carrier-carrier scattering-induced dephasing (Rossi, Haas, and Kuhn, 1994; Haas, Rossi, and Kuhn, 1996).

4. Second order: Screening

In the previous section the carrier-carrier scattering terms were derived in the second Born approximation. While this gives well-defined, finite results on a quantum-kinetic level (El Sayed, Bányai, and Haug, 1994), it is well known that in the semiclassical limit the total scattering rate for a bare Coulomb potential diverges due to the long-range nature of this interaction. Usually, this divergence is removed by taking a screened Coulomb potential whose screening is described, for example, by the Lindhard formula. This dielectric function is obtained by studying the response of the carrier system to an external potential within the random-phase approximation (Haug and Koch, 1993), i.e., in the

present case, from the first-order carrier-carrier contributions. However, as shown by several authors in the field of plasma physics in the early 1960s (Lenard, 1960; Balescu, 1961; Guernsey, 1962; Wyld and Fried, 1963), screening appears self-consistently within the second-order density-matrix approach. Some recent derivations applied to condensed-matter physics can be found in the work of Hohenester and Pötz (1997) and Bonitz (1998). Here we shall briefly review the derivation of the dynamically screened scattering rates by essentially following Wyld and Fried (1963) and restricting the discussion to the homogeneous single-band case.

The equation of motion for the distribution function in a one-band model is given by

$$i\hbar\frac{d}{dt}f_{\mathbf{k}}=\sum_{\mathbf{k}',\mathbf{q}}V_{\mathbf{q}}[\delta K_{\mathbf{k},\mathbf{k}',\mathbf{k}'+\mathbf{q},\mathbf{k}-\mathbf{q}}-\delta K_{\mathbf{k}-\mathbf{q},\mathbf{k}'+\mathbf{q},\mathbf{k}',\mathbf{k}}]. \tag{90}$$

The equation of motion for the two-particle correlations is obtained in the same way as in the previous section, leading to three-particle density matrices. While there the three-particle correlations were factorized into single-particle density matrices only, now all factorizations into lower-order correlations are included. Thus additional contributions appear due to a factorization of a three-particle density matrix into a distribution function times a two-particle correlation. Neglecting the three-particle correlations, we obtain the resulting equation of motion:

$$i\hbar\frac{d}{dt}\delta K_{\mathbf{k},\mathbf{k}',\mathbf{k}'+\mathbf{q},\mathbf{k}-\mathbf{q}}=(\mathcal{E}_{\mathbf{k}-\mathbf{q}}+\mathcal{E}_{\mathbf{k}'+\mathbf{q}}-\mathcal{E}_{\mathbf{k}'}-\mathcal{E}_{\mathbf{k}})\times\delta K_{\mathbf{k},\mathbf{k}',\mathbf{k}'+\mathbf{q},\mathbf{k}-\mathbf{q}}+\sum_{i=1}^{5}S_i, \tag{91}$$

where the renormalized energies are $\mathcal{E}_{\mathbf{k}}=\epsilon_{\mathbf{k}}-\Sigma_{\mathbf{q}}V_{\mathbf{q}}f_{\mathbf{k}-\mathbf{q}}$. A series of five terms that describe different physical phenomena results from the factorization (Wyld and Fried, 1963).

S_1 leads to the scattering in Born approximation as discussed in the previous section:

$$S_1=(V_{\mathbf{q}}-V_{\mathbf{k}-\mathbf{k}'-\mathbf{q}})[f_{\mathbf{k}}f_{\mathbf{k}'}(1-f_{\mathbf{k}'+\mathbf{q}})(1-f_{\mathbf{k}-\mathbf{q}})-f_{\mathbf{k}-\mathbf{q}}f_{\mathbf{k}'+\mathbf{q}}(1-f_{\mathbf{k}'})(1-f_{\mathbf{k}})]; \tag{92a}$$

S_2 gives rise to the screening of the Coulomb potential in the random-phase approximation (RPA);

$$S_2=V_{\mathbf{q}}\Big[(f_{\mathbf{k}}-f_{\mathbf{k}-\mathbf{q}})\sum_{\mathbf{k}''}\delta K_{\mathbf{k}'',\mathbf{k}',\mathbf{k}'+\mathbf{q},\mathbf{k}''-\mathbf{q}}+(f_{\mathbf{k}'}-f_{\mathbf{k}'+\mathbf{q}})\sum_{\mathbf{k}''}\delta K_{\mathbf{k},\mathbf{k}'',\mathbf{k}''+\mathbf{q},\mathbf{k}-\mathbf{q}}\Big]; \tag{92b}$$

S_3 contains exchange corrections to the screening, which are necessary to satisfy the correct antisymmetry of δK upon exchange of two particles:

$$S_3=-V_{\mathbf{k}-\mathbf{k}'-\mathbf{q}}\Big[(f_{\mathbf{k}'}-f_{\mathbf{k}-\mathbf{q}})\sum_{\mathbf{k}''}\delta K_{\mathbf{k},\mathbf{k}'',\mathbf{k}''+\mathbf{k}-\mathbf{k}'-\mathbf{q},\mathbf{k}'+\mathbf{q}}+(f_{\mathbf{k}}-f_{\mathbf{k}'+\mathbf{q}})\sum_{\mathbf{k}''}\delta K_{\mathbf{k}'',\mathbf{k}',\mathbf{k}-\mathbf{q},\mathbf{k}''-\mathbf{k}+\mathbf{k}'+\mathbf{q}}\Big]; \tag{92c}$$

S_4 describes the repeated scattering of two particles from each other and leads to the exact T matrix:

$$S_4=(1-f_{\mathbf{k}-\mathbf{q}}-f_{\mathbf{k}'+\mathbf{q}})\sum_{\mathbf{q}'}V_{\mathbf{q}'}\delta K_{\mathbf{k},\mathbf{k}',\mathbf{k}'+\mathbf{q}+\mathbf{q}',\mathbf{k}-\mathbf{q}-\mathbf{q}'}-(1-f_{\mathbf{k}}-f_{\mathbf{k}'})\sum_{\mathbf{q}'}V_{\mathbf{q}'}\delta K_{\mathbf{k}-\mathbf{q}',\mathbf{k}'+\mathbf{q}',\mathbf{k}'+\mathbf{q},\mathbf{k}-\mathbf{q}}; \tag{92d}$$

and, finally, S_5 contains terms that in the Green's-function language would be called vertex corrections to the screening terms S_2 and S_3:

$$\begin{aligned}S_5=&-(f_{\mathbf{k}}-f_{\mathbf{k}-\mathbf{q}})\sum_{\mathbf{q}'}V_{\mathbf{q}'}\delta K_{\mathbf{k}-\mathbf{q}',\mathbf{k}',\mathbf{k}'+\mathbf{q},\mathbf{k}-\mathbf{q}-\mathbf{q}'}\\&-(f_{\mathbf{k}'}-f_{\mathbf{k}'+\mathbf{q}})\sum_{\mathbf{q}'}V_{\mathbf{q}'}\delta K_{\mathbf{k},\mathbf{k}'+\mathbf{q}',\mathbf{k}'+\mathbf{q}+\mathbf{q}',\mathbf{k}-\mathbf{q}}\\&-(f_{\mathbf{k}'}-f_{\mathbf{k}-\mathbf{q}})\sum_{\mathbf{q}'}V_{\mathbf{q}'}\delta K_{\mathbf{k},\mathbf{k}'+\mathbf{q}',\mathbf{k}'+\mathbf{q},\mathbf{k}-\mathbf{q}+\mathbf{q}'}\\&-(f_{\mathbf{k}}-f_{\mathbf{k}'+\mathbf{q}})\sum_{\mathbf{q}'}V_{\mathbf{q}'}\delta K_{\mathbf{k}-\mathbf{q}',\mathbf{k}',\mathbf{k}'+\mathbf{q}-\mathbf{q}',\mathbf{k}-\mathbf{q}}.\end{aligned} \tag{92e}$$

Due to the divergence of $V_{\mathbf{q}}$ for small $\mathbf{q}$, the direct term in S_1 and the term S_2 are expected to dominate, since they involve no summation over the Coulomb matrix element. Keeping only these contributions is equivalent to the random-phase approximation. The solution of Wyld and Fried is based on the observation that, in this case, Eq. (91) can be factorized in the following sense: If the operator $\hat{F}_{\mathbf{k},\mathbf{q}}=c^{\dagger}_{\mathbf{k}-\mathbf{q}/2}c_{\mathbf{k}+\mathbf{q}/2}$ satisfies the operator analog of the linearized Vlasov equation, i.e.,

$$\frac{d}{dt}\hat{F}_{\mathbf{k},\mathbf{q}}=\frac{1}{i\hbar}(\mathcal{E}_{\mathbf{k}+\mathbf{q}/2}-\mathcal{E}_{\mathbf{k}-\mathbf{q}/2})\hat{F}_{\mathbf{k},\mathbf{q}}-\frac{1}{i\hbar}V_{\mathbf{q}}(f_{\mathbf{k}+\mathbf{q}/2}-f_{\mathbf{k}-\mathbf{q}/2})\sum_{\mathbf{k}'}\hat{F}_{\mathbf{k}',\mathbf{q}}, \tag{93}$$

then Eq. (91) with only the direct part of S_1 and S_2 is a direct consequence of Eq. (93). Such a factorization property is also the basis for the derivation of screening in Hohenester and Pötz (1997). By solving Eq. (93) in the Markov approximation and assuming an initially uncorrelated system, we can calculate the two-particle correlation. With this result Eq. (90) reads

$$\begin{aligned}\frac{d}{dt}f_{\mathbf{k}}=&-\frac{2\pi}{\hbar}\sum_{\mathbf{k}',\mathbf{q}}\left|\frac{V_{\mathbf{q}}}{\varepsilon[\mathbf{q},(\mathcal{E}_{\mathbf{k}-\mathbf{q}}-\mathcal{E}_{\mathbf{k}})/\hbar]}\right|^2\\&\times\delta(\mathcal{E}_{\mathbf{k}-\mathbf{q}}+\mathcal{E}_{\mathbf{k}'+\mathbf{q}}-\mathcal{E}_{\mathbf{k}'}-\mathcal{E}_{\mathbf{k}})[f_{\mathbf{k}}f_{\mathbf{k}'}(1-f_{\mathbf{k}'+\mathbf{q}})\\&\times(1-f_{\mathbf{k}-\mathbf{q}})-f_{\mathbf{k}-\mathbf{q}}f_{\mathbf{k}'+\mathbf{q}}(1-f_{\mathbf{k}'})(1-f_{\mathbf{k}})].\end{aligned} \tag{94}$$

This corresponds to the Boltzmann equation with the Coulomb potential dynamically screened by the Lindhard dielectric function,

$$\varepsilon(\mathbf{q},\omega)=1-V_{\mathbf{q}}\sum_{\mathbf{k}}\frac{f_{\mathbf{k}}-f_{\mathbf{k}-\mathbf{q}}}{\mathcal{E}_{\mathbf{k}}-\mathcal{E}_{\mathbf{k}-\mathbf{q}}-\hbar\omega}. \tag{95}$$

Without the Markov approximation, Eq. (91) with the contributions S_1 and S_2 serves as a starting point for a quantum-kinetic investigation of carrier-carrier scattering, including the buildup of screening at early times.

5. Third order: Collisional broadening

The next order in the hierarchy is obtained in the same way as in the case of carrier-phonon interaction: The equations of motion for three-particle correlations have to be set up and the resulting four-particle density matrices have to be factorized into all kinds of lower-order terms. Among the many possible factorizations there is one class of terms having the structure of self-energy corrections to the second-order equation, thus resulting in second-order energy renormalizations and collisional broadening terms in the equation for the two-particle correlation. Here, however, due to the strong dominance of small-angle scattering, particularly at low densities, this approximation overestimates the broadening in a much more dramatic way than in carrier-phonon scattering. Such a strong overestimation of the collisional broadening due to carrier-carrier scattering when in-scattering terms are neglected has been studied by Rossi *et al.* (1994) and Haas *et al.* (1996) for the case of carrier photogeneration. In particular, it has been shown how the inclusion of additional terms with the structure of in-scattering contributions leads to the correct physical behavior. Within the Green's-function approach a strong violation of energy conservation and unphysically large broadening resulting from an exponentially decaying memory function—corresponding to a Lorentzian spectral function—have been demonstrated (Bonitz *et al.*, 1999). In the same paper the authors show that again the replacement of the exponential by a hyperbolic secans improves the results but does not restore energy conservation. On the other hand, neglecting the decay of the retarded Green's function—which is equivalent to taking the second-order density-matrix theory—is in surprisingly good agreement with the results of a two-time Green's-function calculation.

6. Coulomb interaction in doped semiconductors

In the previous sections we have derived equations of motion for the case of an intrinsic (or undoped) semiconductor. If, in contrast, the semiconductor is doped, the doping impurities can provide or accept electrons or holes, thereby changing their charge state. In this case the Coulomb interaction with the carriers bound at impurities has to be taken into account as well. In general, this interaction contributes at each order to our equations of motion. The first-order or Hartree term describes the electrostatic potential produced by the charged impurities. It is necessary to maintain charge neutrality. In a homogeneous system it is a divergent term at $\mathbf{q}=0$ which exactly cancels the divergence of the other Coulomb contributions. In inhomogeneous systems it is responsible for built-in fields. Examples of this case are modulation-doped quantum-well structures in which impurities provide conduction electrons to the quantum wells. The second-order terms give rise to carrier-impurity scattering processes that contribute to momentum relaxation, and they may also lead to Auger- or impact-ionization-like transitions between free and bound carrier states. In this section we shall address a specific case which is important if optical transitions between free and bound states are involved. Experiments based on such transitions, in particular the study of band-to-acceptor luminescence, have provided valuable information on ultrafast carrier dynamics in optically excited semiconductors, as will be discussed in more detail in Sec. III.A.3.

Let us consider a homogeneous semiconductor that is slightly p-doped with shallow acceptors. At zero temperature the Fermi level is in the middle between the top of the valence band and the acceptor level. Thus at sufficiently low temperatures the acceptors are unoccupied, and it is convenient to treat the acceptor occupation in an electron picture. We thus denote by $s_i^\dagger$ and s_i the creation and destruction of an electron at the acceptor position $\mathbf{r}_i$. Within the hydrogenic impurity model the wave function of the acceptor state is given by

$$\psi(\mathbf{r})=u_V(\mathbf{r})\phi(\mathbf{r}-\mathbf{r}_i), \tag{96}$$

where u_V denotes the periodic part of the Bloch function at the top of the valence band and ϕ is the $1s$ hydrogen wave function. If we again neglect Coulomb terms leading to transitions between impurity levels and free carrier states, which for the purpose studied here are not important, we have three additional contributions to the Coulomb interaction Hamiltonian, due to electron-acceptor, hole-acceptor, and acceptor-acceptor interactions. For sufficiently low doping concentration and negligible occupation of the acceptor levels, the acceptor-acceptor interaction is not important, and the Hamiltonian is given by

$$\begin{aligned}\mathbf{H}_{cc}^{a}&=\mathbf{H}_{cc}^{ea}+\mathbf{H}_{cc}^{ha}\\&=\sum_{\mathbf{k},\mathbf{q},i}V_{\mathbf{q}}^{i}c_{\mathbf{k}-\mathbf{q}}^{\dagger}s_i^{\dagger}s_ic_{\mathbf{k}}-\sum_{\mathbf{k},\mathbf{q},i}V_{\mathbf{q}}^{i}d_{\mathbf{k}-\mathbf{q}}^{\dagger}s_i^{\dagger}s_id_{\mathbf{k}},\end{aligned} \tag{97}$$

where the Coulomb matrix elements are

$$V_{\mathbf{q}}^{i}=\frac{e^2}{\mathcal{V}\varepsilon_r}\int d\mathbf{r}d\mathbf{r}'\,|\phi(\mathbf{r}'-\mathbf{r}_i)|^2\frac{e^{i\mathbf{q}\mathbf{r}}}{|\mathbf{r}-\mathbf{r}'|}, \tag{98}$$

which in the case of the $1s$ wave function reduces to

$$V_{\mathbf{q}}^{i}=V_{\mathbf{q}}e^{i\mathbf{q}\mathbf{r}_i}\beta_{\mathbf{q}}=V_{\mathbf{q}}e^{i\mathbf{q}\mathbf{r}_i}[1+(\tfrac{1}{2}qa_B)^2]^{-2}. \tag{99}$$

Here, $V_{\mathbf{q}}$ is the Coulomb matrix element of the homogeneous semiconductor [Eq. (81)] and a_B is the acceptor Bohr radius.

The relevant dynamical variable to describe optical transitions between the conduction band and the impurity level is the band-to-acceptor polarization,

$$p^a_{\mathbf{k}}=\sum_i e^{i\mathbf{k}\mathbf{r}_i}\langle s^\dagger_i c_{\mathbf{k}}\rangle=\sum_i e^{i\mathbf{k}\mathbf{r}_i}p^i_{\mathbf{k}}. \tag{100}$$

The first-order contribution to its equation of motion due to the complete (band and impurity) Coulomb interaction is given by

$$\frac{d}{dt}p^a_{\mathbf{k}}|^{(cc,1)}=-\frac{1}{i\hbar}\sum_{\mathbf{q}} V_{\mathbf{q}}(f^e_{\mathbf{k}+\mathbf{q}}p^a_{\mathbf{k}}-\beta_{\mathbf{q}}f^e_{\mathbf{k}}p^a_{\mathbf{k}+\mathbf{q}}). \tag{101}$$

Here, the first term is due to the renormalization of the conduction band by electron-electron interaction, while the second term gives rise to Coulomb enhancement and excitonic effects in the transition (we have again neglected terms involving acceptor occupations). Both terms are proportional to the electron distribution function and therefore negligible at low densities.

The second-order contribution is obtained in the same way as the interband polarization. Here we shall give only the result in the semiclassical limit, which can be written in a form similar to Eq. (85b):

$$\begin{aligned}\frac{d}{dt}p^a_{\mathbf{k}}|^{(cc,2)}=&-\sum_{\mathbf{q}}[\mathcal{W}^{e(cc,2)}_{\mathbf{k}-\mathbf{q},\mathbf{k}}p^a_{\mathbf{k}}-\beta_{\mathbf{q}}\mathcal{W}^{e(cc,2)}_{\mathbf{k},\mathbf{k}-\mathbf{q}}p^a_{\mathbf{k}-\mathbf{q}}]\\&-\sum_{\mathbf{q},i}[\beta^2_{\mathbf{q}}\mathcal{W}^{a(cc,2)}_{\mathbf{k}-\mathbf{q},\mathbf{k}}e^{i(\mathbf{k}-\mathbf{q})\mathbf{r}_i}p^i_{\mathbf{k}}\\&-\beta_{\mathbf{q}}\mathcal{W}^{a(cc,2)}_{\mathbf{k},\mathbf{k}-\mathbf{q}}e^{i\mathbf{k}\mathbf{r}_i}p^i_{\mathbf{k}-\mathbf{q}}],\end{aligned} \tag{102}$$

where the matrix $\mathcal{W}^{e(cc,2)}_{\mathbf{k},\mathbf{k}-\mathbf{q}}$ is given in Eq. (87) and the matrix $\mathcal{W}^{a(cc,2)}_{\mathbf{k},\mathbf{k}-\mathbf{q}}$ is

$$\begin{aligned}\mathcal{W}^{a(cc,2)}_{\mathbf{k},\mathbf{k}-\mathbf{q}}=&\frac{\pi}{\hbar}|V_{\mathbf{q}}|^2\sum_{\nu=e,h}\sum_{\mathbf{k}'}\delta(\epsilon^\nu_{\mathbf{k}'+\mathbf{q}}-\epsilon^\nu_{\mathbf{k}'})\\&\times f^\nu_{\mathbf{k}'}(1-f^\nu_{\mathbf{k}'+\mathbf{q}}).\end{aligned} \tag{103}$$

If the impurity positions are randomly distributed, this last part vanishes. In contrast to interband polarization, here we do not have an exact symmetry between in- and out-scattering terms because the matrix elements for electron-electron and electron-impurity interaction are different. However, for $\mathbf{q}$ values smaller than the inverse Bohr radius of the impurity we have $\beta_{\mathbf{q}}\approx 1$ and the symmetry is approximately recovered, leading again to a strong compensation between the two terms.

F. Carrier-photon interaction

Typically, the laser pulses used to excite semiconductors in the ultrafast regime have a very high degree of coherence and are well described by a classical light field, as was done in the previous sections. However, there are certain features that can only be described in terms of a quantum-mechanical treatment of the electromagnetic radiation. Among these are all kinds of phenomena that affect the photon statistics, like the generation of squeezed light by nonlinear optical techniques (Fox *et al.*, 1995; Dabbicco *et al.*, 1996) or the optical Stark effect with nonclassical light (Altevogt, Puff, and Zimmermann, 1997). The most important process, however, which requires a quantum description of light, is spontaneous emission. Often the characteristic time scales for spontaneous emission are much longer than those for other interaction processes like carrier-carrier or carrier-phonon scattering. Therefore, for the modeling of the ultrafast carrier dynamics, it can be neglected. However, in luminescence experiments the spontaneously emitted photons are the quantities that are detected, and a theory is required that relates the properties of the emitted radiation to the carrier dynamics. In this section we shall derive equations of motion describing the rate of spontaneously emitted photons.

The quantized light field is described by creation and destruction operators $a^\dagger_{\mathbf{q}\nu}$ and $a_{\mathbf{q}\nu}$ for a photon with wave vector $\mathbf{q}$ and polarization component ν. The free-photon Hamiltonian is then given by

$$\mathbf{H}_l=\sum_{\mathbf{q},\nu}\hbar\omega_{\mathbf{q}}a^\dagger_{\mathbf{q}\nu}a_{\mathbf{q}\nu}, \tag{104}$$

where the dispersion relation is $\omega_{\mathbf{q}}=cq$, c being the velocity of light.

The exact form of the interaction Hamiltonian, as well as the interpretation of the photon operators, depends on the choice of gauge. In the Coulomb gauge, by neglecting terms quadratic in the field, we obtain the carrier-light Hamiltonian

$$\mathbf{H}_{cl}=\sum_{ij,\mathbf{q},\nu}[\mu^{ij}_{\mathbf{q},\nu}c^\dagger_i a_{\mathbf{q}\nu}d^\dagger_j+\mu^{ij*}_{\mathbf{q},\nu}d_j a^\dagger_{\mathbf{q}\nu}c_i], \tag{105}$$

where we have considered interband transitions only in the rotating-wave approximation. The multipole form of the interaction can be obtained by performing the Power-Zienau-Woolley transformation (Cohen-Tannoudji, Dupont-Roc, and Grynberg, 1989; Kira *et al.*, 1999; Savasta and Girlanda, 1999), which results in the same form of the interaction Hamiltonian but with different matrix elements, and an additional field-independent term. This latter term—the dipole self-energy—has the same operator structure as the electron-hole interaction. For the present case (in which we are only interested in the properties of the spontaneously emitted photons and neglect the feedback on the carrier dynamics) the choice of the gauge plays a minor role; the properties are essentially determined by the structure of the carrier-light Hamiltonian [Eq. (105)]. A recent review of the quantum theory of carrier-light interaction in semiconductors is that of Kira *et al.* (1999).

1. First order: Coherent electromagnetic fields

The structure of the above light-matter Hamiltonian is similar to that of carrier-phonon interaction. Therefore the structure of the resulting equations of motion is also similar, the main difference being that carrier-phonon interaction is an intraband process, while carrier-photon interaction is an interband process. To first order in the correlation expansion, coherent photon amplitudes are excited according to

$$\frac{d}{dt}\langle a_{\mathbf{q}\nu}\rangle = i\omega_{\mathbf{q}}\langle a_{\mathbf{q}\nu}\rangle + \frac{1}{i\hbar}\sum_{ij}\mu^{ij*}_{\mathbf{q},\nu}p_{ji}. \tag{106}$$

These coherent amplitudes correspond to a classical coherent electromagnetic field, and a description on this level coincides with the classical treatment of the light field in the previous sections. In particular, Eq. (106) shows that the interband polarization acts as a source for a classical light field.

2. Second order: Absorption and luminescence

Even in the absence of a coherent amplitude, photons can be emitted. These incoherent photons are described by the average photon occupation number,

$$N^{\mathrm{inc}}_{\mathbf{q}\nu} = \langle a^{\dagger}_{\mathbf{q}\nu}a_{\mathbf{q}\nu}\rangle - |\langle a_{\mathbf{q}\nu}\rangle|^2. \tag{107}$$

In the absence of a coherent contribution, the rate of change of this variable determines the photon flux in the direction $\mathbf{q}$. This photon flux is obtained from the equation of motion

$$\frac{d}{dt}N^{\mathrm{inc}}_{\mathbf{q}\nu} = -\frac{1}{i\hbar}\sum_{ij}[\mu^{ij}_{\mathbf{q}\nu}r^{ji*}_{\mathbf{q}\nu} - \mu^{ij*}_{\mathbf{q}\nu}r^{ji}_{\mathbf{q}\nu}], \tag{108}$$

where we have introduced the incoherent photon-assisted density matrices

$$r^{ji}_{\mathbf{q}\nu} = \langle (a^{\dagger}_{\mathbf{q}\nu} - \langle a^{*}_{\mathbf{q}\nu}\rangle)d_j c_i\rangle. \tag{109}$$

Thus, in complete analogy with carrier-phonon interaction, these photon-assisted density matrices appear as new dynamical variables. Their temporal evolution is determined by the equation of motion

$$\begin{aligned}\frac{d}{dt}r^{j_1i_1}_{\mathbf{q}\nu} &= \frac{1}{i\hbar}[\epsilon^h_{j_1} + \epsilon^e_{i_1} - \hbar\omega_{\mathbf{q}}]r^{j_1i_1}_{\mathbf{q}\nu} \\ &\quad - \frac{1}{i\hbar}\sum_{i_2,j_2}\mu^{i_2j_2}_{\mathbf{q}\nu}(\langle c^{\dagger}_{i_2}d^{\dagger}_{j_2}d_{j_1}c_{i_1}\rangle - p^{*}_{j_2i_2}p_{j_1i_1}) \\ &\quad - \frac{1}{i\hbar}\sum_{i_2,\mathbf{q}',\nu'}\mu^{i_2j_1}_{\mathbf{q}'\nu'}\langle (a^{\dagger}_{\mathbf{q}\nu} - \langle a^{*}_{\mathbf{q}\nu}\rangle)c^{\dagger}_{i_2}a_{\mathbf{q}'\nu'}c_{i_1}\rangle \\ &\quad - \frac{1}{i\hbar}\sum_{j_2,\mathbf{q}',\nu'}\mu^{i_1j_2}_{\mathbf{q}'\nu'}\langle (a^{\dagger}_{\mathbf{q}\nu} - \langle a^{*}_{\mathbf{q}\nu}\rangle)d_{j_1}a_{\mathbf{q}'\nu'}d^{\dagger}_{j_2}\rangle.\end{aligned} \tag{110}$$

Here, only the single-particle Hamiltonian in a time-independent basis has been used for the evolution of the carrier operators. We shall address the role of interaction mechanisms in Sec. II.F.5. From Eq. (110) it can be seen that the source term for the emission of incoherent photons (first term on the rhs) is a two-particle density matrix, the function N introduced in Eq. (73), where the interband coherent part has been subtracted. However, it may still include intraband coherences. If, in accordance with our correlation-expansion scheme, all two-particle correlations are neglected, the terms on the rhs can be factorized into products of single-particle density matrices according to

$$\begin{aligned}\frac{d}{dt}r^{j_1i_1}_{\mathbf{q}\nu}|^{(cl)} &= -\frac{1}{i\hbar}\sum_{i_2,j_2}\mu^{i_2j_2}_{\mathbf{q}\nu}f^{e}_{i_2i_1}f^{h}_{j_2j_1} \\ &\quad + \frac{1}{i\hbar}(N^{inc}_{\mathbf{q}\nu} + |\langle a_{\mathbf{q}\nu}\rangle|^2) \\ &\quad \times\left(1 - \sum_{i_2}\mu^{i_2j_1}_{\mathbf{q}\nu}f^{e}_{i_2i_1} - \sum_{j_2}\mu^{i_1j_2}_{\mathbf{q}\nu}f^{h}_{j_2j_1}\right).\end{aligned} \tag{111}$$

The first source term gives rise to spontaneous emission, while the second one gives rise to absorption and stimulated emission. In the following we shall neglect this second term, since we assume that the photons immediately leave the system, making their occupation number negligible.

In the semiclassical limit, when the photon-assisted density matrices are adiabatically eliminated and only diagonal density matrices are taken into account, we get the following rate of emitted photons:

$$\frac{d}{dt}N^{\mathrm{inc}}_{\mathbf{q}\nu} = \frac{2\pi}{\hbar}\sum_{ij}|\mu^{ij}_{\mathbf{q}\nu}|^2\delta(\epsilon^h_j + \epsilon^e_i - \hbar\omega_{\mathbf{q}})f^{e}_{ii}f^{h}_{jj}, \tag{112}$$

i.e., the well-known Fermi's golden rule result for which the luminescence intensity is proportional to the product of electron and hole distribution functions of the optically coupled states.

3. Homogeneous system

The carrier-photon interaction Hamiltonian in momentum representation is given by

$$\mathbf{H}_{cl} = \sum_{\mathbf{k},\mathbf{q},\nu}[\mu_{\mathbf{q},\nu}c^{\dagger}_{\mathbf{k}}a_{\mathbf{q}\nu}d^{\dagger}_{-\mathbf{k}+\mathbf{q}} + \mu^{*}_{\mathbf{q},\nu}d_{-\mathbf{k}+\mathbf{q}}a^{\dagger}_{\mathbf{q}\nu}c_{\mathbf{k}}]. \tag{113}$$

Then, the rate of emitted photons in the semiclassical limit reads

$$\frac{d}{dt}N^{\mathrm{inc}}_{\mathbf{q}\nu} = \frac{2\pi}{\hbar}\sum_{\mathbf{k}}|\mu_{\mathbf{q}\nu}|^2\delta(\epsilon^h_{-\mathbf{k}+\mathbf{q}} + \epsilon^e_{\mathbf{k}} - \hbar\omega_{\mathbf{q}})f^{e}_{\mathbf{k}}f^{h}_{-\mathbf{k}+\mathbf{q}}. \tag{114}$$

In many cases the momentum of the photon is negligible compared to other characteristic momenta in the carrier dynamics, and replacing $\mathbf{k}-\mathbf{q}$ by $\mathbf{k}$ on the rhs of Eq. (114) is a very good approximation.

4. Transitions between band and impurity states

The theory developed so far for interband transitions is easily translated to transitions between band and impurity states. The band-to-acceptor interaction Hamiltonian reads

$$\mathbf{H}_{cl} = \sum_{i,\mathbf{k},\mathbf{q},\nu}[\mu_{\mathbf{q},\nu}\gamma_{\mathbf{k}}c^{\dagger}_{\mathbf{k}}a_{\mathbf{q}\nu}s_i + \mu^{*}_{\mathbf{q},\nu}\gamma_{\mathbf{k}}s^{\dagger}_i a^{\dagger}_{\mathbf{q}\nu}c_{\mathbf{k}}], \tag{115}$$

where $\gamma_{\mathbf{k}} = 8(\pi a_B^3/\mathcal{V})^{1/2}[1+(ka_B)^2]^{-2}$ is the Fourier transform of the acceptor wave function. After factorization and under the assumption of a negligible acceptor occupation, this yields for the spectrum

$$\frac{d}{dt}N^{\rm inc}_{\mathbf{q}\nu}=\frac{2\pi}{\hbar}\sum_{\mathbf{k}}|\mu_{\mathbf{q}\nu}|^2|\gamma_{\mathbf{k}}|^2\delta(\epsilon^e_{\mathbf{k}}-\epsilon^a-\hbar\omega_{\mathbf{q}})f^e_{\mathbf{k}}, \quad (116)$$

i.e., the same result as for the band-to-band case, in which the hole distribution function is replaced by the time-independent quantity $|\gamma_{\mathbf{k}}|^2$. Here, ϵ^a is the energy of the acceptor level in the electron picture. This shows that band-to-acceptor luminescence spectra provide direct information on the electron distribution function.

5. Influence of other interaction mechanisms

In the previous sections only the contributions of the single-particle Hamiltonian to the equation of motion for the photon-assisted density matrix have been taken into account. Of course, like its semiclassical counterpart, the interband polarization, the photon-assisted density matrix will also be influenced by other interaction mechanisms. We can easily obtain the contributions due to these interaction Hamiltonians by noticing that we can write the equation of motion as

$$\frac{d}{dt}r^{j_1i_1}_{\mathbf{q}\nu}|^{(cc,cp)}=\left\langle(a^\dagger_{\mathbf{q}\nu}-\langle a^*_{\mathbf{q}\nu}\rangle)\frac{d}{dt}(d_jc_i)|^{(cc,cp)}\right\rangle. \quad (117)$$

Thus we obtain exactly the same operator combinations as in the case of interband polarization, which are only multiplied by a photon creation operator. After factorization, if this polarization is replaced by the photon-assisted density matrix, all terms linear in the interband polarization that have been derived in the previous sections remain the same. Terms without an interband polarization do not contribute, since we have neglected photon-induced intraband transitions in the Hamiltonian. Terms with higher powers of the interband polarization give additional contributions where one of the polarizations is replaced by the photon-assisted density matrix. In many cases, however, particularly if luminescence from band states instead of exciton states is studied, these terms are of minor importance.

The results obtained in the previous sections for the interband polarization can now be directly applied to the photon-assisted density matrix. The first-order contributions due to carrier-phonon and carrier-carrier interaction are obtained by simply adding the respective self-energies [Eqs. (48) and (76)] to the single-particle energies in Eq. (110). In particular, in the case of a homogeneous system we obtain (Kuhn and Rossi, 1992b)

$$\frac{d}{dt}r^{\mathbf{k}}_{\mathbf{q}\nu}=\frac{1}{i\hbar}\sum_{\mathbf{k}'}\alpha_{\mathbf{k}\mathbf{k}'}(\omega_{\mathbf{q}})r^{\mathbf{k}'}_{\mathbf{q}\nu}-\frac{1}{i\hbar}\mu_{\mathbf{k}}f^e_{\mathbf{k}}f^h_{-\mathbf{k}}, \quad (118)$$

where

$$\alpha_{\mathbf{k}\mathbf{k}'}(\omega_{\mathbf{q}})=\left[\epsilon^e_{\mathbf{k}}+\epsilon^h_{-\mathbf{k}}-\hbar\omega-\sum_{\mathbf{k}''}V_{\mathbf{k}-\mathbf{k}''}(f^e_{\mathbf{k}''}+f^h_{-\mathbf{k}''})\right]\times\delta_{\mathbf{k}\mathbf{k}'}-(1-f^e_{\mathbf{k}}-f^h_{-\mathbf{k}})V_{\mathbf{k}-\mathbf{k}'}. \quad (119)$$

This equation, supplemented by the respective stimulated terms as well as by a phenomenological dephasing rate and combined with the respective equations for electron, hole, and photon distribution functions, has been called the *semiconductor luminescence equation* (Kira, Jahnke, and Koch, 1998).

The semiclassical luminescence spectrum is given by

$$\frac{d}{dt}N^{\rm inc}_{\mathbf{q}\nu}=\frac{1}{i\hbar}\sum_{\mathbf{k},\mathbf{k}'}\{\mu_{\mathbf{k}}\mu^*_{\mathbf{k}'}[\alpha^{-1}(\omega_{\mathbf{q}})]_{\mathbf{k}\mathbf{k}'}-\mu^*_{\mathbf{k}}\mu_{\mathbf{k}'}[\alpha^{*-1}(\omega_{\mathbf{q}})]_{\mathbf{k}\mathbf{k}'}\}f^e_{\mathbf{k}'}f^h_{-\mathbf{k}'}. \quad (120)$$

With the bare Coulomb potential and in the absence of band-gap renormalization, the inverse of the matrix α—including an infinitesimal imaginary part—corresponds to the exciton propagator, which can be calculated analytically. Taking into account screening, band-gap renormalization, and a finite dephasing rate, we can calculate the inverse numerically by using techniques that have been developed for the calculation of quasiequilibrium absorption spectra (Schmitt-Rink, Löwenau, and Haug, 1982; Haug, 1988).

The second-order contributions due to carrier-phonon and carrier-carrier interaction are given by

$$\frac{d}{dt}r^{\mathbf{k}}_{\mathbf{q}\nu}|^{(2)}=-\sum_{\mathbf{q}}(\mathcal{W}_{\mathbf{k}-\mathbf{q},\mathbf{k}}r^{\mathbf{k}}_{\mathbf{q}\nu}-\mathcal{W}_{\mathbf{k},\mathbf{k}-\mathbf{q}}r^{\mathbf{k}-\mathbf{q}}_{\mathbf{q}\nu}), \quad (121)$$

where the transition matrices are the same as in Eqs. (64) and (87). Thus the same compensation effects between in- and out-scattering terms apply here as well. This will be discussed in more detail in Sec. III.A.2.

Including these terms, the equation of motion for the photon-assisted density matrix again has the same form as in Eq. (118), but with the matrix $\tilde{\alpha}$ given by

$$\tilde{\alpha}_{\mathbf{k}\mathbf{k}'}(\omega_{\mathbf{q}})=\left[\epsilon^e_{\mathbf{k}}+\epsilon^h_{-\mathbf{k}}-\hbar\omega_{\mathbf{q}}-\sum_{\mathbf{k}''}V_{\mathbf{k}-\mathbf{k}''}(f^e_{\mathbf{k}''}+f^h_{-\mathbf{k}''})-i\hbar\sum_{\mathbf{k}''}\mathcal{W}_{\mathbf{k}'',\mathbf{k}}\right]\delta_{\mathbf{k}\mathbf{k}'}-(1-f^e_{\mathbf{k}}-f^h_{-\mathbf{k}})V_{\mathbf{k}-\mathbf{k}'}+i\hbar\mathcal{W}_{\mathbf{k},\mathbf{k}'}. \quad (122)$$

For sufficiently slowly varying distribution functions, the semiclassical spectrum is again obtained by inverting this matrix, which now includes broadening due to carrier-phonon and carrier-carrier scattering processes. A numerical solution of the equation of motion for the photon-assisted density matrix yields the quantum-kinetic spectrum.

Band-to-acceptor spectra, including many-body and dephasing processes, can be obtained in the same way, by replacing the self-energies and transition matrices with those derived in Sec. II.E.6 for the band-to-acceptor polarization.

G. Theoretical modeling of typical experiments

Virtually all experiments in the ultrafast time domain are carried out in the optical regime, which means that the semiconductor is optically excited by a short laser

pulse and the detected signal is again electromagnetic radiation. Therefore the modeling of such experiments has to take into account three basic features: the creation of electronic excitations by the exciting light field, the subsequent carrier dynamics in the semiconductor, and the generation of the emitted electromagnetic radiation. The excitation of the semiconductor by a classical electromagnetic field has been treated in Sec. II.C, while the generation of coherent and incoherent radiation has been described in Sec. II.F. For the modeling of the carrier dynamics we have to distinguish between two cases: excitation by a single pulse, as is typical of luminescence or terahertz-emission experiments, and excitation by two pulses traveling in different directions, as is the case in pump-probe and four-wave-mixing experiments.

If the semiconductor is excited by a single pulse with a sufficiently large spatial extension, the equations of motion as derived in Sec. II for the homogeneous case can be directly applied. In this case the direction of the incident pulse is the only preferred direction, and the coherent emission will also take place in this direction. Due to disorder, light scattering in other directions, the so-called *Rayleigh scattering*, is also possible. An incoherent emission of photons, on the other hand, may occur in any direction; this is usually called *luminescence*. Since in many cases it is difficult to distinguish between these two contributions, the more general name *secondary emission*, including both phenomena, has become common usage. Here we shall concentrate on some aspects related to luminescence. Recent results on Rayleigh scattering and on other aspects of the secondary emission have been presented by Wang *et al.* (1995), Haacke *et al.* (1997), Birkedal and Shah (1998), Woerner and Shah (1998), Garro *et al.* (1999), and Haacke *et al.* (2000).

Many luminescence experiments have been interpreted on a purely incoherent basis. In this case the carrier dynamics are completely described in terms of distribution functions, and their temporal evolution is dictated by Boltzmann equations. The spectral and temporal shapes of the corresponding generation and emission rates are obtained from Fermi's golden rule. Within this approach the luminescence spectrum due to band-to-band transitions is a direct probe of the product of electron and hole distribution functions at the corresponding transition energy, while the band-to-acceptor spectrum directly monitors the electron distribution function. Because the Boltzmann equation is a rate equation, it is well suited to stochastic simulations based on the well-known Monte Carlo method. Sophisticated programs involving a large variety of scattering mechanisms as well as details of the band structure have been developed and applied to many experimental investigations (Osman and Ferry, 1987; Goodnick and Lugli, 1988; Stanton, Bailey, and Hess, 1988; Lugli *et al.*, 1989; Rieger *et al.*, 1989; Hohenester *et al.*, 1993; Rota *et al.*, 1993, 1995; Supancic *et al.*, 1996). If coherence phenomena do not play an important role—as is typically the case on not-too-short time scales—a good agreement between theory and experiment has been achieved and much has been learned about the characteristic times of the various scattering processes. To overcome the problem of screening, which is particularly important for carrier-carrier scattering processes, molecular-dynamics schemes were developed that directly simulate in phase space the dynamics of an ensemble of interacting electrons, while still treating the interactions with the lattice within a Monte Carlo scheme. Compared to Monte Carlo simulations using a time-dependent quasistatic screening model, the molecular-dynamics results showed a faster initial broadening at high carrier densities, which is in better agreement with experiments (Hohenester *et al.*, 1993; Rota *et al.*, 1993). However, as will be discussed in more detail in Sec. III.A, it turns out that for this initial broadening the inclusion of coherence phenomena may be essential.

Coherence in the photogeneration process is taken into account by treating the interband polarization as an independent dynamical variable. If the scattering processes are treated on a semiclassical level, it is still possible to use a generalized Monte Carlo approach to treat the scattering terms in the equations for the distribution functions (Kuhn and Rossi, 1992a, 1992b) or in the equations for the polarization (Rossi *et al.*, 1994; Haas *et al.*, 1996), but direct-integration methods have also been widely used (Rappen, Peter, and Wegener, 1994; Jahnke and Koch, 1995; Jahnke *et al.*, 1996; Pötz, 1996b; Joschko *et al.*, 1997).

Coherence and correlation phenomena in the photoemission process are included by taking into account the photon-assisted density matrices introduced in Sec. II.F. As discussed there, on this level excitonic effects, Coulomb enhancement, and renormalization, as well as broadening due to scattering processes, can be included. If memory effects ("electron-photon quantum kinetics") are neglected, the photon-assisted density matrices can be adiabatically eliminated and the spectrum is obtained by performing a matrix inversion in which, however, the matrix is a function of time.

Typical terahertz signals constitute coherently emitted electromagnetic radiation. Therefore a quantized treatment of the field is not necessary in this case. Instead, they are calculated directly from the intraband polarization or from the oscillating current density induced by the exciting light field, which act as sources for a classical field.

If the semiconductor is excited by two or more pulses traveling in different directions or by a strongly localized pulse, the excitation corresponds to a spatially inhomogeneous electric-field distribution and thus the full theory, including nondiagonal single-particle density matrices, has to be used. If the typical length scales introduced by the excitation are sufficiently large, however, the Wigner representation in combination with the gradient expansion—as introduced in Sec. II.C.3—can be conveniently employed. The characteristic length scale in a two-pulse pump-probe or four-wave-mixing experiment is the period of the transient grating created in the sample. If λ is the wavelength of the exciting pulses and α the angle between the two incident directions, this pe-

riod is given by $\lambda/[2\sin(\alpha/2)]$, which is typically at least in the micrometer range. Since in the absence of strong electric fields transport processes over this distance can usually be neglected on a femtosecond time scale, the dynamics are well described by the lowest-order contribution in the gradient expansion, i.e., by the equations of motion for the homogeneous case in which all the quantities now depend parametrically on the spatial coordinate $\mathbf{r}$. For an exciting electric field of the form

$$\mathbf{E}(\mathbf{r},t)=\mathbf{E}_1(t)e^{i\mathbf{q}_1\mathbf{r}}+\mathbf{E}_2(t)e^{i\mathbf{q}_2\mathbf{r}}+\text{c.c.}$$
$$=e^{i\mathbf{q}_1\mathbf{r}}[\mathbf{E}_1(t)+\mathbf{E}_2(t)e^{i(\mathbf{q}_2-\mathbf{q}_1)\mathbf{r}}]+\text{c.c.}, \quad (123)$$

all dynamical variables can be expanded in a Fourier series (Lindberg, Binder, and Koch, 1992) as[5]

$$f_{\mathbf{k}}(\mathbf{r})=\sum_n f_{\mathbf{k}}^{(n)}e^{in(\mathbf{q}_2-\mathbf{q}_1)\mathbf{r}},$$

$$p_{\mathbf{k}}(\mathbf{r})=e^{i\mathbf{q}_1\mathbf{r}}\sum_n p_{\mathbf{k}}^{(n)}e^{in(\mathbf{q}_2-\mathbf{q}_1)\mathbf{r}}. \quad (124)$$

Here, $f_{\mathbf{k}}^{(0)}$ is the spatially averaged distribution function, $f_{\mathbf{k}}^{(1)}$ and $f_{\mathbf{k}}^{(-1)}$ describe transient grating terms, and higher orders of $f_{\mathbf{k}}$ describe a nonsinusoidal shape of this grating. $p_{\mathbf{k}}^{(0)}$ and $p_{\mathbf{k}}^{(1)}$ describe polarizations traveling in the directions of the pulses; thus, if pulse 2 is the probe pulse, pump-probe signals are calculated from $p_{\mathbf{k}}^{(1)}$. In particular, assuming an optically thin sample by neglecting any propagation effects, as is always done in this review, the differential transmission spectrum $\Delta T(\omega)$ is obtained from the total polarization in the probe direction $P^{(1)}=\Sigma_{\mathbf{k}}Mp_{\mathbf{k}}^{(1)}$ by Fourier transformation: according to

$$\Delta T(\omega)\sim\frac{\mathrm{Im}[E_2^*(\omega)\delta P^{(1)}(\omega)]}{|E_2(\omega|^2}, \quad (125)$$

where $\delta P^{(1)}$ is the difference between the polarization calculated with and without the pump pulse (Lindberg and Koch, 1988b; Balslev, Zimmermann, and Stahl, 1989).

The diffracted polarizations $p_{\mathbf{k}}^{(2)}$ and $p_{\mathbf{k}}^{(-1)}$ give rise to four-wave-mixing signals. Again, in the absence of propagation effects, the emitted fields are essentially proportional to the polarizations $P^{(\nu)}=\Sigma_{\mathbf{k}}Mp_{\mathbf{k}}^{(\nu)}$, where $\nu=2$ and -1; therefore both temporally and spectrally resolved signals are directly given by $|P(t)|^2$ and $|P(\omega)|^2$, respectively. Since the feedback from higher to lower orders in the Fourier expansion is usually not very strong, the series is truncated either at the desired order or at most one order above. With this technique the calculation of pump-probe and four-wave-mixing signals requires increasing the number of variables by a factor of about 4 with respect to the single-pulse calculation. An alternative method that avoids the increase in the number of variables has been proposed by Bányai *et al.* (1995; Haug and Jauho, 1996). It is based on the observation that if the phase difference ϕ between the pulses is treated as a continuous variable equal to $(\mathbf{q}_2-\mathbf{q}_1)\mathbf{r}$ and the dynamics are calculated for all phases ϕ, the polarization components in the various directions can be obtained by a Fourier transform,

$$p_{\mathbf{k}}^{(n)}=\frac{1}{2\pi}\int_0^{2\pi}p_{\mathbf{k}}(\phi)e^{in\phi}d\phi. \quad (126)$$

This method is particularly useful in quantum-kinetic calculations, in which the number of variables in the homogeneous case is often already very large and a further increase is not possible due to memory limitations.

III. SELECTED EXPERIMENTAL AND THEORETICAL RESULTS

A. Line shape of luminescence spectra

As mentioned above, measurements of the luminescence spectrum were among the first optical experiments to yield information on nonequilibrium carrier dynamics in semiconductors, and they are still widely applied to a variety of semiconductor materials and structures. For a long time they were rather successfully interpreted in terms of a fully incoherent picture based on the Boltzmann equation and transition rates obtained from Fermi's golden rule. However, it turned out that several features in the spectra—particularly in spectral regions directly related to the carrier photogeneration process—were hard to explain. In this section we shall discuss effects due to a coherent description of carrier dynamics. For this purpose we shall first compare the carrier photogeneration process treated in an incoherent picture with the corresponding coherent description based on the semiconductor Bloch equations. Then we shall analyze the photoemission process on the same level. Finally, we shall show that this coherent treatment indeed provides a much better explanation of experimentally observed band-to-acceptor luminescence spectra.

1. Coherent carrier photogeneration

According to Fermi's golden rule, the generation rate of electrons and holes is given by a product of temporal and spectral shapes of the exciting laser pulse, as obtained in the case of a Gaussian pulse in Eq. (33). In a coherent picture, on the other hand, carrier generation is a two-step process according to Eq. (26): First, the light field creates an interband polarization and then the polarization itself interacts again with the field, creating electron and hole populations. The photogeneration rates obtained in these two pictures are plotted at four different times in Fig. 3 for the case of a 150-fs pulse centered at 1.68 eV and material parameters corresponding to bulk GaAs. In the case of Fermi's golden

[5]It should be noted that this Fourier expansion only holds in the case of a rotating-wave approximation and in the absence of Coulomb terms that do not conserve the number of electron-hole pairs. Otherwise, the clear separation between distribution functions and polarizations is lost and a different expansion involving additional Fourier components has to be performed.

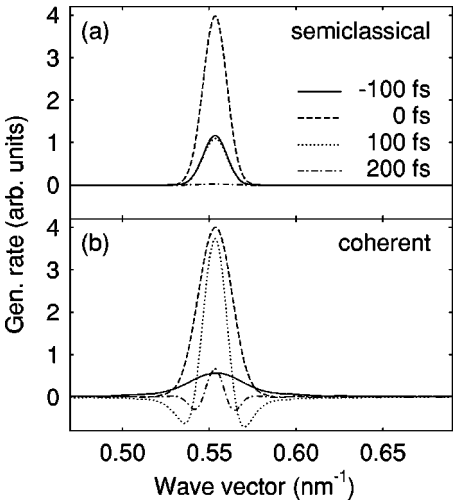

FIG. 3. Generation rate of a 150-fs laser pulse as a function of wave vector at different times: (a) semiclassical and (b) coherent picture. No dephasing processes have been taken into account. After Kuhn and Rossi, 1992b.

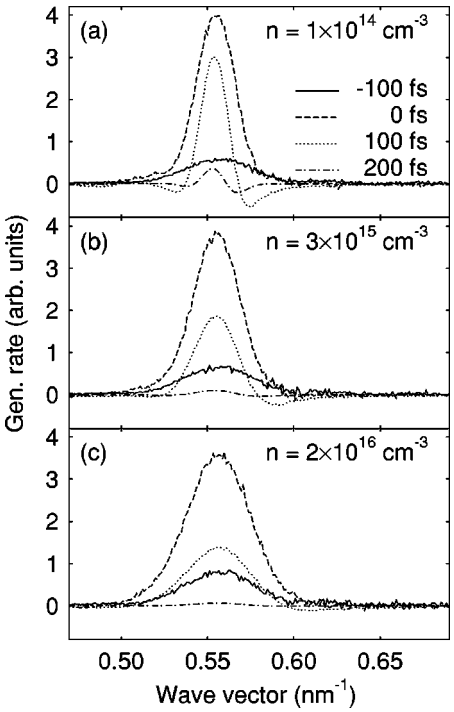

FIG. 4. Coherent generation rate of a 150-fs pulse at three different densities, including dephasing due to carrier-carrier and carrier-phonon scattering. After Leitenstorfer *et al.*, 1996.

rule, the spectral shape is time independent, except for the phase-space-filling terms, which are responsible for the slight difference between the curves at -100 fs and 100 fs. In contrast, the generation rate obtained from the Bloch equations in the absence of carrier-phonon and carrier-carrier scattering exhibits a pronounced time dependence of the spectral shape. The generation starts out very broad; with increasing time the shape becomes narrower, and negative values appear in the wings. From a physical point of view this can be easily understood: As in the semiclassical case, the spectral width is determined by energy-time uncertainty. Due to causality, however, only the time from the onset of the laser pulse up to the observation time determines the broadening, leading to a spectrally very broad rate at early times. With increasing time, the energy uncertainty decreases, and since there is still complete phase coherence between the carriers and the laser field, those carriers generated off-resonance perform a stimulated recombination leading to negative wings. As a result, the time-integrated generation rate agrees with the semiclassical case as long as phase-space filling is not important, and one should expect that for measurements performed after the exciting pulse has gone, there should be no big difference.

The situation changes if scattering processes are taken into account. The semiclassical rate is not affected by these processes, since on a Boltzmann level all interaction processes are treated independently. In the Bloch case, on the other hand, the generation rate is still given by Eq. (26); the polarization dynamics, however, are strongly influenced by carrier-phonon and carrier-carrier interactions. In the present case of a homogeneous system and an excitation high up in the band, the most important contributions are given by the second-order terms, which lead to a dephasing of the interband polarization.

Figure 4 shows generation rates for different pulse intensities (specified by the final carrier density) obtained from the semiconductor Bloch equations, taking into account first-order carrier-carrier contributions (Hartree-Fock) as well as second-order carrier-carrier and carrier-phonon contributions on a Markovian level according to Eqs. (62) and (85). Now the shape of the generation rate becomes strongly density dependent. Due to dephasing by scattering processes, coherence is lost and, as a consequence, the stimulated recombination processes in the wings are inhibited, thereby reducing the narrowing of the spectral shape with increasing time. The dominant process for this density dependence is carrier-carrier scattering. At lower densities dephasing is essentially due to carrier-phonon scattering only. The corresponding dephasing rate is of the order of 200 fs; therefore, on the time scale of the pulse, it is not yet very efficient. We observe only a slight reduction of the negative parts. With increasing density, however, the loss of coherence increases and the negative parts are more and more reduced. The generation rate remains broad during the pulse, leading to a much broader carrier distribution after the pulse, compared to the semiclassical case. In Sec. III.A.3 we shall show how this broadening of the carrier generation process influences band-to-acceptor spectra.

It should be noted that a physically reasonable density dependence is obtained only if both in- and out-scattering-type second-order contributions as given in Eq. (85) are included, particularly in the case of carrier-carrier scattering. Sometimes it has been argued that, due to random phases, in-scattering contributions can be neglected. Then, the scattering terms reduce to a **k**-dependent dephasing rate, given by the total out-

scattering rate. As discussed in detail by Rossi *et al.* (1994) and Haas *et al.* (1996), this results in an essentially density-independent, very strong broadening. The physical reason for this strong overestimation of the dephasing at low densities is the assumption inherent in this approximation that each scattering process completely destroys the coherence. However, at low densities most of the two-body scattering processes are characterized by a very small momentum transfer $\mathbf{q}$, which, in turn, leads to a very small energy exchange and thus to very small dephasing.

In addition to the scattering-induced broadening of the generation rate, there are, of course, other cases in which the semiclassical rate [Eq. (33)] no longer holds. Close to the semiconductor band gap, carrier-light interaction is strongly influenced by excitonic effects. In the semiconductor Bloch equations such effects are described by the first-order carrier-carrier contributions, in particular by the internal field. Here, a semiclassical generation rate can again be obtained by adiabatic elimination of the polarization, which, however, has to be performed in an exciton basis. If the laser pulse intensity is very high, the assumption of slowly varying distribution functions is no longer satisfied. Here, the semiconductor Bloch equations give rise to Rabi-type oscillations, well known from the physics of two-level systems. Since a continuum of energies is involved in band-to-band excitations, no complete Rabi oscillations are possible; nevertheless, the total generation rate still exhibits nonmonotonic behavior (Kuhn and Rossi, 1992b; Fürst, Leitenstorfer, Nutsch, *et al.*, 1997). Even for excitonic excitation, which is closer to a two-level model, Coulomb effects and the presence of the continuum strongly modify the Rabi oscillations, but in this case multiple oscillations with a frequency depending linearly on the field amplitude have been observed (Schülzgen *et al.*, 1999).

2. Luminescence line shape

Luminescence is the inverse process to the generation of carriers by light absorption. Therefore features similar to those discussed in the previous section should occur in the emission process as well, leading again to modifications in the luminescence spectra when compared to the Fermi's golden rule result. The theoretical description is somewhat more complicated, since, as discussed in Sec. II.F, it requires a quantum-mechanical treatment of the light field in which the photon-assisted density matrix, instead of the interband polarization, is the relevant variable introduced by the interaction. Nevertheless, the many-body contributions appear in the same way as in the case of the interband polarization, since neither carrier-phonon nor carrier-carrier interactions couple directly to the photons. Therefore, the same scattering matrices responsible for the broadening of the generation process give rise to the broadening of the band-to-band luminescence spectrum.

In order to focus on the broadening of the luminescence spectrum—and to avoid the broadening of the distribution function due to the scattering of the excited carriers—here, we show luminescence spectra obtained for a stationary distribution function of electrons and holes, generated by a laser pulse according to the models in the previous section (Kuhn, Rossi, *et al.*, 1996; Leitenstorfer *et al.*, 1996). Since the distribution functions after the pulse are constant, the spectra are obtained by inverting the matrix in Eq. (122). In Figs. 5(a)–(c) luminescence spectra, calculated according to four different models, are plotted for three different carrier densities. The dot-dashed lines show the fully semiclassical result obtained by calculating both generation and luminescence according to Fermi's golden rule. In this case the spectrum is simply given by the square of the exciting laser spectrum multiplied by the density of states. The dashed lines show the luminescence spectra obtained by solving the semiconductor Bloch equations, taking into account the broadening of the generation process, while the luminescence process is described by the semiclassical formula, thus introducing no additional broadening. The dotted lines show the opposite case: semiclassical generation and luminescence including broadening. These curves essentially agree with the dashed ones, which again demonstrates the fact that it is the same physics that broadens the transitions. Finally, the solid lines display the spectra in which broadening has been included for both the generation and emission processes. From these results it is clear that, with rising density, the semiclassical model increasingly underestimates the width of the luminescence spectra; the broadening of both generation and emission processes has to be taken into account.

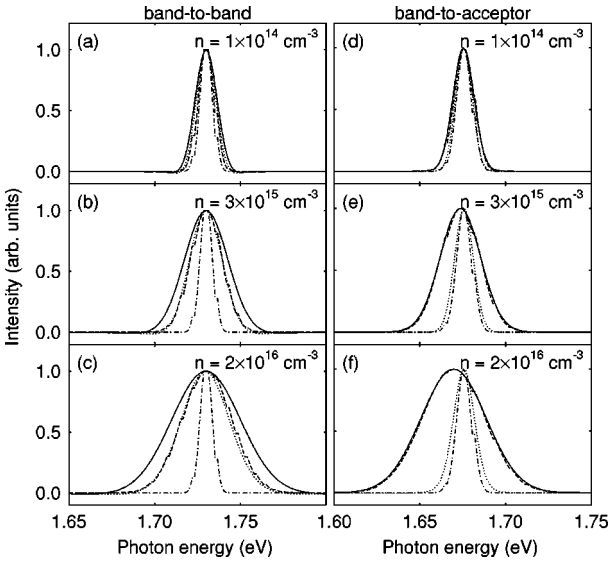

FIG. 5. Spectral profile of band-to-band [(a)–(c)] and band-to-acceptor [(d)–(f)] luminescence at different densities calculated for a carrier distribution generated by a 150-fs pulse: dot-dashed line, semiclassical generation and recombination; dashed line, broadened generation and semiclassical recombination; dotted line, semiclassical generation and broadened recombination; solid line, broadened generation and recombination. After Leitenstorfer *et al.*, 1996.

Instead of measuring band-to-band luminescence, in *p*-doped semiconductors one can measure band-to-acceptor luminescence, which, as has been mentioned above, has the advantage that it does not involve free holes. Therefore it is usually easier to interpret. Let us now look at the broadening in these experiments. Parts (d)–(f) of Fig. 5 show band-to-acceptor spectra calculated under the same conditions as in parts (a)–(c) for band-to-band spectra. Here, we no longer find an agreement between the dashed and dotted lines; instead, the dashed lines essentially agree with the solid ones. The reason for this behavior can be understood as follows: Since the generation is a band-to-band transition, while the emission is a band-to-acceptor transition, there is no longer symmetry between the two processes and there is no reason why the broadening should be the same. In fact, the broadening of the generation process is much greater, which can be traced back to the fact that dephasing of band-to-acceptor transitions is due to scattering processes of the electrons only, while the dephasing of band-to-band transitions is due to scattering processes of both electrons and holes, the latter usually being much more efficient because of the much higher density of states. Therefore we can conclude that for band-to-acceptor spectra the broadening of the emission process is negligible compared to that of the generation process.

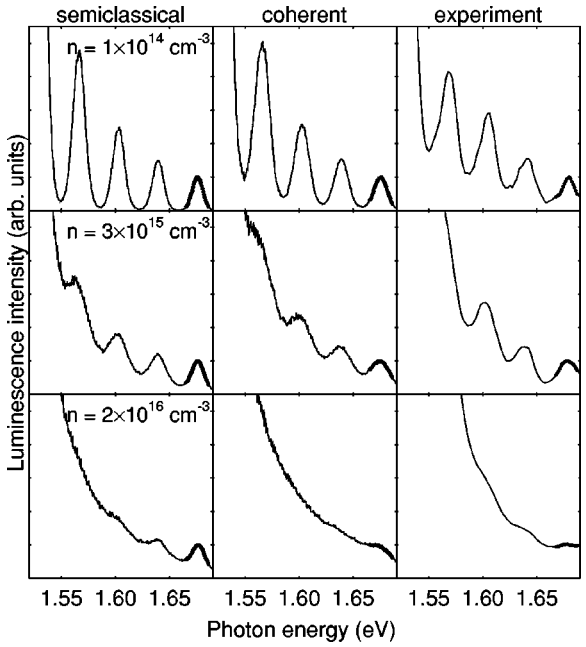

FIG. 6. Band-to-acceptor luminescence spectra at three different excitation densities: left and center panels, theoretically calculated; right panel, experimentally observed. The unrelaxed peak (heavy lines) reflects the broadening of the generation processes as included in the coherent model. After Leitenstorfer, Lohner, Elsaesser *et al.*, 1994.

3. Band-to-acceptor luminescence spectra

In the previous section we have clearly seen that a proper inclusion of the interband polarization dynamics—in particular their density-dependent dephasing—should noticeably modify luminescence spectra. Therefore the question arises whether such calculations can improve the agreement with experimentally observed spectra (Leitenstorfer, Lohner, Elsaesser, *et al.*, 1994; Leitenstorfer *et al.*, 1996). Figure 6 demonstrates that this is indeed the case. Here, time-integrated band-to-acceptor spectra calculated on a semiclassical (Boltzmann) as well as on a coherent (semiconductor Bloch) level for three different densities are compared to experimental results. In agreement with the findings of the previous section, here the broadening of the emission process has been neglected in the calculations. At low densities the spectra exhibit pronounced phonon replicas due to the emission of optical phonons, while carrier-carrier scattering has essentially no effect at the lowest density. In contrast, with increasing density the replicas are more and more washed out due to increasing carrier-carrier scattering. The overall behavior is similar in the Boltzmann and Bloch cases; however, there are remarkable differences, particularly in the region of the peak at the highest energy (marked by heavy lines), which are due to those carriers' not yet having emitted a phonon. In the Boltzmann case this peak is visible up to the highest density because in this picture the carriers are always generated with a narrow distribution, which is subsequently broadened by carrier-carrier scattering. In contrast, in the Bloch case the generation process is broadened as discussed above, which is clearly in much better agreement with the experimental results.

B. Coherent features in pump-probe experiments

Much like luminescence experiments, pump-probe experiments in the band-to-band region have been performed for many years to obtain information on the dynamics of carrier distribution functions. Measurements of the transmission change of a probe pulse due to a previous pump pulse were among the first time-resolved studies of the nonequilibrium dynamics in semiconductors (Shank *et al.*, 1979), and the transmission change has been completely interpreted in terms of Pauli blocking of the optical transitions. However, the direct source for a differential transmission or reflection signal is a third-order polarization created in the sample by the pump and probe pulses. Therefore, on a time scale of the order of the dephasing time, the coherent dynamics of this polarization will influence the signal. Besides the usual phase-space-filling term present when the pump pulse precedes the probe pulse, there are two additional contributions which are also well known from two-level systems (Chachisvilis, Fidder, and Sundström, 1995): First, if the probe pulse precedes the pump pulse by a time delay of the order of or shorter than the dephasing time, the pump pulse perturbs the decay of the probe polarization by suddenly increasing the dephasing rate. This gives rise to the perturbed free polarization decay. Second, if the pulses overlap temporally, they induce a grating in the sample which can diffract the pump pulse

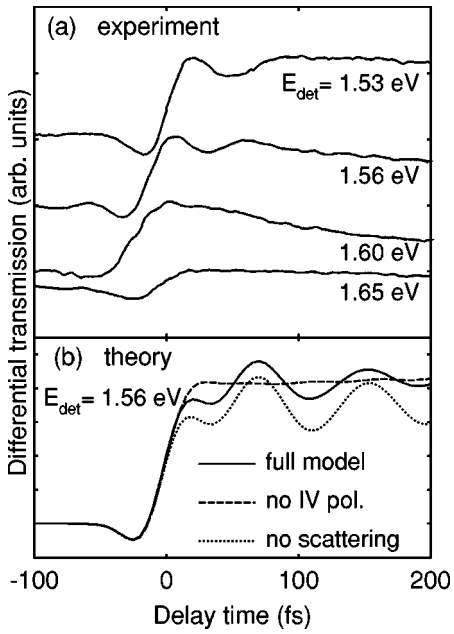

FIG. 7. Differential transmission signals after band-to-band excitation of bulk GaAs with 20-fs pulses: (a) experimentally observed signals at four different energies; (b) calculated signal at 1.56 eV: solid line, the full model; dashed line, without inter-valence-band (IV) polarization; dotted line, without scattering. After Joschko *et al.*, 1997, 1998.

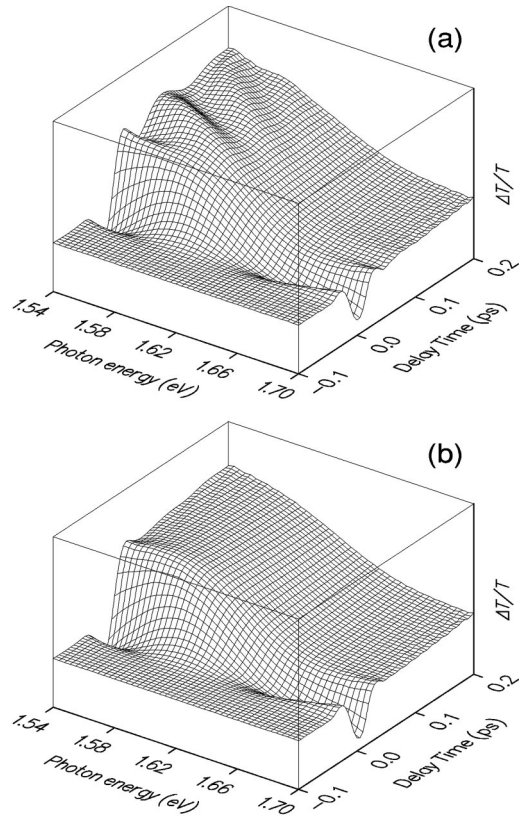

FIG. 8. Differential transmission spectra calculated (a) with and (b) without inter-valence-band polarizations.

into the probe direction. If the probe pulse precedes the pump pulse, these phenomena give rise to spectral oscillations in the differential transmission with a frequency determined by the time delay between both pulses (Fluegel *et al.*, 1987; Lindberg and Koch, 1988c; Likforman *et al.*, 1995). This shows that, on time scales comparable to or shorter than dephasing times, pump-probe spectra are quite complicated to interpret. Grating effects can be even more complicated if, for example, in spatially resolved pump-probe experiments, a nearly collinear excitation has to be used. In this case different, diffracted orders can no longer be distinguished, leading to a superposition of pump-probe, four-wave-mixing, and possibly higher-order contributions (Otremba *et al.*, 1999). Besides these features general to pump-probe experiments, there are additional modifications in a semiconductor due to many-body effects. Electron and hole distributions give rise to band-gap renormalization and, therefore, to a spectral shift. Furthermore, they modify the Coulomb enhancement, which again may lead to an induced absorption in some spectral regions (Fürst, Leitenstorfer, Laubereau, and Zimmermann, 1997). Coulomb correlation effects are even more pronounced in the excitonic region of the spectrum. Here it has been shown that Coulomb sources may even strongly dominate the spectra (Bartels *et al.*, 1997). In particular, in the case of pumping and probing with two countercircularly polarized laser pulses, Pauli blocking—as well as other mean-field contributions—is completely absent and only correlations give rise to a signal (Smith *et al.*, 1994; Axt, Victor, and Stahl, 1996; Sieh *et al.*, 1999). In the following we shall address in more detail a specific coherent feature in band-to-band spectra.

The Pauli blocking terms in a density-matrix theory involve not only distribution functions—i.e., diagonal density-matrix elements—but, if the optical excitation overlaps spectrally with several transitions, also off-diagonal elements describing phase coherence within a given band or between different conduction or valence bands, respectively. Since such off-diagonal elements oscillate in time with a frequency given by the corresponding energy splitting, they give rise to quantum beats in pump-probe signals when plotted as a function of the delay time between pump and probe pulse. In the excitonic region such quantum beats have been observed for many years in different systems, where the interfering states were given by excitons in coupled quantum wells (Leo, Göbel, *et al.*, 1991), spin states in a magnetic field (Bar-Ad and Bar-Joseph, 1991) as well as heavy- and light-hole excitons (Schmitt-Rink *et al.*, 1992). In the band-to-band regime, on the other hand, there is in many cases a continuous variation of splitting energies, for example, in the case of heavy- and light-hole bands. Therefore, even if a superposition is excited, it is not obvious whether quantum beats can be observed in pump-probe signals.

Figure 7(a) shows experimentally observed pump-probe signals at different detection energies obtained from bulk GaAs excited by 20-fs pump and probe pulses at 1.61 eV (Joschko *et al.*, 1997). The pulses overlap with a broad manifold of transitions from the heavy- and the

light-hole band to the conduction band, but they do not overlap with the exciton at about 1.5 eV and therefore clearly probe band-to-band transitions. While under such conditions a spectrally integrated signal exhibits no oscillations, here oscillations are clearly visible on the low-energy side, in particular at 1.56 eV. The variation of the oscillation frequency with the excess energy gives a clear hint that these are indeed heavy-hole/light-hole quantum beats. This interpretation is confirmed by theoretical results obtained from the semiconductor Bloch equations. In Fig. 7(b) the calculated signal at 1.56 eV (solid line) is compared with the results of calculations in which the inter-valence-band polarizations (dashed line) and the carrier-carrier and carrier-phonon scattering (dashed line) have been switched off. Figures 8(a) and (b) show the complete spectra as functions of the photon energy and the delay time with and without inter-valence-band polarization, respectively. If the inter-valence-band polarizations (off-diagonal elements of the hole density matrix) are switched off, these oscillations are absent, unambiguously demonstrating their origin as heavy-hole/light-hole quantum beats in the continuum. From an analysis of the various contributions in the theoretical model, the spectra can be understood in detail (Joschko *et al.*, 1998): The strong asymmetry with respect to the spectral center of the pulses is due to the Coulomb enhancement, which strongly increases the low-energy part; the negative feature around zero time delay is mainly due to the grating effect discussed above; and the damping of the oscillations is due to a combination of dephasing by scattering processes and of the inhomogeneous broadening of the transition frequencies.

The occurrence of quantum beats in spectrally resolved signals can be easily understood from a three-band model of noninteracting carriers. Assuming that the pump pulse at time $-T_D$ creates electron and heavy- and light-hole distributions $f^e_{\mathbf{k}}$, $f^h_{\mathbf{k}}$, and $f^l_{\mathbf{k}}$, as well as an inter-valence-band polarization $f^{lh}_{\mathbf{k}}=\tilde{f}^{lh}_{\mathbf{k}}\exp[(i\omega^{lh}_{\mathbf{k}}-\Gamma^{lh})(t+T_D)]$, where $\hbar\omega^{lh}_{\mathbf{k}}$ is the heavy-hole/light-hole splitting energy at a given $\mathbf{k}$ and Γ^{lh} the corresponding dephasing rate, the linear susceptibility due to a probe pulse at time $t=0$ is given by

$$\begin{aligned}\chi(\omega)=&\sum_{\mathbf{k}}\frac{|M^h|^2(f^e_{\mathbf{k}}+f^h_{\mathbf{k}})}{\hbar\omega-\epsilon^e_{\mathbf{k}}-\epsilon^h_{\mathbf{k}}+i\hbar\Gamma^h}\\&+\sum_{\mathbf{k}}\frac{|M^l|^2(f^e_{\mathbf{k}}+f^l_{\mathbf{k}})}{\hbar\omega-\epsilon^e_{\mathbf{k}}-\epsilon^l_{\mathbf{k}}+i\hbar\Gamma^l}\\&+\sum_{\mathbf{k}}\frac{M^{l*}M^h\tilde{f}^{lh}_{\mathbf{k}}}{\hbar\omega-\epsilon^e_{\mathbf{k}}-\epsilon^h_{\mathbf{k}}+i\hbar\Gamma^h}\frac{E(\omega+\omega^{lh}_{\mathbf{k}})}{E(\omega)}\\&\times e^{(-i\omega^{lh}_{\mathbf{k}}-\Gamma^{lh})T_D}+\sum_{\mathbf{k}}\frac{M^{h*}M^l\tilde{f}^{lh}_{\mathbf{k}}*}{\hbar\omega-\epsilon^e_{\mathbf{k}}-\epsilon^l_{\mathbf{k}}+i\hbar\Gamma^l}\\&\times\frac{E(\omega-\omega^{lh}_{\mathbf{k}})}{E(\omega)}e^{(i\omega^{lh}_{\mathbf{k}}-\Gamma^{lh})T_D}.\end{aligned}\tag{127}$$

Here, Γ^h and Γ^l are interband dephasing rates of the heavy-hole-to-conduction-band and light-hole-to-conduction-band transitions, respectively, M^h and M^l are the corresponding dipole matrix elements, and $E(\omega)$ is the Fourier transform of the electric field of the probe pulse. We have assumed that the distribution functions as well as the inter-valence-band polarization envelope $\tilde{f}^{lh}_k$ are slowly varying during the probe pulse. This result clearly shows that there are oscillating contributions in the spectrum (third and fourth terms). They are damped not only by Γ^{lh}, but also by inhomogeneous broadening, since at a given frequency ω, a range of $\mathbf{k}$ states (the corresponding width being determined by the interband dephasing rate) around the resonant transition frequency contributes to the susceptibility. Furthermore, these terms involving inter-valence-band polarizations depend on the spectral shape of the probe pulse, and they are shifted towards lower (third term) and higher (fourth term) frequency compared to the diagonal (first and second) term. The question remains why oscillations are seen only on the low-energy side in both the experimental and the theoretical spectra. This behavior is also confirmed by Eq. (127) when the $\mathbf{k}$ summation is performed. It turns out that when we calculate the imaginary part of the susceptibility, the two terms resulting from the decomposition $\exp(\pm i\omega^{lh}_{\mathbf{k}}T_D)=\cos\omega^{lh}_{\mathbf{k}}T_D \pm i\sin\omega^{lh}_{\mathbf{k}}T_D$ in the third term add constructively, while in the fourth term they oscillate out of phase, thus canceling each other.

Recently, heavy-hole/light-hole quantum beats in the band-to-band continuum—in particular, their dephasing dynamics—have also been analyzed on the level of a Coulomb quantum-kinetic approach (Mieck and Haug, 1999). It has been found that they should persist in pump-probe spectra even in the density range between 10^{17} and 10^{18} cm^{-3}. In the excitonic part of the spectrum the heavy-hole/light-hole systems more closely resemble a three-level system, and one might expect a simpler interpretation. However, it turns out that here Coulomb effects are even more important. In particular, Coulomb-induced correlations between excitons may even change the sign of the signal or modify the phase of the beats (Bartels *et al.*, 1997), and they efficiently couple heavy-hole and light-hole excitons (Meier *et al.*, 2000).

C. Temporal and spectral shape of four-wave-mixing signals

In a four-wave-mixing experiment the sample is excited by two pulses traveling in directions $\mathbf{q}_1$ and $\mathbf{q}_2$, and the signal is measured in the diffracted direction $2\mathbf{q}_2-\mathbf{q}_1$. If the sample is optically thin, it is usually a good assumption to model the emitted electric field directly by the optical polarization in this direction. To lowest order this is a third-order polarization, but, of course, with increasing power of the pulses, higher-order polarizations also contribute to the signal. For the case of a two-level system and pulses arriving at times $t=-T_D$ and $t=0$, respectively, with pulse durations shorter than the dephasing time, it can be shown that the third-order

polarization in the diffracted direction is directly proportional to the value of the phase-conjugated polarization at $t=0$ created by the first pulse at $t=-T_D$. Since the time-integrated signal decays with a time constant $T_2/2$, this technique provides direct information on the dephasing time T_2. As a function of time, the polarization decays with the dephasing time; it exhibits a free polarization decay. If instead of a single two-level system an inhomogeneously broadened ensemble of such systems is considered, the signal is not emitted immediately after the second pulse due to interference of the different frequency contributions. Instead, its maximum occurs at time $t=T_D$: It exhibits photon-echo behavior. The time-integrated signal in this case decays with a time constant of $T_2/4$. Such an echo signal was first observed in magnetic resonance (Hahn, 1950), here called the spin echo, with dephasing times of the order of 10 ms. In the visible range the first photon echoes were observed in ruby (Kurnit *et al.*, 1964; Abella *et al.*, 1966) with dephasing times of the order of 100 ns.

In a semiconductor the spectrum consists of both a discrete excitonic and a continuous band-to-band part. Furthermore, depending on the sample and the experimental conditions, the exciton line may be either homogeneously or inhomogeneously broadened. Therefore one might expect a more complicated temporal behavior of the four-wave-mixing signal, depending on a variety of parameters. For inhomogeneously broadened two-dimensional excitons in quantum wells excited by 12.6-ps pulses, it was shown during the early stages of coherent spectroscopy in semiconductors that this system exhibits a photon echo (Schultheis *et al.*, 1985). Similar results were obtained for excitons in mixed crystals (Noll *et al.*, 1990). For weak disorder, however, the signals can only be understood in detail if the Coulomb interaction is also included in the model (Jahnke *et al.*, 1994).

For homogeneously broadened excitons it was found that the expected free polarization decay is modified by many-body effects, which, particularly at higher excitation power, strongly dominate the temporal shape of the signal (Leo, Wegener, *et al.*, 1990; Kim, Shah, Damen, *et al.*, 1992; Mycek *et al.*, 1992; Weiss *et al.*, 1992). This behavior is qualitatively well reproduced by calculations based on the semiconductor Bloch equations (Wegener *et al.*, 1990; Lindberg *et al.*, 1992). The most prominent deviation from the two-level case, which also manifests itself in the time-integrated signal, is the appearance of a contribution at negative delay times. Qualitatively, this can be understood on the mean-field level on the basis of a two-level system, which, in addition to the external field, is subject to a local field proportional to the polarization. Here, the polarization created by the first pulse in the direction $\mathbf{q}_2$, which is still present at the arrival of the second pulse, can be diffracted into the observed direction $2\mathbf{q}_2-\mathbf{q}_1$. This contribution, however, is removed by sufficiently strong inhomogeneous broadening. At positive delay times the Coulomb interaction gives rise to a delayed contribution in the signal, the delay being determined by the dephasing time. Besides these mean-field effects of the Coulomb interaction, there are also modifications to the noninteracting carrier case which are related to electronic correlations induced by the Coulomb interaction. As has been shown in detail in Sec. II.E.2, such correlations give rise to nonlinear scattering and relaxation terms. This type of dephasing has been introduced in a simplified way as *excitation-induced dephasing* (Wang *et al.*, 1993; Hu *et al.*, 1994), i.e., a dephasing rate that increases linearly with the carrier density. However, these correlations lead to more than just dephasing. Variables like $B_{j_1,i_1,j_2,i_2}=\langle d_{j_1}c_{i_1}d_{j_2}c_{i_2}\rangle$, which were not discussed in Sec. II because in a correlation expansion they enter at a higher order, include effects related to biexcitons as well as exciton-exciton correlations (Axt and Stahl, 1994b). They again modify four-wave-mixing signals; in particular, they give rise to biexcitonic quantum beats with a frequency determined by the biexciton binding energy (Pantke *et al.*, 1993; Mayer *et al.*, 1994; Bartels *et al.*, 1995). Even if bound biexcitons are excluded due to excitation with two pulses of the same circular polarization, the signals are strongly dominated by such Coulomb correlations, particularly at negative delay times (Kner *et al.*, 1998). We shall come back to the features of biexcitons and exciton-exciton correlations in Sec. III.H when discussing Coulomb quantum kinetics. Quantitatively, it has been found that correlation effects are typically more important than local field corrections for the deviations of four-wave-mixing signals in the excitonic regime from the limiting case of noninteracting two-level systems described by the optical Bloch equations.

In the band-to-band continuum case, which, at least in the limit of noninteracting carriers, is equivalent to an inhomogeneously broadened ensemble of two-level systems, a photon echo behavior is expected. The dephasing in this case was studied as a function of carrier density by using 6-fs pulses (Becker *et al.*, 1988), and the signal was indeed attributed to a photon echo. However, in that work the signal was not time resolved; therefore a clear proof was not possible. A clear photon echo behavior, as found in calculations based on the semiconductor Bloch equations for the case of excitation in the band-to-band continuum (Lindberg *et al.*, 1992; Glutsch, Siegner, and Chemla, 1995), was observed by Lohner *et al.* (1993) after spectral filtering of the continuum contribution, and recently by Hügel *et al.* (1999) in room-temperature measurements with 11-fs pulses. In the following we shall discuss in more detail the results obtained by Lohner *et al.*

In that experiment a bulk GaAs sample was excited by 100-fs pulses slightly above the band edge but still overlapping with the exciton. The diffracted signal was then spectrally as well as temporally analyzed. The spectrally resolved signal for zero time delay at four different excitation densities is shown in Fig. 9(a). The spectrum of the laser pulse is included in Fig. 9(b) as a dashed line. Even if the pulse maximum is in the band, at low densities the spectrum is completely determined by the exciton. Such a strong enhancement of the exciton contribution has been found in quantum wells by scanning

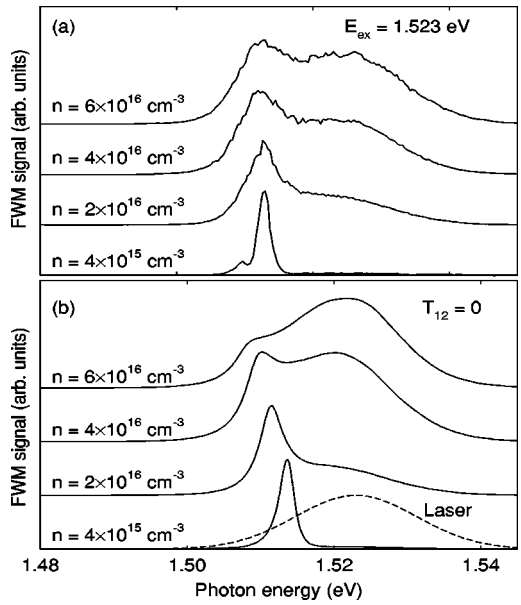

FIG. 9. Spectrally resolved four-wave-mixing (FWM) signals of bulk GaAs excited by two 100-fs pulses with zero delay, 4 meV above the band gap: (a) experimental and (b) theoretical results at different excitation densities. After Lohner *et al.*, 1993.

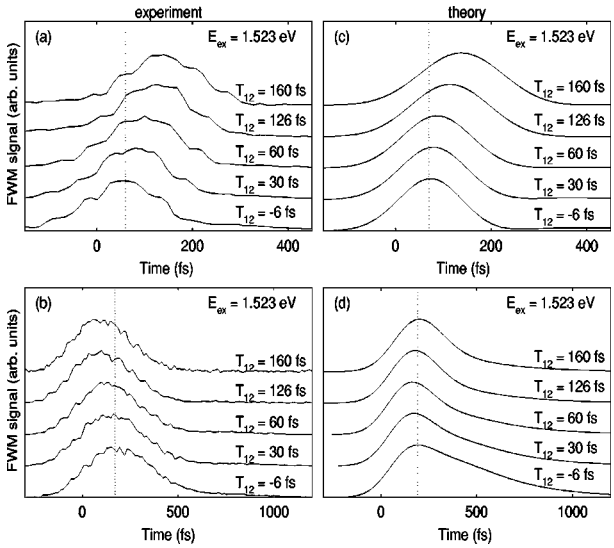

FIG. 10. Measured [(a), (b)] and calculated [(c), (d)] temporally resolved four-wave-mixing (FWM) signals for different delay times: (a), (c) after filtering at the excitation frequency; (b), (d) after filtering at the exciton frequency. After Lohner *et al.*, 1993.

the excitation frequency across the exciton line (Kim, Shah, Cunningham, *et al.*, 1992). With increasing density the exciton is screened and an additional free-carrier contribution appears which is essentially given by the pulse spectrum. This behavior is qualitatively well reproduced by calculations based on the semiconductor Bloch equations, as shown in Fig. 9(b). The slight differences, in particular the slight redshift of the exciton and the stronger free-carrier contribution at higher densities, can be attributed to limitations of the quasistatic screening model used in these calculations and to possible uncertainties in the exact determination of the density. The interesting point here is that the exciton is still clearly visible at densities more than one order of magnitude higher than the Mott density at $T=10$ K (Ulbrich, 1988), which demonstrates that the nonequilibrium distribution is much less effective in screening the electron-hole interaction. At a given density the spectral shape of the signal also strongly depends on the delay (Leitenstorfer, Lohner, Rick, *et al.*, 1994): With increasing negative delay, the excitonic contribution increases, since here the continuum contribution vanishes due to inhomogeneous broadening. For positive delay times the excitonic contribution is decreasing faster than the continuum contribution, which can be attributed to destructive interference between the polarizations of bound and unbound states. A similar two-component behavior of the spectrally resolved four-wave-mixing signal was found at the direct gap of germanium (Rappen *et al.*, 1993).

As one might expect from the discussion above, the temporal shape of the signal in this case will be quite complicated. However, by performing a spectral filtering at either the exciton or excitation frequency, one can extract the two characteristic signal types. This is shown in Figs. 10(a) and (b) for the experimental data and 10(c) and (d) for the theoretical results. The continuum contribution [Figs. 10(a) and (c)] exhibits clear photon echo behavior, while the excitonic contribution [Figs. 10(b) and (d)] exhibits essentially a free polarization decay modified by many-body effects as discussed above. This demonstrates that in a semiconductor these types of signals, which were initially shown to be characteristic of different atomic or magnetic systems, occur simultaneously, and furthermore they can be clearly separated.

If the semiconductor is excited with a shorter pulse higher up in the band, the excitonic contribution is essentially absent and the time-resolved four-wave-mixing signal exhibits photon echo behavior. This is clearly seen in Figs. 11(a) and (b), where experimental and theoretical results, respectively, are shown corresponding to an excitation with 11-fs pulses centered at 50 meV above the band gap (Hügel *et al.*, 1999). The calculations

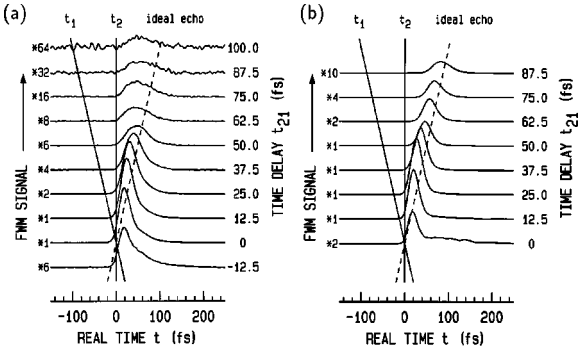

FIG. 11. Temporally resolved four-wave-mixing (FWM) signals for different delay times for the case of excitation by 11-fs pulses centered 50 meV above the band edge: (a) experiment; (b) theory. After Hügel *et al.*, 1999.

shown here are based on a quantum-kinetic treatment of Coulomb and carrier-phonon scattering processes in terms of nonequilibrium Green's functions, which takes into account the dynamical buildup of screening.

D. Coherent control phenomena

The existence of a four-wave-mixing signal in the case of temporally nonoverlapping laser pulses in different directions is clear proof of the coherence in the material. Coherence means that the system is characterized not only by amplitudes but also by phases. This phase sensitivity is demonstrated even more clearly by coherent-control experiments, in which the response of the system is measured after excitation with two temporally nonoverlapping phase-locked laser pulses in the same direction. In a semiclassical picture the first laser pulse creates a certain density of electron-hole pairs. If the system is far from inversion, then a second pulse simply adds another density, which, in the case of equal pulse intensities, is essentially the same as the first pulse. In a coherent picture, as has been discussed in detail above, first a polarization is created and then the interaction of the polarization with the light field leads to the generation of a carrier density. Thus the second pulse may interfere constructively or destructively with the polarization left over from the first pulse. In the absence of dephasing, constructive interference results in a final carrier density that is four times the density of the first pulse alone, while in the case of destructive interference, all carriers generated by the first pulse are removed, leaving an unexcited sample. Therefore, as a function of the delay time between the pulses, the final carrier density exhibits an oscillatory behavior. In the presence of dephasing, these oscillations are damped with increasing delay time until finally, for times much longer than the dephasing time, the semiclassically expected result—i.e., twice the density generated by the first pulse—is recovered.

This was shown by Heberle *et al.* (1995) for excitons in quantum wells. Experimental and theoretical results for the case of two pulses with different intensities are plotted in Fig. 12 at different delay times (Heberle *et al.*, 1996). The sensitivity with respect to the delay time (here given in units of $T_{hh}=2\pi/E_{hh}$, where E_{hh} is the energy of the heavy-hole exciton), as well as the decreasing splitting between the constructive and destructive curves with increasing delay time, is clearly visible. In the experiment the density was extracted from the differential reflectivity change, measured with a third pulse. The deviations from a constant value after the pulses are due to the fact that this quantity is not exactly proportional to the density; instead, as discussed in Sec. III.B.1, it also depends on intraband coherences and the time-dependent momentum distribution of the carriers.

Coherent-control techniques using two temporally separated phase-locked pulses have been applied to a variety of systems. If the pulses are perpendicularly polarized, they do not interfere directly and therefore their relative phase does not influence the total exciton density. However, they may control the spin density in a quantum well sample (Heberle *et al.*, 1996). This can be best understood by decomposing the pulses into their circular polarization components. The first pulse creates a superposition of excitons with spin $s_z=+1$ and $s_z=-1$. If the delay time is $t_{12}=(n\pm 1/4)T_{hh}$, one of the circular components of the second pulse interferes constructively with the corresponding polarization component created by the first pulse, while the other component interferes destructively. As a result, one of the angular momentum components is removed and the other is enhanced, leaving a net angular momentum in the sample. At integer or half-integer multiples of T_{hh}, the interference effectively results in a linear polarization, thus creating no net angular momentum.

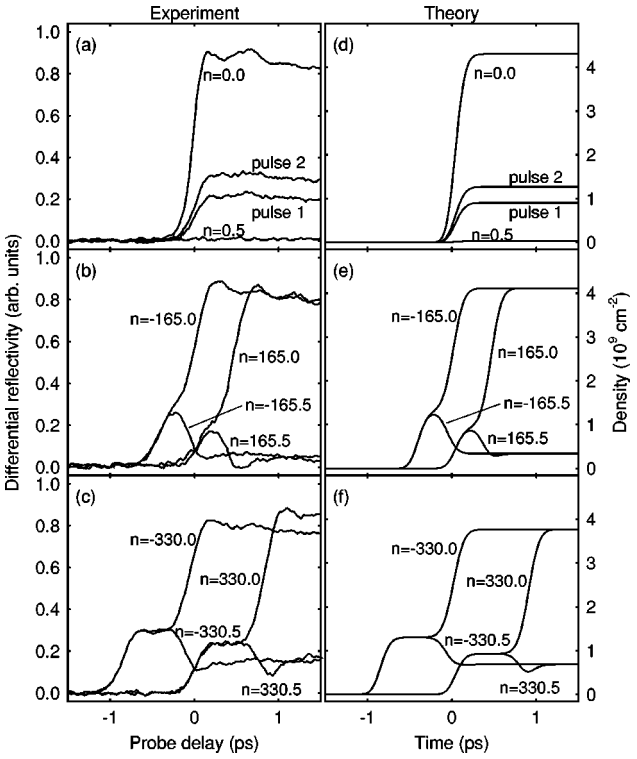

FIG. 12. Coherent-control signals for excitation of a GaAs quantum well structure with two phase-locked pulses of slightly different intensities centered at the heavy-hole exciton at delay times of n times the heavy-hole exciton oscillation period: (a)–(c), measured differential reflection of a probe pulse; and (d)–(f), calculated exciton densities. In (a) and (d) only the signals corresponding to an excitation by pulse one or two have been included. After Heberle *et al.*, 1996.

All kinds of quantum beats can be coherently controlled. They arise due to the excitation of a superposition of two energetically separated levels by a short laser pulse with a spectrum overlapping both transitions. In general, the delay times corresponding to destructive interference of the two transitions are different. Therefore it is possible to select delay times when one component is selectively switched off, removing the quantum beats from the signal (Kuhn *et al.*, 1999). This has been shown for heavy-hole/light-hole beats in quantum wells (Heberle *et al.*, 1995), quantum beats due to charge oscilla-

tions in coupled quantum wells (Luo *et al.*, 1993; Planken *et al.*, 1993), and phonon quantum beats (Wehner *et al.*, 1998; Steinbach *et al.*, 1999). We shall come back to the case of phonon quantum beats in Sec. III.G when we discuss quantum-kinetic phenomena.

In the case of degenerate final states of an optical transition, coherent-control techniques can be used for selective excitations. Here, the quantum interference between a one-photon and a two- or three-photon transition is typically used to control the final states. Based on such an approach, the outcome of chemical reactions (Brumer and Shapiro, 1995) or the photoionization of atoms (Chen, Yin, and Elliot, 1990) can be controlled. In a semiconductor this technique allows one to create a photocurrent in the absence of an applied voltage because the superposition of the light pulses removes the symmetry between the generation of carriers with opposite momenta (Dupont *et al.*, 1995; Atanasov *et al.*, 1996; Haché *et al.*, 1997), which is always present if a single pulse is used. Again, another type of phase-dependent, i.e., coherently controlled, carrier dynamics is obtained in semiconductor nanostructures if interband and intersubband transitions are simultaneously excited by phase-locked fields in their respective frequency ranges (Pötz, 1997a, 1997b, 1998).

E. Charge oscillations in double quantum wells

For all the phenomena discussed in the previous sections, spatial inhomogeneities were irrelevant for the carrier dynamics. In pump-probe and four-wave-mixing experiments inhomogeneities introduced by the different pulse directions, particularly the induced transient grating, were necessary for selecting the desired optical signal; however, all space dependences were treated parametrically and thus all spatial transport phenomena were neglected. This was justified by the large length scales in the micrometer range. The situation changes if inhomogeneities occur on a nanometric scale. In this and the following section, we shall discuss some phenomena related to the spatial dynamics of optical carrier excitation in the growth direction of multiple quantum well structures.

In an asymmetric double quantum well with a sufficiently thin barrier, the states in the two wells are coupled due to tunneling. Typically, in the flat-band case this coupling is not very strong because of the different energies of bound states in the two wells. By applying an electric field, however, one can bring states in the wide and narrow wells into resonance (see the inset in Fig. 13). The resulting delocalized states are then energetically separated by the tunnel splitting and, if the spectral width of the exciting laser pulse is larger than this splitting, a superposition of the two states is excited, leading to quantum beats, as discussed above for the case of heavy and light holes. Such beats have been observed both in the differential transmission and in the four-wave-mixing signal (Leo, Shah, *et al.*, 1991, 1992). The difference with respect to the heavy-hole/light-hole case, however, is the fact that here the superposition leads to

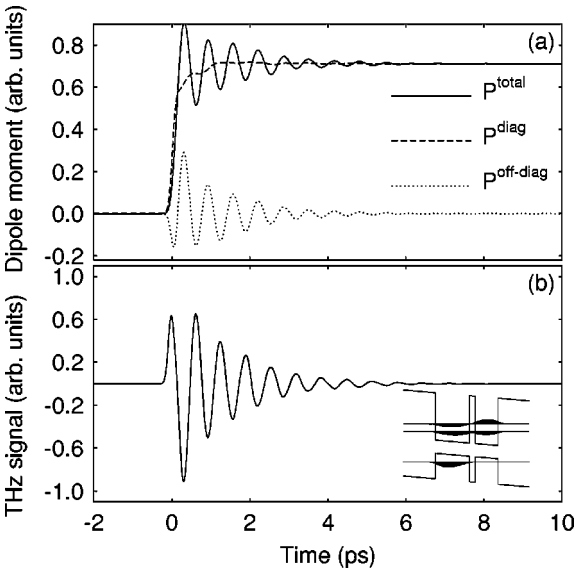

FIG. 13. Oscillating wave packet in a GaAs/AlGaAs asymmetric double quantum well structure: (a) dipole moment (solid line, total moment; dashed line, diagonal contribution; dotted lines, off-diagonal contribution) and; (b) emitted electromagnetic radiation. The inset shows the band edges and the electronic states. After Kuhn *et al.*, 1994.

a spatial oscillation of the electronic wave packet. Since the hole states are not in resonance, the holes essentially remain in the wide well. Thus an oscillating dipole moment is created. Neglecting the interband cotributions, which oscillate much faster, we obtain the dipole moment from the density matrices according to

$$\mathbf{P}=\sum_{i_1 i_2}\sum_{\mathbf{k}}\mathbf{M}^{e}_{i_1 i_2}f^{e}_{i_1 i_2,\mathbf{k}}-\sum_{j_1 j_2}\sum_{\mathbf{k}}\mathbf{M}^{h}_{j_1 j_2}f^{h}_{j_2 j_1,\mathbf{k}}, \qquad (128)$$

where $\mathbf{M}^{e}_{i_1 i_2}$ and $\mathbf{M}^{h}_{j_1 j_2}$ are the electron and hole dipole matrix elements between subbands i_1 and i_2 or j_1 and j_2, respectively, and $\mathbf{k}$ is the in-plane momentum. In Fig. 13(a) the dipole moment excited by a 160-fs laser pulse is plotted as a function of time. This result is obtained from a solution of the semiconductor Bloch equations including two electron and one hole subband (Binder, Kuhn, and Mahler, 1994; Kuhn, Binder, *et al.*, 1994). Here, the dashed and dotted lines show the diagonal and off-diagonal contributions, respectively. The off-diagonal part describes the coherent superposition; it oscillates and finally decays due to dephasing processes.[6] The diagonal part approaches a finite value due to the different localizations of electrons and holes. According to classical electrodynamics, such a time-dependent dipole moment emits electromagnetic radiation proportional to its second derivative, which is plotted in Fig.

[6]Here dephasing has been treated by phenomenological interband and intersubband rates. Results in which the dephasing due to carrier-carrier scattering has been treated on the semiclassical (Boltzmann-Bloch) level can be found in the articles of Pötz, Žiger, and Kocevar (1995), Pötz (1996a), and Binder (1997).

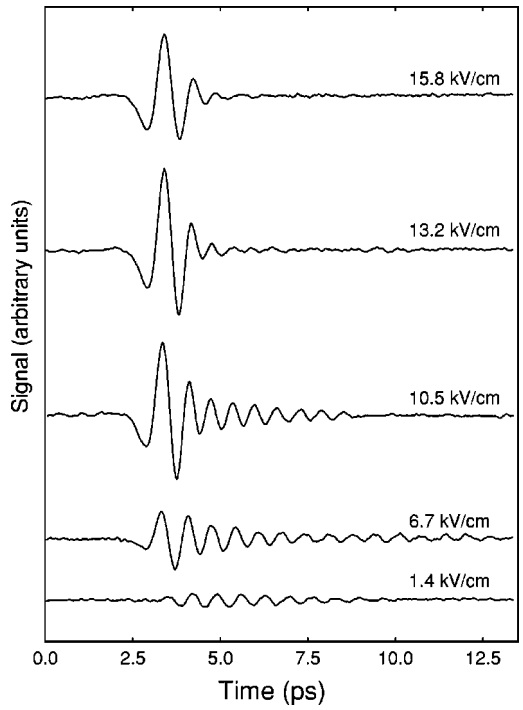

FIG. 14. Measured coherent electromagnetic transients emitted from an asymmetric double-quantum well structure at different bias fields for a photon energy of 1.54 eV. After Roskos *et al.*, 1992.

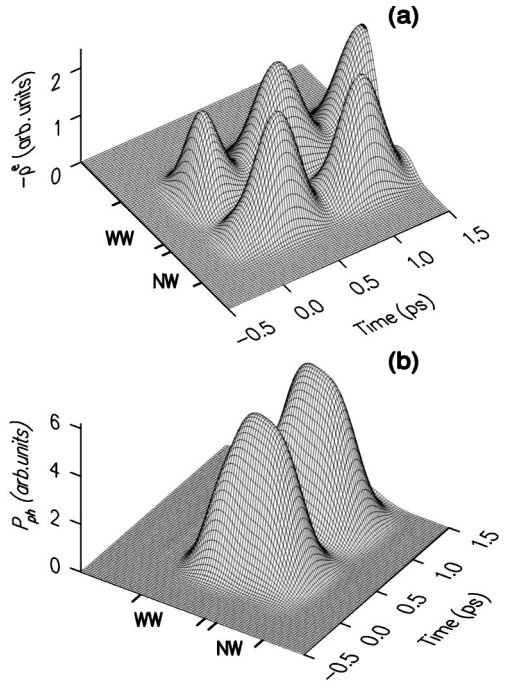

FIG. 15. Oscillating wave packet in the asymmetric double quantum well structure of Fig. 13: (a) electron charge density; (b) induced lattice polarization as functions of position and time.

13(b).[7] Such radiation in the terahertz range has indeed been observed experimentally (Roskos *et al.*, 1992; Nuss *et al.*, 1994). Figure 14 shows electromagnetic transients emitted from an asymmetric double quantum well structure with the same parameters as above at different values of the bias field (Roskos *et al.*, 1992). A coherent emission of terahertz radiation has also been observed in superlattices, as will be discussed in the next section.

Spatial inhomogeneities give rise to two additional features included in the general theory discussed above which are absent in the homogeneous case: coherent phonons and Hartree contributions. An oscillating electronic wave packet polarizes the crystal lattice. This lattice polarization is described by coherent optical phonons according to Eq. (60). Figure 15 shows the electron charge density as well as the lattice polarization as functions of space and time. It can clearly be seen that whenever the electronic wave packet is localized in the narrow well, the lattice polarization is maximal, while it essentially vanishes if the electrons are in the wide well, where their charge density is compensated by the holes. The coherent-phonon amplitudes increase linearly with the density of excited carriers. Therefore they give a density-dependent contribution to the electron and hole self-energies [Eq. (48)]. As shown by the squares in Fig. 16, they tend to reduce the frequency of the electronic oscillation. However, the Hartree terms also increase linearly with carrier density and give rise to density-dependent self-energies [Eq. (76)]. It turns out that they tend to increase the oscillation frequency (triangles in Fig. 16). If both contributions are taken into account, the latter dominates, as shown by the diamonds. Physically, this density dependence can be well understood from classical electrodynamics: The Hartree terms describe the electrostatic forces between electrons and holes. They are attractive, thus increasing the oscillation frequency. These forces, however, are screened by the lattice, which reduces this increase. These calculations

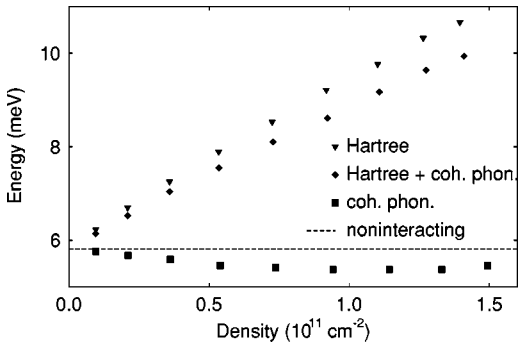

FIG. 16. Oscillation frequency of the dipole moment in the asymmetric double quantum well structure of Fig. 13 as a function of the excited carrier density for free carriers, including space-charge effects (Hartree terms), and/or coherent phonons. After Binder, Preisser, and Kuhn, 1997.

[7]It should be noted that the oscillation frequencies are determined by the exciton energies. The additional appearance of single-particle energies in the spectrum under certain conditions is an artifact of the truncation of the hierarchy as discussed by Axt, Bartels, and Stahl (1996) and Haring Bolivar *et al.* (1997).

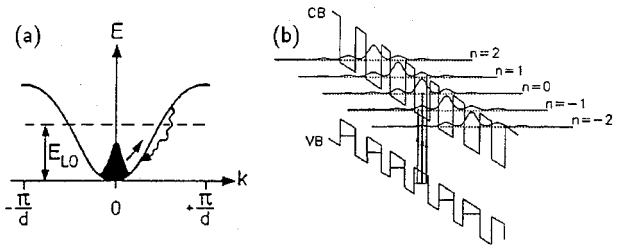

FIG. 17. Bloch oscillations and Wannier-Stark localization in superlattices: (a) the field-induced coherent motion of an electronic wave packet initially created at the bottom of a miniband in the Bloch (miniband) picture; (b) transitions from the valence band (VB) to the conduction band (CB) of a superlattice in the Wannier-Stark picture. Here, the width of the miniband exceeds the LO phonon energy E_{LO}, so that LO phonon scattering is possible. After (a) von Plessen *et al.*, 1994 and (b) Waschke *et al.*, 1993.

therefore include the lattice screening on a fully dynamical and microscopic basis. Frequency changes due to induced electric fields have been used to obtain direct information on the spatial dynamics of charge oscillations in superlattices (Lyssenko *et al.*, 1997).

F. Bloch oscillations and Wannier-Stark localization in superlattices

Ever since the initial applications of quantum mechanics to the dynamics of electrons in solids, the analysis of Bloch electrons moving in a homogeneous electric field has been of central importance. By employing semiclassical arguments, Bloch (1928) demonstrated that a wave packet, given by a superposition of single-band states peaked about some quasimomentum $\hbar\mathbf{k}$, moves with a group velocity given by the gradient of the energy-band function with respect to the quasimomentum and that the rate of change of the quasimomentum is proportional to the applied field $\mathbf{F}$. This is often referred to as the "acceleration theorem":

$$\hbar\dot{\mathbf{k}} = e\mathbf{F}. \tag{129}$$

Thus, in the absence of interband tunneling and scattering processes, the quasimomentum of a Bloch electron in a homogeneous and static electric field will be uniformly accelerated into the next Brillouin zone in a repeated-zone scheme (or equivalently undergoes an umklapp process back into the first zone). The corresponding motion of the Bloch electron through the periodic energy-band structure, shown in Fig. 17(a), is called *Bloch oscillation*; it is characterized by an oscillation period $\tau_B = h/(eFd)$, where d denotes the lattice periodicity in the field direction.

There are two mechanisms impeding a fully periodic motion: interband tunneling and scattering processes. Interband tunneling is an intricate problem and still is the subject of a continuing debate. Early calculations of the tunneling probability into other bands in which the electric field is represented by a time-independent scalar potential were made by Zener (1934), who used a Wentzel-Kramers-Brillouin generalization of Bloch functions; by Houston (1940), who used accelerated Bloch states (Houston states); and subsequently by Kane (1959) and Argyres (1962), who employed the crystal momentum representation. Their calculations led to the conclusion that the tunneling rate per Bloch period is much less than unity for electric fields up to 10^6 V/cm for typical band parameters corresponding to elemental or compound semiconductors.

Despite the apparent agreement among these calculations, the validity of employing the crystal momentum representation or Houston functions to describe electrons moving in a nonperiodic (crystal plus external field) potential has been disputed. The starting point of the controversy was the original paper by Wannier (1960). He pointed out that, due to the translational symmetry of the crystal potential, if $\phi(\mathbf{r})$ is an eigenfunction of the scalar-potential Hamiltonian (corresponding to the perfect crystal plus the external field) with eigenvalue ϵ, then any $\phi(\mathbf{r}+n\mathbf{d})$ is also an eigenfunction with eigenvalue $\epsilon+n\Delta\epsilon$, where $\Delta\epsilon = eFd$ is the so-called Wannier-Stark splitting and $\mathbf{d}$ is the primitive lattice vector along the field direction. He concluded that the translational symmetry of the crystal gives rise to a discrete energy spectrum, the so-called *Wannier-Stark ladder*. The states corresponding to these equidistantly spaced levels are localized, as schematically shown in Fig. 17(b) for the case of a semiconductor superlattice.

The existence of such energy quantization was disputed by Zak (1968), who pointed out that in an infinite crystal the scalar potential $-\mathbf{F}\cdot\mathbf{r}$ is not bounded, which implies a continuous energy spectrum. Thus the main point of the controversy was related to the existence (or absence) of Wannier-Stark ladders. More precisely, the point was to decide whether interband tunneling [neglected in the original calculation by Wannier (1960)] is strong enough to destroy the Wannier-Stark energy quantization (and the corresponding Bloch oscillations).

It was only during the last decade that this controversy came to an end. From a theoretical point of view, most of the formal problems related to the nonperiodic nature of the scalar potential (superimposed on the periodic crystal potential) were finally removed by using a vector potential representation of the applied field (Kittel, 1963; Krieger and Iafrate, 1986). Within such a vector potential picture, upper boundaries for the interband tunneling probability were established at a rigorous level, showing that an electron may execute a number of Bloch oscillations before tunneling out of the band (Krieger and Iafrate, 1986; Nenciu, 1991), in qualitatively good agreement with the earlier predictions of Zener (1934) and Kane (1959).

The second mechanism impeding a fully periodic motion is scattering by phonons, impurities, etc. [see Fig. 17(a)]. This results in lifetimes shorter than the Bloch period τ_B for all reasonable values of the electric field, so that Bloch oscillations should not be observable in conventional solids.

In superlattices, however, the situation is much more favorable because of the smaller Bloch period τ_B resulting from the small width of the mini-Brillouin zone in the field direction (Bastard, 1989).

Indeed, the existence of Wannier-Stark ladders as well as Bloch oscillations in superlattices has been confirmed by a number of recent experiments (Shah, 1999). The photoluminescence and photocurrent measurements of the biased GaAs/GaAlAs superlattices performed by Mendez and co-workers (1988), together with the electroluminescence experiments by Voisin and co-workers (1988), provided the earliest evidence of field-induced Wannier-Stark ladders in superlattices. A few years later, Feldmann and co-workers (1992) were able to measure Bloch oscillations in the time domain through a four-wave-mixing experiment originally suggested by von Plessen and Thomas (1992). A detailed analysis of the Bloch oscillations in the four-wave-mixing signal (which reflects the interband dynamics) was also performed by Leo and co-workers (Leo, Haring Bolivar, *et al.*, 1992; Leisching *et al.*, 1994).

In addition to the above interband polarization analysis, Bloch oscillations have been detected by monitoring the intraband polarization, which, in turn, is reflected by anisotropic changes in the refractive index (Shah, 1999). Measurements based on transmittive electro-optic sampling were performed by Dekorsy and co-workers (1994; Dekorsy, Ott, *et al.*, 1995). Finally, Bloch oscillations were measured through a direct detection of terahertz radiation in semiconductor superlattices (Waschke *et al.*, 1993; Roskos *et al.*, 1994).

1. Two equivalent pictures

Let us now apply the theoretical approach presented in Sec. II to the case of a semiconductor superlattice in the presence of a uniform (space-independent) electric field. The noninteracting carriers within the superlattice crystal will then be described by the Hamiltonian $\mathbf{H}_c^0$ in Eq. (5), where now the electrodynamic potentials $\mathbf{A}_2$ and φ_2 (in the following simply denoted as $\mathbf{A}$ and φ) correspond to a homogeneous electric field $\mathbf{E}_2(\mathbf{r},t) = \mathbf{F}(t)$.

As pointed out in Sec. II.A, the natural quantum-mechanical representation is given by the eigenstates of this Hamiltonian:

$$\left[\frac{\left[-i\hbar\nabla_{\mathbf{r}}+\frac{e}{c}\mathbf{A}(\mathbf{r},t)\right]^2}{2m_0}-e\varphi(\mathbf{r},t)+V^l(\mathbf{r})\right]\phi_n(\mathbf{r}) = \epsilon_n\phi_n(\mathbf{r}). \tag{130}$$

However, due to the gauge freedom discussed in Sec. II, there is an infinite number of possible combinations of $\mathbf{A}$ and φ—and therefore of possible Hamiltonians—that describe the same homogeneous electric field $\mathbf{F}(t)$. In particular, one can identify two independent choices: the vector-potential gauge

$$\mathbf{A}(\mathbf{r},t) = -c\int_{t_0}^{t}\mathbf{F}(t')dt', \quad \varphi(\mathbf{r},t)=0 \tag{131}$$

and the scalar-potential gauge

$$\mathbf{A}(\mathbf{r},t)=0, \quad \varphi(\mathbf{r},t) = -\mathbf{F}(t)\cdot\mathbf{r}. \tag{132}$$

As shown by Rossi (1998), the two independent choices correspond to the well-known Bloch oscillation and Wannier-Stark pictures, respectively. They simply reflect two equivalent quantum-mechanical representations and therefore, any physical phenomenon can be described in both pictures.

More specifically, within the vector potential picture [Eq. (131)], the eigenfunctions ϕ_n in Eq. (130) are the so-called accelerated Bloch states (or Houston states; Houston, 1940; Kittel, 1963; Krieger and Iafrate, 1986). As discussed by Rossi (1998), this time-dependent representation constitutes a natural basis for the description of Bloch oscillations, i.e., it provides a rigorous quantum-mechanical derivation of the acceleration theorem [Eq. (129)], thus showing that this is not a simple semiclassical result.[8] Within this representation, Bloch oscillations are fully described by the diagonal terms of the intraband density matrix (semiclassical distribution functions). Therefore nondiagonal elements describing phase coherence between different Bloch states do not contribute to the intraminiband dynamics. However, they are of crucial importance for the description of interminiband dynamics, i.e., field-induced Zener tunneling, which in this Bloch state representation originates from the time variation of our basis states [see Eq. (23)].

In contrast, within the scalar potential picture [Eq. (132)], the eigenfunctions ϕ_n in Eq. (130) are the well-known Wannier-Stark states (Wannier, 1960). Contrary to the previous Bloch picture, within this representation the intraminiband Bloch dynamics originate from a quantum interference between different Wannier-Stark states, thus involving nondiagonal elements of the intraband density matrix.

In the remainder of this section we shall review a few simulated experiments on ultrafast carrier dynamics in semiconductor superlattices (Je *et al.*, 1995; Koch *et al.*, 1995; Meier *et al.*, 1995; Rossi *et al.*, 1995; Rossi, Gulia, *et al.*, 1996; Rossi, Meier, *et al.*, 1996). In this case, the Bloch representation discussed in Sec. III.F.1 was employed, limiting the set of interband density-matrix elements to the diagonal ones, i.e., $i=j$. In addition, incoherent scattering processes were treated within the usual Markov limit discussed in Sec. II.D. Due to the relatively low electric fields considered, the "intracollisional

[8]The acceleration theorem [Eq. (129)] and the corresponding Bloch oscillation dynamics are often regarded as a semiclassical result compared to the Wannier-Stark picture. On the contrary, they correspond to two different fully quantum-mechanical pictures.

field effect" (Brunetti, Jacoboni, and Rossi, 1989)—i.e., the action of the field during the scattering process—was neglected.[9]

In the simulated experiments reviewed here, the following superlattice model was employed: The energy dispersion and the corresponding wave functions along the growth direction ($k_\parallel$) were computed within the well-known Kronig-Penney model (Bastard, 1989), while for the in-plane direction ($k_\perp$) an effective-mass model was used. Only coupling to GaAs bulk phonons was considered. This, of course, is a simplifying approximation which neglects any superlattice effect on the phonon dispersion, such as confinement of optical modes in the wells and barriers and the presence of interface modes (Rücker, Molinari, and Lugli, 1992; Molinari, 1994). However, while these modifications have important consequences for phonon spectroscopies (like Raman scattering), they are far less decisive for transport phenomena.[10]

2. Bloch oscillation analysis

We shall start by discussing the scattering-induced damping of Bloch oscillations. In particular, we shall show that in the low-density limit this damping is mainly determined by optical-phonon scattering (Rossi, Meier, *et al.*, 1995, 1996), while at high densities the main mechanism responsible for the suppression of Bloch oscillations is found to be carrier-carrier scattering (Rossi, Gulia, *et al.*, 1996).

All of the simulated experiments presented in this section refer to the superlattice structure considered by Meier *et al.* (1995): 111-Å GaAs wells and 17-Å $Al_{0.3}Ga_{0.7}As$ barriers. For such a structure there has been experimental evidence for terahertz emission from Bloch oscillations (Roskos *et al.*, 1994).

In the first set of simulated experiments, an initial distribution of photoexcited carriers (electron-hole pairs) is generated by a 100-fs Gaussian laser pulse in resonance with the first miniband exciton ($\hbar\omega_L \approx 1540$ meV). The strength of the applied electric field is assumed to be 4 kV/cm, which corresponds to a Bloch period ($\tau_B = h/eFd$) of about 800 fs.

In the low-density limit (corresponding to a weak laser excitation), incoherent scattering processes do not alter the Bloch oscillation dynamics. This is due to the following reasons: In agreement with recent experimental (Roskos *et al.*, 1994; von Plessen *et al.*, 1994) and theoretical (Meier *et al.*, 1995; Rossi, Meier, *et al.*, 1995, 1996) investigations, at low temperature, scattering with LO phonons is not permitted and scattering with acoustic phonons is unimportant for superlattices characterized by a miniband width smaller than the LO phonon energy—as for the structure considered here—and for laser excitations close to the band gap. Moreover, in this low-density regime carrier-carrier scattering plays no role: Due to the quasielastic nature of Coulomb collisions, most of the scattering processes in the low-density limit are characterized by a very small momentum transfer. As a consequence, the momentum relaxation along the growth direction is negligible. As a result, on this picosecond time scale the carrier system exhibits coherent Bloch oscillation dynamics, i.e., negligible scattering-induced dephasing. This can be clearly seen from the time evolution of the carrier distribution as a function of $k_\parallel$ (i.e., averaged over $k_\perp$) shown in Fig. 18. During the laser photoexcitation ($t=0$) the carriers are generated around $k_\parallel=0$, where the transitions are close to resonance with the laser excitation. According to the acceleration theorem, the electrons are then shifted in **k** space. When the carriers reach the border of the first Brillouin zone, they are Bragg reflected. After about 800 fs, corresponding to the Bloch period τ_B, the carriers have completed one oscillation in **k** space. As expected, the carriers execute Bloch oscillations without losing the synchronism of their motion by scattering. This is again shown in Figs. 18(b)–(d), where we have plotted (b) the mean kinetic energy, (c) the current, and (d) its time derivative, which is proportional to the emitted far field, i.e., the terahertz radiation. All three quantities exhibit oscillations characterized by the same Bloch period τ_B. Due to the finite width of the carrier distribution in **k** space [see Fig. 18(a)], the amplitude of the oscillations of the kinetic energy is somewhat smaller than the miniband width. Since the scattering-induced dephasing is negligible for this excitation condition, the oscillations of the current are symmetric around zero, which implies

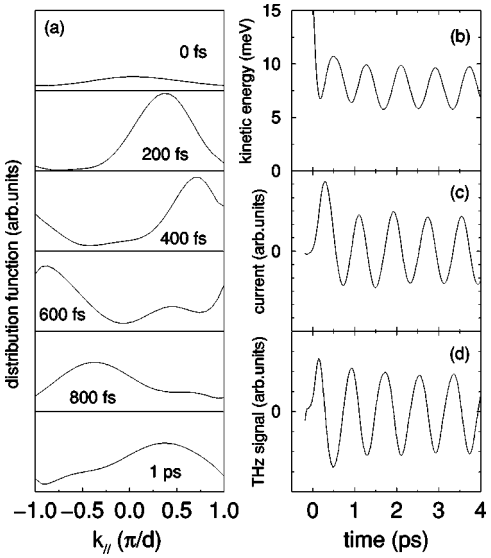

FIG. 18. Full Bloch oscillation dynamics corresponding to a laser photoexcitation resonant with the first-miniband exciton: (a) time evolution of the electron distribution as a function of $k_\parallel$; (b) average kinetic energy; (c) current; and (d) terahertz signal corresponding to the Bloch oscillations in (a).

[9]A detailed analysis of the intracollisional field effect in superlattices in the high-field regime can be found in Hader *et al.* (1997), where numerical solutions based on Wannier-Stark and plane-wave bases are compared.

[10]Indeed, it is now well known (Molinari, 1994) that the total scattering rates are sufficiently well reproduced if the phonon spectrum is assumed to be bulklike.

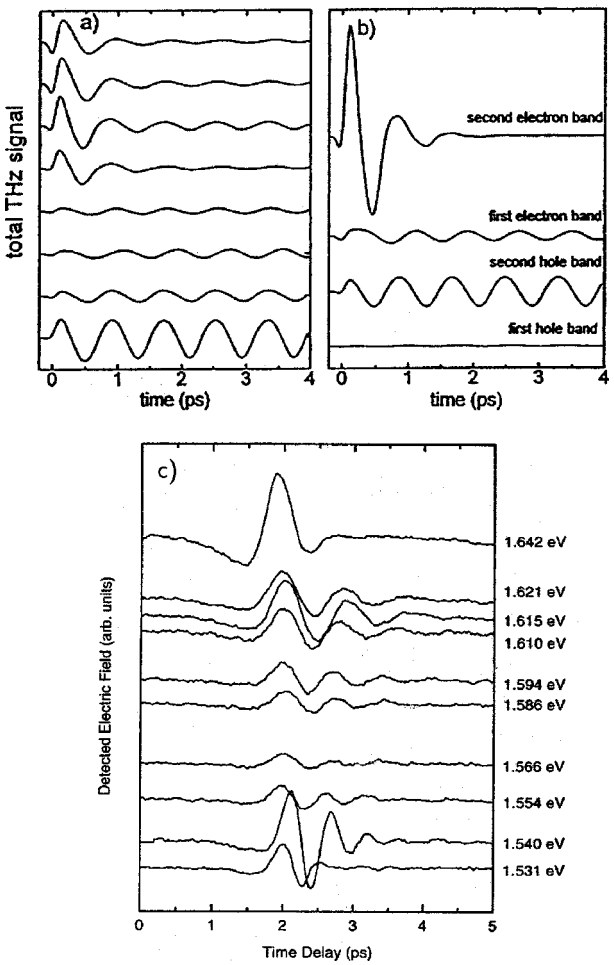

FIG. 19. Bloch oscillations corresponding to laser photoexcitation high in the band: (a) total terahertz signals for eight different spectral positions of the exciting laser pulse (1540, 1560,..., 1680 meV, from bottom to top); (b) individual terahertz signals of the electrons and holes in the different bands for a central spectral position of the laser pulse of 1640 meV; (c) experimentally observed terahertz transients for different excitation energies extending from just below the fundamental band gap up to well into the second miniband. After [(a), (b)] Koch *et al.*, 1995 and (c) Roskos *et al.*, 1994.

that the time average of the current is equal to zero, i.e., there is no dissipation.

As already pointed out, this ideal Bloch oscillation regime is typical of laser excitation close to the gap in the low-density limit. Let us now discuss the case of laser photoexcitation high in the band, still at low densities. Figure 19(a) shows the terahertz signal as obtained from a set of simulated experiments corresponding to different laser excitations (Meier *et al.*, 1995). The different traces correspond to the emitted terahertz signal for increasing excitation energies. We can clearly see the presence of Bloch oscillations in all cases. However, the oscillation amplitude and decay (effective damping) is excitation dependent.

In the case of laser excitation resonant with the first miniband exciton considered above (see Fig. 18), we have a strong terahertz signal. The amplitude of the signal decreases when the excitation energy is increased. Additionally, there are also some small changes in the phase of the oscillations, which are induced by the electron-LO phonon scattering.

When the laser energy comes into resonance with the transitions between the second electron and hole minibands ($\hbar\omega_L \approx 1625$ meV), the amplitude of the terahertz signal increases again. The corresponding terahertz transients show an initial part, which is strongly damped, and some oscillations for longer times that are much less damped. For a better understanding of these results, we show in Fig. 19(b) the individual terahertz signals, originating from the two electron and two heavy-hole minibands for the excitation with $\hbar\omega = 1640$ meV. The Bloch oscillations performed by the electrons within the second miniband are strongly damped due to intra- and interminiband LO phonon scattering processes (Meier *et al.*, 1995; Rossi *et al.*, 1995). Since the width of this second miniband (45 meV) is somewhat larger than the LO phonon energy, intraminiband scattering is also possible whenever the electrons are accelerated into the high-energy region of the miniband. The terahertz signal originating from electrons within the first miniband shows an oscillatory behavior with a small amplitude and a phase that is determined by the time the electrons need to relax down to the bottom of the band.

At the same time, the holes in both minibands exhibit undamped Bloch oscillations, since the minibands are so close in energy that no LO phonon emission can occur under these excitation conditions. The analysis shows that at early times the tetrahertz signal is mainly determined by the electrons within the second miniband. At later times the observed signal is due to heavy holes and electrons within the first miniband.

The above theoretical analysis closely resembles experimental observations obtained for a superlattice structure very similar to the one modeled here as shown in Fig. 19(c) (Roskos *et al.*, 1994). In these experiments terahertz emission from Bloch oscillations was found. For some excitation conditions the oscillations were associated with resonant excitation of the second miniband. The general behavior of the magnitude of the signals, the oscillations, and the damping are close to the results shown in Figs. 19(a) and (b). In superlattices with a miniband width larger than the LO phonon energy, it has been found that the terahertz radiation may even be enhanced by phonon emission because this process gives rise to a narrowing of the electron distribution (Wolter *et al.*, 1997).

Finally, in order to study the density dependence of the Bloch oscillation damping, let us go back to the case of laser excitations close to the gap. Figure 20(a) shows the total (electrons plus holes) terahertz radiation as a function of time for three different carrier densities. With increasing carrier density, carrier-carrier scattering becomes more and more important: Due to Coulomb screening, the momentum transfer in carrier-carrier scattering increases (its typical value being comparable to the screening wave vector). This can be seen in Fig.

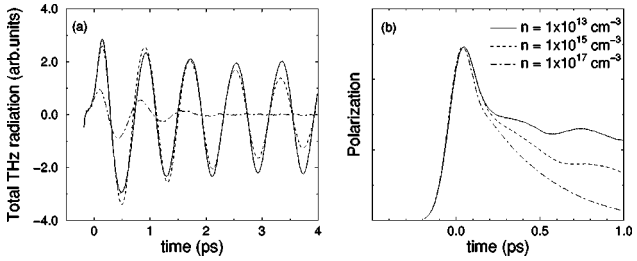

FIG. 20. Bloch oscillations corresponding to laser photoexcitation close to the gap: (a) total terahertz radiation as a function of time; (b) incoherently summed polarization as a function of time. After Rossi, Gulia, *et al.*, 1996.

20(a), where for increasing carrier densities we realize an increasing damping of the terahertz signal. However, for the highest carrier density considered here, we also deal with a damping time of the order of 700 fs, which is much longer than the typical dephasing time, i.e., the decay time of the interband polarization, associated with carrier-carrier scattering. The dephasing time is typically investigated by means of four-wave-mixing measurements, and such multipulse experiments can be simulated as well (Lohner *et al.*, 1993; Leitenstorfer, Lohner, Rick, *et al.*, 1994). From a theoretical point of view, a qualitative estimate of the dephasing time is given by the decay time of the *incoherently summed polarization* (Kuhn and Rossi, 1992b). Figure 20(b) shows this incoherently summed polarization as a function of time for the same three carrier densities as Fig. 20(a). As expected, the decay times are always much shorter than the corresponding damping times of the terahertz signals [note the different time scales in Figs. 20(a) and (b)]. This difference, discussed in more detail by Rossi, Gulia, *et al.*, (1996) and Rossi (1998), can be understood as follows: The fast decay times of Fig. 20(b) reflect the interband dephasing, i.e., the sum of the electron and hole scattering rates. In particular, for the Coulomb interaction this means the sum of electron-electron, electron-hole, and hole-hole scattering. As in the case of bulk GaAs discussed in Sec. III.A, this last contribution is known to dominate and determines the dephasing time scale. On the other hand, the total terahertz radiation in Fig. 20(a) is the sum of the electron and hole contributions. However, due to the small value of the hole miniband width compared to that of the electron, the electron contribution dominates. This means that the terahertz damping in Fig. 20(a) mainly reflects the damping of the electron contribution. This decay, in turn, reflects the intraband dephasing of electrons, which is due to electron-electron and electron-hole scattering only, i.e., there are no hole-hole contributions.

From the above analysis we can conclude that the decay time of the terahertz radiation due to carrier-carrier scattering differs considerably from the corresponding dephasing times obtained from a four-wave-mixing experiment: The first is a measurement of the intraband dephasing, while the second reflects the interband dephasing.[11]

G. Carrier-phonon quantum kinetics

Most of the theoretical results discussed so far have been obtained by treating energy relaxation and dephasing processes on a semiclassical level, i.e., in terms of scattering rates. The *Markov approximation* leading to these rates, however, always assumes a separation between the time scales relevant for the interaction-induced correlations and the dynamics of distribution functions or the envelope of polarizations. On a femtosecond time scale this separation is no longer satisfied and quantum-kinetic phenomena are of increasing importance either because they quantitatively modify the semiclassical results or because they introduce completely new features not present in a semiclassical picture. In the following sections we shall review some phenomena in which quantum kinetics play an essential role. We shall concentrate on carrier-phonon quantum kinetics and then discuss a few results of the currently very active field of Coulomb quantum kinetics.

1. Memory effects and energy-time uncertainty

As discussed in the theory part of this review, in the density-matrix formalism each interaction mechanism introduces new types of dynamical variables. For the interaction with a classical light field, these correspond to the various interband polarizations, while for the carrier-phonon coupling they are given by phonon-assisted density matrices. Semiclassical transition rates are obtained if these new variables are adiabatically eliminated by means of the Markov approximation. In the previous sections we have extensively discussed phenomena that showed the failure of this approximation in the case of the interband polarization and that could only be explained by treating the interband polarization as an independent dynamical variable. In particular, in Sec. III.A.1 we discussed the time-dependent broadening of carrier photogeneration associated with these dynamics.

Similarly, the carrier-phonon interaction is treated on the quantum-kinetic level if the phonon-assisted density matrices are obtained from the solution of equations of motion like Eq. (53). The full set of equations for the case of a homogeneous semiconductor can be found in Schilp *et al.* (1994a).

Broadening phenomena related to electron-phonon quantum kinetics can be observed most clearly in a one-band model in which this is the only type of interaction.

[11]We stress that this difference between intraband and interband dephasing in superlattices is the same as was discussed in Sec. III.A.3 for the case of bulk semiconductors, where the broadening of the photoexcited carrier distribution is mainly determined by the decay of the interband polarization (interband dephasing), while the subsequent energy broadening of the electron distribution is due to electron scattering only (intraband dephasing; see Fig. 6).

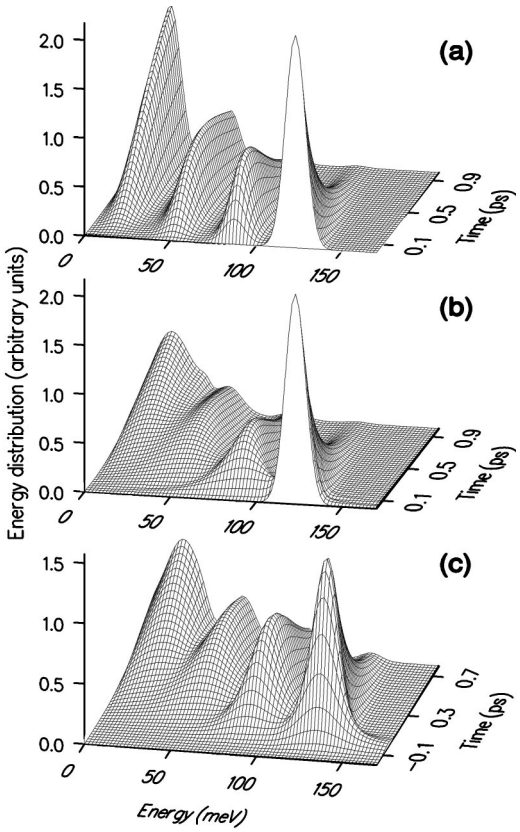

FIG. 21. Electron distribution functions in bulk GaAs: (a) semiclassical calculation; (b) and (c) quantum-kinetic calculations. (a) and (b) show the relaxation of a given initial distribution in a one-band model, while (c) is the result of a two-band calculation for the case of an excitation by a 100-fs laser pulse. After Schilp, Kuhn, and Mahler, 1994a, 1994c.

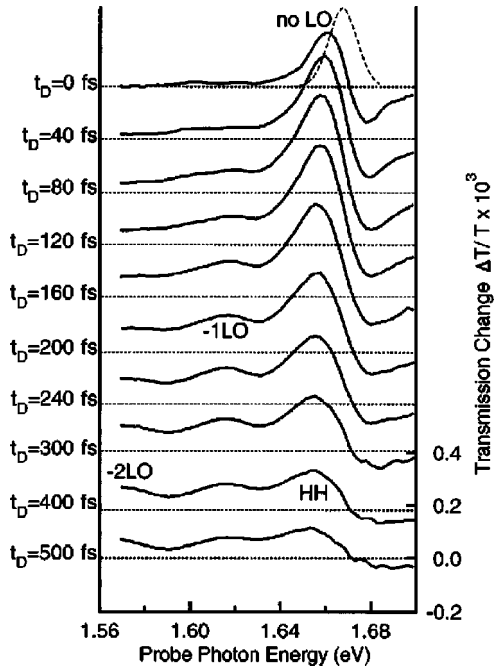

FIG. 22. Spectrally resolved transmission changes in GaAs measured for different time delays at a carrier density of 8×10^{14} cm^{-3} (the dashed line denotes the excitation spectrum). After Fürst, Leitenstorfer, Laubereau, and Zimmermann, 1997.

In Figs. 21(a) and (b) we compare the electron distributions as functions of energy and time obtained from a semiclassical (Boltzmann) and a quantum-kinetic calculation; here we consider the energy relaxation of an initial Gaussian distribution within a one-band electron model interacting with LO phonons. In the semiclassical case replicas due to the emission of one, two, or three phonons appear on the low-energy side. Due to energy conservation in each scattering process, they exhibit the same spectral shape of the initial distribution, in complete analogy with the time-independent shape of the semiclassical generation rate in Fig. 3. The quantum-kinetic result, on the other hand, exhibits a strong time-dependent broadening. The replicas are initially very broad; with increasing time they become narrower and approach the semiclassical shape. This is again a consequence of energy-time uncertainty: At early times the single-particle energy is not yet a well-defined quantity. Figure 21(c) shows the distribution functions for the more realistic case of a two-band semiconductor (Schilp *et al.*, 1994a, 1994b) in which the carriers are generated by a 100-fs laser pulse. Now there is a time-dependent broadening due to both the light absorption and the phonon emission process. The former is responsible for the broadening of the highest energy peak, while the latter broadens the subsequent replicas. It can be clearly seen that there is initially no minimum between two replicas; these minima build up with increasing time due to destructive interference at the semiclassically forbidden transitions. Such time-dependent broadening due to phonon scattering were observed in two-color pump-probe experiments (Fürst, Leitenstorfer, Laubereau, and Zimmermann, 1997) in which electron-hole pairs were generated by a 120-fs laser pulse and the transmission change of a weak, spectrally broad 25-fs pulse was measured. The corresponding differential transmission spectra for various delay times between pump and probe pulse are shown in Fig. 22. The same features were also obtained in calculations based on the Green's-function formalism (Bányai *et al.*, 1992; Tran Thoai and Haug, 1993; Schmenkel, Bányai, and Haug, 1998) as well as in exactly solvable models of electron-phonon interaction (Meden *et al.*, 1996; Schönhammer and Wöhler, 1997; Schönhammer 1998).

2. Nonequilibrium phonons and energy conservation

In the previous section we have seen that energy-time uncertainty is a characteristic feature of quantum kinetics. However, in the absence of an external light field, we have a closed electron-phonon system, and the energy of such a closed system should be constant without any uncertainty. Here we want to address the question of energy conservation in greater detail. In the semiclassical case the system is completely determined by the distribution functions of electrons and holes. In the relaxation process the electrons lose energy, which is taken up by the phonons. This is shown in Fig. 23(a), where

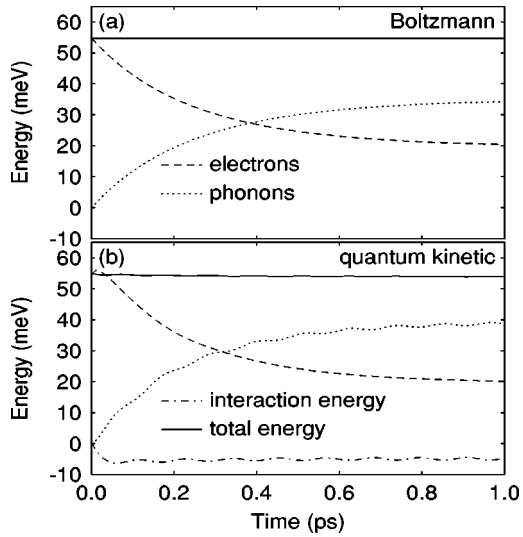

FIG. 23. One-band model including nonequilibrium phonons in bulk GaAs: (a) semiclassical and (b) quantum-kinetic calculation of total energy (solid line), as well as contributions due to electrons (dashed lines), phonons (dotted line), and carrier-phonon interaction (dot-dashed line) as functions of time.

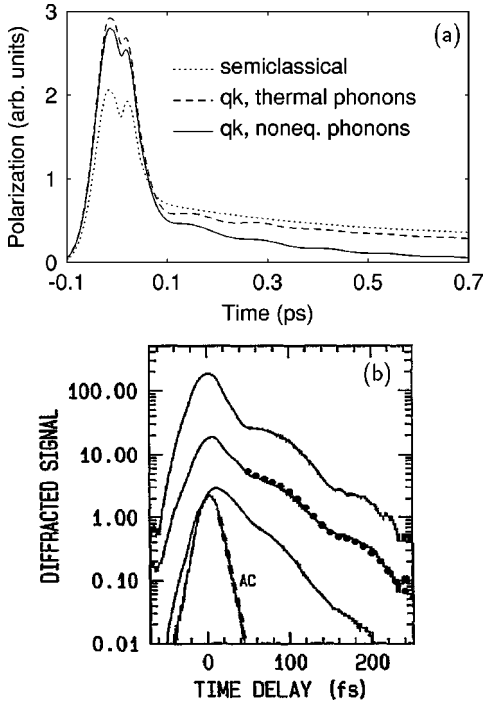

FIG. 24. Phonon quantum beats: (a) incoherently summed polarization as a function of time in bulk GaAs after excitation by a 50-fs pulse: dotted line, semiclassical calculation; dashed line, quantum-kinetic (qk) calculation with thermal phonons; solid line, quantum kinetic calculation with nonequilibrium phonons. (b) Four-wave-mixing signals at different densities exhibiting phonon quantum beats: solid line, experiment; dotted line, theory. After (a) Schilp *et al.*, 1995 and (b) Bányai *et al.* (1995).

the mean energies of the electrons and phonons are plotted as functions of time for the case of relaxation from a given initial distribution. As is clear from the semiclassical scattering rates, the sum of the two energies is a constant. Figure 23(b) shows the same energies obtained from the quantum-kinetic calculation. Now the sum of electron and phonon energy is no longer constant; however, if the interaction energy given by the expectation value of the interaction Hamiltonian is included, a constant total energy is recovered (Schilp *et al.*, 1995). The initial increase of the electron and phonon energies is balanced by the buildup of a negative interaction energy due to electron-phonon correlations. Thus we directly observe the buildup of polarons from an initially uncorrelated electron-phonon system.

In Sec. II.D.4 we discussed how the correlation expansion could be continued to take into account higher-order correlations. As shown there, neglecting the off-diagonal part and treating the diagonal part in Markov approximation results in a complex self-energy describing a damping of electron-phonon correlations. However, it has been shown both analytically and numerically that this approximation violates the conservation of the total energy (Schilp *et al.*, 1995). In addition, it strongly overestimates the broadening of the distribution functions, in clear contrast to results known from exactly solvable models and from experiments. However, if all terms of the next order are taken into account, it can be shown analytically that energy conservation is again satisfied. Numerically, this "fourth Born approximation" has been studied for a one-dimensional model (Zimmermann *et al.*, 1998). It turns out that in many cases it is a better approximation to completely neglect third-order terms than to use the Markovian self-energy approximation.

The interaction energy in Fig. 23(b) has a contribution that oscillates with the phonon frequency. These oscillations can be traced back analytically to the divergence at $\mathbf{q}=0$ in the Fröhlich coupling matrix element, since this gives rise to a divergence in the frequency spectrum of the phonon-assisted density matrices (Binder, Schilp, and Kuhn, 1998). Also, in the case of the phonon energy the oscillations are due to phonons with very small wave vectors mainly in a range that is semiclassically not allowed. In the semiclassically allowed region the nonequilibrium phonon distribution in a bulk semiconductor is quite close to its semiclassical value. In a one-dimensional system, however, this is different. Here the semiclassical model yields very sharp peaks in the phonon distribution because, for an electron with a given momentum, the emission of phonons with only two distinct wave vectors is compatible with energy and momentum conservation. In contrast, in the quantum-kinetic case energy-time uncertainty leads to a smooth distribution function (Binder *et al.*, 1998).

3. Phonon quantum beats

Phonon quantum kinetics modify the carrier distribution functions that can be measured, for example, in pump-probe experiments. However, experimentally observable signals are in general changed only quantita-

tively. For a clear proof of quantum kinetics, it would be desirable to have a phenomenon that is present only in a quantum-kinetic treatment. The situation is similar to the case of the coherent interband polarization discussed above: An explicit treatment of that variable quantitatively changes the carrier photogeneration process; phenomena like four-wave-mixing or coherent control in the case of temporally nonoverlapping pulses are simply not present if the polarization is adiabatically eliminated. Such a phenomenon, which is present only due to carrier-phonon quantum kinetics, has indeed been found: If the semiconductor is excited by a sufficiently short laser pulse, the interband polarization exhibits an oscillatory decay, the oscillation frequency being of the order of the phonon frequency (Tran Thoai and Haug, 1993; Schilp *et al.*, 1994a, 1995; Bányai, Vu, and Haug, 1998). This is shown in Fig. 24(a) where the incoherently summed polarization is plotted as a function of time. While in the semiclassical case it is smoothly decaying, in quantum-kinetic cases with both thermal and nonequilibrium phonons, oscillations are present. These oscillations are phonon quantum beats, and they arise due to the simultaneous excitation of a direct optical transition and a phonon-assisted one; therefore they rely on an electron-phonon correlation. The faster decay of the polarization in the presence of nonequilibrium phonons is due to enhanced phonon absorption. Phonon quantum beats have been experimentally observed in time-integrated four-wave-mixing experiments. Figure 24(b) shows the diffracted signal at different densities after excitation of bulk GaAs with two 14.2-fs pulses (Bányai *et al.*, 1995). The dots are results of quantum-kinetic calculations. Phonon quantum beats have also been obtained in the case of quantum wells (Wehner *et al.*, 1998).

Like other quantum beat phenomena, electron-phonon quantum beats can be controlled by a second phase-locked pulse (Wehner *et al.*, 1998; Steinbach *et al.*, 1999). If the delay time corresponds to destructive interference on the phonon-assisted transition, the beats are eliminated from the signal, as can be clearly seen in Fig. 25(a), where the incoherently summed polarization is plotted as a function of time for the case of excitation with two phase-locked 15-fs pulses whose delay time varies from 42.8 fs (top) to 48.2 fs (bottom) in steps of 0.3 fs (Axt *et al.*, 1999; Kuhn *et al.*, 1999). Figure 26 shows corresponding experimentally observed four-wave-mixing signals (Wehner *et al.*, 1998) for similar excitation conditions. Qualitatively, the appearance of phonon quantum beats and their coherent control can be understood quite well in terms of a simple model based on a two-level system coupled to a single phonon mode. This model has the advantage of being exactly solvable and thus the linear as well as the nonlinear response can be given exactly (Axt *et al.*, 1999; Castella and Zimmermann, 1999). Here the linear spectrum consists of a series of lines separated by the phonon energy corresponding to the zero-phonon line and sidebands due to phonon-assisted transitions (Mahan, 1990); thus the excitation of phonon quantum beats by a pulse that spectrally overlaps with at least two lines becomes obvious. Since for this model the exact solution is known, it can also be applied to systems with a stronger electron-phonon coupling in which the quantum-kinetic approach based on the correlation expansion breaks down. Indeed, it has been shown that the coherent control of phonon quantum beats in ZnSe—where clear signatures of multiphonon transitions are observed—can be well explained (Steinbach *et al.*, 1999). The drawback of this simple model is, however, that it does not provide any dephasing, which has to be put in by hand. Therefore it cannot reproduce another interesting feature seen in experiment, namely, the fact that the decay of the four-wave-mixing signals also depends on the phase difference between the two exciting pulses. This behavior is well reproduced by the quantum-kinetic semiconductor model, as is shown in Fig. 25(b), where the inverse of the decay time extracted from the curves in Fig. 25(a) is plotted as a function of the delay time between the pulses. This clearly demonstrates that scattering processes can be influenced as long as the correlation between initial and final states has not yet died out.

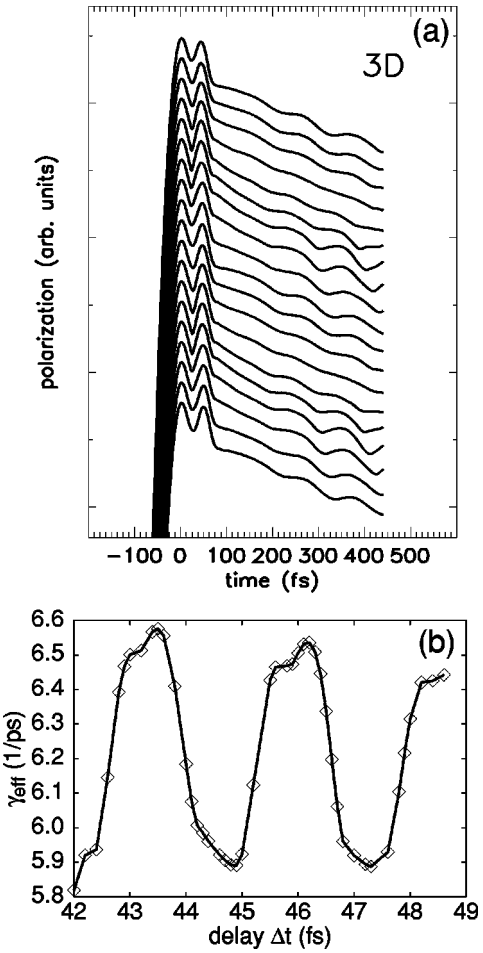

FIG. 25. Incoherently summed polarization: (a) excitation with a pair of phase-locked 15-fs pulses with delay times ranging from 42.8 fs (top) to 48.2 fs (bottom) in steps of 0.3 fs; (b) extracted decay constant as a function of the delay time. Parameters refer to bulk GaAs. After Axt *et al.*, 1999.

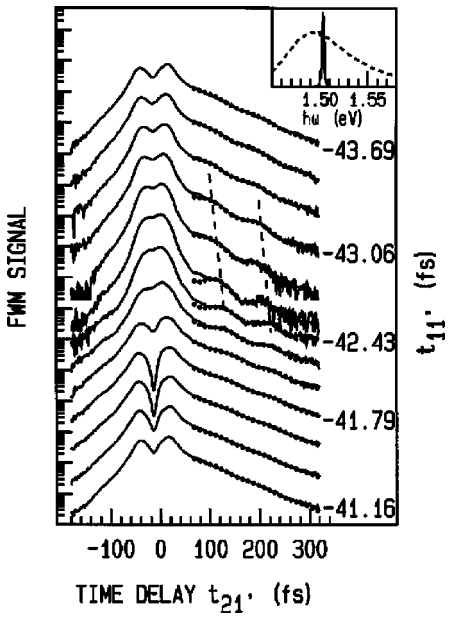

FIG. 26. Four-wave-mixing (FWM) signals in GaAs measured for the case of excitation with a pair of phase-locked 15-fs pulses with different delay times. After Wehner *et al.*, 1998.

4. Carrier-phonon quantum kinetics in inhomogeneous systems

In the results obtained from a quantum-kinetic treatment of carrier-phonon interaction discussed so far, we have always assumed a spatially homogeneous excitation. Technically, this means that the single-particle density matrices depend on only one wave vector $\mathbf{k}$, and the phonon-assisted density matrices depend on two wave vectors. In the case of an inhomogeneous excitation, this corresponds to the zeroth order in a gradient expansion, as discussed in Sec. II.C.3. This is a good approximation if all inhomogeneities—introduced, for example, by the exciting laser pulses—occur on sufficiently large length scales, such that transport phenomena are not relevant on the ultrafast time scale considered in this review. However, much like the time scales the length scales in optical experiments are also continuously reduced; therefore the interest in optically induced transport phenomena on ultrafast time scales is rapidly increasing.

Depending on the required spatial resolution, different experimental techniques have been developed to perform a spatially resolved optical excitation and/or detection. Spot sizes of the order of 1 μm have been achieved by using lenses or microscope objectives (Yoon, Wake, and Wolfe, 1992; Otremba *et al.*, 1999). The theoretical limitation of this technique, which is given by the diffraction limit of about $\lambda/2$, where λ is the wavelength of the light, can be overcome by using a solid immersion lens. A spot size of 355 nm corresponding to 0.41λ was demonstrated with this method (Vollmer *et al.*, 1999). Alternatively, the light can be transmitted through holes in metal masks with diameters in the micron and submicron range (Hillmer *et al.*, 1988; Gammon *et al.*, 1996; Sönnichsen *et al.*, 2000). The highest spatial resolution, of the order of 100 nm and less, can be achieved by using scanning near-field optical microscopes (Betzig *et al.*, 1991; Hess *et al.*, 1994; Richter *et al.*, 1997; Guenther *et al.*, 1999). In this case transport processes occur on a femtosecond time scale.

The semiclassical description of transport phenomena is again based on the Boltzmann picture in which scattering events occur locally in space and time between states with well-defined energy and momentum. The dynamical variable in the semiclassical theory is the single-particle distribution function. Its closest analog in quantum mechanics is the Wigner function defined in Eq. (37). Formally, the scattering terms are obtained from the equation of motion for the Wigner function as the zeroth order in the gradient expansion discussed in Sec. II.C.3, together with the Markov approximation, which is equivalent to a zeroth-order gradient expansion in time. In the previous sections we have clearly seen that on ultrafast time scales the conservation of the single-particle energies, which appears as a result of the Markov approximation, is no longer satisfied. Instead, energy-time uncertainty strongly affects the dynamics. Similarly, on very short length scales the assumption of slowly varying dynamical variables, which is the basis for the gradient expansion, is no longer fulfilled. The uncertainty relation between position and momentum makes scattering process nonlocal in space. Both kinds of uncertainty relations are treated correctly if, in the case of carrier-phonon interaction, the single-particle and the phonon-assisted density matrices are taken as independent dynamical variables. Here the quantum-kinetic treatment has the additional advantage of being independent of the choice of the single-particle basis. This is in clear contrast to the semiclassical Boltzmann case, in which the Markov approximation requires selecting the initial and final states of a scattering process, which, in turn, depends on this basis.

In this section we shall discuss a few phenomena related to the spatiotemporal dynamics of locally generated carriers. By using a short-pulse excitation through a near-field microscope, a spatially localized wave packet of electrons and holes is created. The subsequent dynamics of such a wave packet strongly depend on the excitation condition (Steininger *et al.*, 1996; Hanewinkel *et al.*, 1999): An excitation resonant with the 1*s* exciton creates electron-hole pairs that are strongly bound, and the resulting wave packet exhibits spatial broadening. An excitation high up in the band-to-band continuum produces electron-hole pairs, which, in the absence of phonon interaction, propagate like pulses through the sample. Electron-hole correlation effects are of minor importance in this case. Phonon emission leads to energy loss and thus to carrier group-velocity relaxation; as a consequence, it induces spatial broadening of the pulses with a subsequent transition from a ballistic to a diffusive transport regime (Steininger *et al.*, 1997; Knorr *et al.*, 1998). This behavior, which can be well understood on a semiclassical level of description, is again modified on ultrashort time scales by quantum-kinetic features. In Fig. 27 the Wigner function $f^e_{\mathbf{k}}(\mathbf{r})$ for a Gaussian wave packet prepared at time $t=0$ at $z=0$

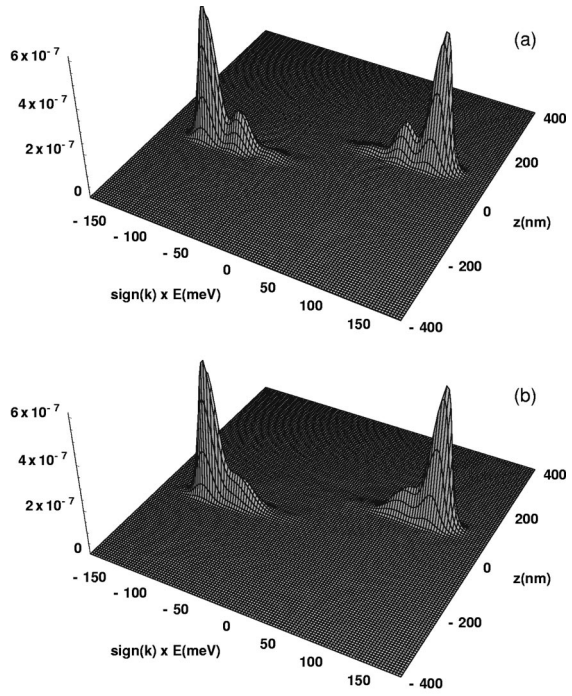

FIG. 27. Wigner function at $t=100$ fs for a Gaussian wave packet in a GaAs quantum wire prepared at $t=0$, $z=0$, and $E=120$ meV: (a) semiclassical and (b) quantum-kinetic calculation.

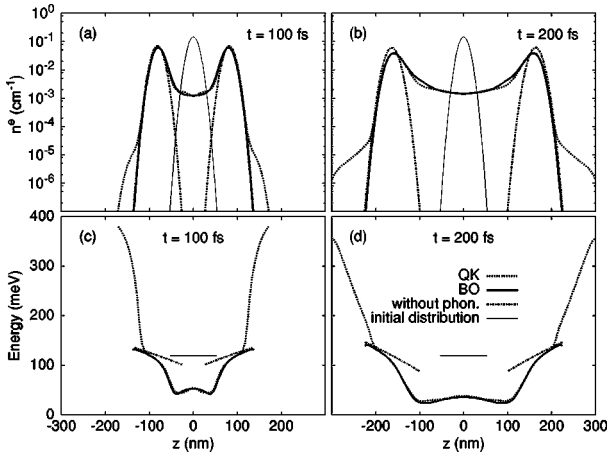

FIG. 28. GaAs quantum wire along the wire axis at different times for an initial excess energy of 120 meV: (a) and (b) electron densities; (c) and (d) spatially resolved mean kinetic energies obtained from a semiclassical calculation of a Bloch oscillation (solid lines), a quantum-kinetic (QK; dotted lines), and a noninteracting-carrier (dot-dashed lines) calculation. The thin lines represent the initial values at time $t=0$. After Herbst *et al.*, 2000.

with an excess energy of 120 meV is plotted at time $t=100$ fs. It is obtained from a semiclassical [Fig. 27(a)] and a quantum-kinetic [Fig. 27(b)] treatment of carrier-phonon interaction. These calculations have been performed for a GaAs cylindrical quantum wire model with a single subband. The broadening of the phonon replicas due to energy-time uncertainty in the quantum-kinetic results—which was discussed above for the case of a bulk semiconductor—is again clearly visible. Here this broadening also affects the spatial dynamics, due to occupation of momentum states inaccessible by semiclassically allowed processes. This phenomenon is analyzed in more detail in Fig. 28, where the electron density $n^e(\mathbf{r})=\mathcal{V}^{-1}\Sigma_{\mathbf{k}}f^e_{\mathbf{k}}(\mathbf{r})$ [Figs. 28(a) and (b)] and the mean kinetic energy $\langle E(\mathbf{r})\rangle=[n^e(\mathbf{r})\mathcal{V}]^{-1}\Sigma_{\mathbf{k}}(\hbar^2k^2/2m)f^e_{\mathbf{k}}(\mathbf{r})$ [Figs. 28(c) and (d)] are plotted along the wire axis after 100 fs and after 200 fs (Herbst, Axt, and Kuhn, 2000). Note that the energies are only plotted at those positions where this quantity is well defined, i.e., where the density is noticeably different from zero. For clarity the initial values have also been included. The results correspond to three levels of the theory: (i) a calculation neglecting phonons (dot-dashed lines), (ii) a calculation including phonon scattering by using the semiclassical Boltzmann approach (solid lines), and (iii) a full quantum-kinetic treatment of the electron-phonon interaction (dotted lines). Without phonons we find the expected ballistic transport of electrons. The distribution remains Gaussian for all times and moves outward along the wire axis. Initially, the energy distribution is, by construction, position independent. Since highly energetic particles cover a longer distance (compared to low-energy ones), at later times the mean kinetic energy increases monotonically with the distance from the origin, as can be clearly seen in Figs. 28(c) and (d). In the low-temperature limit considered here, phonons can only be emitted. Therefore, in the Boltzmann case, electrons can only lose energy, leading to a slowing down, as confirmed by the corresponding electron density in Figs. 28(a) and (b); we now find a noticeable electron density behind the ballistic wave front, but no density is built up ahead of the wave front. Correspondingly, $\langle E(\mathbf{r})\rangle$ is always below the respective value obtained in the ballistic case. Only at the front edge of the wave—formed by carriers that have not yet emitted a phonon—is the ballistic value reached.

In the quantum-kinetic case, also, phonons can only be emitted. Nevertheless, as a consequence of the energy-time uncertainty, it is possible for some of the particles to increase their kinetic energy as long as the collision is not yet complete. The effect of this type of process is clearly visible in Figs. 28(a) and (b), where the quantum-kinetic calculation predicts a small but finite electron occupation ahead of the ballistic wave front, i.e., we find electron densities in space regions that are out of reach from a semiclassical point of view. As shown in Figs. 28(c) and (d), the particles ahead of the ballistic wave front indeed have mean kinetic energies drastically increased compared to the highest values obtained in the ballistic description or in the Boltzmann case. The occurrence of high kinetic energies at early times is known from the quantum-kinetic treatment of the spatially homogeneous case (Schilp *et al.*, 1994a). The new aspect here is that in the spatially inhomogeneous case this effect is accompanied by a spatial separation of the highly energetic particles from the classical wave front. For space regions that could be reached within a semiclassical description, the Boltzmann result

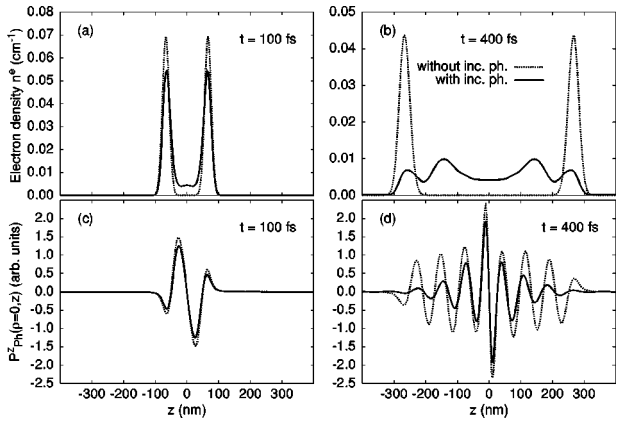

FIG. 29. GaAs quantum wire along the wire axis for an initial excess energy of 80 meV: (a) and (b) electron densities; (c) and (d) z component of the lattice polarization including only coherent phonons (dotted lines) and both coherent and incoherent phonons (solid lines). After Herbst *et al.*, 2000.

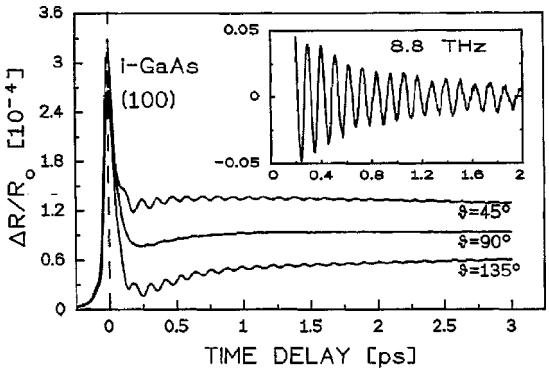

FIG. 30. Time-resolved reflectivity changes of (100)-oriented intrinsic GaAs for the case of excitation with a 50-fs pulse at 2 eV exhibiting oscillations due to the coherent phonons. After Cho *et al.*, 1990.

agrees quite well with the predictions of the quantum-kinetic theory.

Although initially the wire is locally neutral, the motion of the electrons leads to a charge separation inducing an electrical field. According to Eq. (58), the induced potential acts as a source for the generation of coherent phonons. Figure 29 displays the z component of the lattice polarization $\mathbf{P}_{lat}$ [Eq. (60)] along the wire axis after 100 and 400 fs, together with the corresponding electron densities. In addition to the curves obtained from a complete treatment including coherent and incoherent phonons (solid lines), we also plot results where the incoherent phonons have been switched off (dotted lines). Here, spatial oscillations of the phonon polarization, whose amplitudes decrease with increasing distance from the origin, are clearly visible. The spatial extent of the lattice vibrations equals the region between the ballistic wave fronts. The electrons passing a given space position excite lattice vibrations that oscillate with the LO frequency at that site. Because these oscillations start in different sites at different times, the vibrations are translated into spatial modulations. The decrease in the phonon amplitudes is due to the fact that charges accumulated in a small region of a $1d$ wire induce an electric field that decreases with increasing distance, thus reducing the forces responsible for the ion displacements. The inclusion of incoherent phonons leads to an effective damping of the phonon oscillations, which becomes stronger at later times. It should be noted that Eq. (58) is complete within the model considered, i.e., there are no terms left out due to the truncation procedure. It follows that in the absence of anharmonic forces, the only way the incoherent phonons may influence the coherent amplitudes is by their impact on the distribution functions. The damping of the phonon amplitudes is thus due to the spatial broadening of the wave packet and to the corresponding reduction of the induced potentials that generate the coherent phonons. Coherent phonons can be experimentally detected by various techniques either in the optical range or directly in the terahertz frequency range of the phonon oscillations. If coherent phonons are excited close to a surface, they modulate the reflectivity of the crystal and thus give rise to an oscillatory contribution in differential reflection signals. Figure 30 shows such reflectivity changes due to coherent phonons in bulk GaAs that were generated by the charge separation of carriers excited in a strong surface electric field due to Fermi level pinning at the surface (Cho *et al.*, 1990). A recent review on coherent phonon phenomena in condensed matter is that of Dekorsy, Cho, and Kurz (2000).

H. Carrier-carrier quantum kinetics

As in the case of carrier-phonon coupling, in a carrier-carrier interaction the Boltzmann picture of instantaneous scattering events occurring between states with well-defined energies loses its validity over ultrashort time scales. The temporal evolution of the single-particle density matrices is no longer completely determined by specifying their values at a given time. In contrast, it also depends on the values at previous times; the dynamics become non-Markovian. In the density-matrix approach discussed in this review, this corresponds to treating the two-particle density matrices as independent variables and solving the corresponding equations of motion like Eq. (79), in which higher-order correlation terms have been factorized into single-particle density matrices. Besides scattering, the Coulomb interaction in a charged many-particle system, however, gives rise to an additional important feature: The interaction between two carriers is screened by the presence of all the other carriers. It is intuitively clear that the carrier system requires some time to react to a perturbation and thus to build up the screening. The characteristic time is essentially given by the inverse of the plasmon frequency (El Sayed, Schuster, *et al.*, 1994) which, for moderate densities in GaAs, is of the order of 100 fs. Therefore this buildup of screening occurs on the same time scale relevant for quantum-kinetic phenomena. Here,

we shall briefly review some of the results that have been achieved in this currently very active field of Coulomb quantum kinetics.

As discussed above, it takes about 100 fs for the screening to build up. On the other hand, this means that on very short times of the order of 10 fs, screening does not play an important role, and the calculations can be performed with an unscreened potential. It is interesting to note that, while in the Boltzmann case Coulomb scattering rates with an unscreened potential diverge, in a quantum-kinetic treatment all contributions remain finite. On this level it has been found that the incoherently summed interband polarization, as well as time-integrated four-wave-mixing signals, exhibit a nonexponential decay with a density dependence of the characteristic decay time according to $n^{-1/3}$ (El Sayed, Bányai, and Haug, 1994; Vu *et al.*, 1997), thus confirming the measured density dependence (Becker *et al.*, 1988). Furthermore, the ultrafast redistribution of electrons as measured in pump-probe experiments was explained qualitatively (Camescasse *et al.*, 1996). Comparing quantum-kinetic and semiclassical calculations based on the same static screening model, it turned out that the non-Markovian relaxation is slightly delayed with respect to the Markovian one (Schäfer, 1996).

For times approaching 100 fs the buildup of screening has to be taken into account. In the density-matrix approach this requires including additional terms in the equations of motion of the two-particle density matrices, as discussed in Sec. II.E.4. In a Green's-function approach the screened potential is treated as a dynamical variable and a corresponding Dyson equation has to be solved. This leads to a considerable increase in the amount of computation. Nevertheless, such calculations are possible today, and a series of interesting results have been obtained in the past few years. Indeed, the decay of the interband polarization turns out to be in between the results obtained with a bare and with a statically screened Coulomb potential (Bányai, Vu, Mieck, and Haug, 1998). On this level, a good quantitative agreement between theory and experiment has been achieved for both four-wave-mixing (Bányai, Vu, and Haug, 1998; Hügel *et al.*, 1999) and pump-probe signals (Vu *et al.*, 1999). For systems excited by an inhomogeneous external potential, the generation and damping of plasmons has also been studied (Kwong and Bonitz, 2000).

Besides scattering and screening, there are other phenomena in a two- (or multi-) band semiconductor that are related to density matrices involving four operators. Among these are transitions involving two electron-hole pairs, which have attracted considerable interest in recent years. Typically, such two-pair states consist in a bound state, the biexciton, and an exciton-exciton scattering continuum. While the bound biexciton has often been treated in terms of a few-level model, the continuum is more complicated and is directly related to quantum kinetics. In the density-matrix approach the central quantity for these phenomena is the two-pair transition B_{j_1,i_1,j_2,i_2} introduced in Sec. III.C. However, it turns out that for the kind of experimental conditions in which these effects are most important, the correlation expansion method described in this review is not the most useful one for truncating the hierarchy, mainly because it treats all two-particle density matrices on the same level. Instead, virtually all calculations in this field have been based on the dynamics-controlled truncation scheme (Axt and Stahl, 1994a, 1994b; Axt and Mukamel, 1998), in which the variables are classified according to their order in the driving electric field. By formally solving the equation of motion for the two-pair transition, one can derive a memory term in the equation for the interband polarization, which again shows the quantum-kinetic nature of this contribution (Östreich, Schönhammer, and Sham, 1995; Axt, Victor, and Kuhn, 1998). Some aspects related to such Coulomb-induced correlations in pump-probe and four-wave-mixing signals have already been discussed above. These correlations have been found to be particularly important for describing the polarization dependence of pump-probe and four-wave-mixing experiments (Axt *et al.*, 1995; Mayer *et al.*, 1995; Schäfer *et al.*, 1996). One reason for their importance is the fact that the correlated exciton-exciton continuum strongly compensates some mean field contributions and, therefore, it is essential to obtain the correct line shape (Haase *et al.*, 2000) as well as the transient polarization (Bartels *et al.*, 1998) of four-wave-mixing experiments in which both exciton and biexciton contributions are present. Furthermore, such correlations may effectively couple different transitions and thus remove the clear distinction between quantum beats that arise from an interference in the semiconductor material and polarization interference, where the signals interfere in the detector (Phillips and Wang, 1999; Smirl *et al.*, 1999). In higher-order diffracted signals—like in a six-wave-mixing experiment—even density matrices involving six operators have been found to be important for a correct description of the spectra because there are again strong compensation effects (Bolton *et al.*, 2000).

All the investigations discussed so far have been restricted to those contributions of the Coulomb interaction that conserve the number of electron-hole pairs, an approximation that has also been applied in the theory part of this review. In the case of high carrier densities and strong external fields, it is well known that other contributions also become important, leading, for example, to Auger recombination and impact ionization. In particular, the latter process is an interesting candidate for a quantum-kinetic treatment because it involves threshold behavior: Semiclassically, an electron must reach at least an energy corresponding to one band gap above the minimum of the band before it can create an additional electron-hole pair. Since in a quantum-kinetic treatment the scattering process is not instantaneous, the electron can still gain energy from the electric field. Therefore with increasing field the threshold for impact ionization is shifted to lower fields. This has been calculated both for idealized parabolic bands (Quade *et al.*, 1994) and for realistic materials based on full band struc-

tures (Redmer *et al.*, 2000). Formally similar processes occur in doped semiconductor nanostructures, where the Coulomb interaction leads to transitions between different subbands. Here again the threshold behavior of the semiclassical theory is smoothed on short time scales due both to the energy-time uncertainty of the intersubband transition and to an initial fast broadening caused by intrasubband scattering (Prengel, Schöll, and Kuhn, 1997; Prengel and Schöll, 1999a, 1999b).

IV. SUMMARY AND CONCLUSIONS

The aim of the present paper was to provide a review of ultrafast phenomena in photoexcited semiconductors. The primary goal was to present a cohesive discussion of both coherent—i.e., phase-related—and incoherent—i.e., phase-breaking—processes in semiconductor bulk and heterostructures, as well as of their mutual interplay on a subpicosecond time scale. After a brief historical overview and a description of typical experimental techniques, we have shown how different phenomena can be described and explained within the same theoretical framework, based on the density-matrix formalism. By applying a correlation expansion we have derived the contributions to the equations of motion for the relevant kinetic variables corresponding to various interaction mechanisms and we have discussed their physical meaning. Based on this theoretical approach, we have reviewed a number of experimental and theoretical results crucial to understanding the microscopic origin of many ultrafast phenomena in semiconductors.

The main conclusion of the analysis presented in the paper is twofold: On the one hand, purely macroscopic or phenomenological models, commonly used to describe carrier relaxation and dephasing in the early days of ultrafast optics, are no longer adequate for describing the nonequilibrium dynamics of interacting carrier-phonon systems on a subpicosecond time scale. In contrast, a kinetic description—based, for example, on the density-matrix formalism but of course also on other approaches like the Green's-function approach—is required. On the other hand, the study of photoexcited carrier and phonon degrees of freedom on extremely short (femtosecond) time scales shows a variety of phenomena that cannot be explained in terms of the usual semiclassical Boltzmann theory. This is mainly ascribed to a failure of the conventional Markov approximation over ultrashort time scales as well as a failure of the independent treatment of different interaction mechanisms. One is then forced to employ fully quantum-kinetic formulations, which implies extending the set of kinetic variables to higher-order correlation functions like phonon-assisted and specific many-particle density matrices.

Generally speaking, the continuous improvement of time-resolved optical spectroscopy, intimately related to the ability to generate laser-pulse sequences on shorter and shorter time scales, has been accompanied by a progressive refinement of their theoretical description, i.e., from macroscopic to kinetic or quantum-kinetic models.

At this point a few comments are in order. As already mentioned, the field of ultrafast dynamics in semiconductors is so vast that it is not possible to treat all phenomena in a single review. For example, for most of the phenomena discussed in this review, we could treat the exciting light field as an external field and neglect the feedback of the carrier system to this field. This was possible because the samples were assumed to be optically thin. In optically thick samples propagation effects become important, leading, for example, to the formation of polaritons (Fröhlich *et al.*, 1991) and self-induced transmission (Giessen *et al.*, 1998). In this case interaction mechanisms may also give rise to new, renormalized states, for example, between polaritons and phonons, which have been called "phonoritons" (Hanke *et al.*, 1999). Another example is the case of optically coupled subsystems like multiple quantum well structures in which each quantum well "sees" the light field that is coherently emitted by the other wells. Depending on the interwell distance, these fields may add up constructively or destructively, thereby modifying the carrier dynamics in the wells (Hübner *et al.*, 1996). Recent progress in the fabrication and characterization of semiconductor microcavities (Khitrova *et al.*, 1999) offers the possibility of studying ultrafast carrier dynamics in the presence of strong light-matter coupling. Such systems constitute a unique laboratory for the study of basic phenomena related to coupled exciton-light dynamics.

It clearly follows that a proper description of such effects requires treating electromagnetic degrees of freedom explicitly, which implies further extending our set of dynamical variables. If the light field is treated quantum mechanically, photon populations and various photon-assisted density matrices have to be included along with average fields, as described in Sec. II.F. In this respect, there is a natural parallelism between photons and phonons: for both, the strong coupling with carrier degrees of freedom introduces significant correlations in terms of photon- and phonon-assisted density matrices, which results in new renormalized states, i.e., polaritons and polarons, respectively.

All the experiments discussed in this paper have been interpreted in terms of the correlation expansion of the density-matrix approach. The assumption that correlations involving an increasing number of carriers are of decreasing relevance has allowed us to limit the description to a few higher-order density matrices. In the semiclassical case they could even be adiabatically eliminated. Typically, this assumption is fulfilled in the presence of short-range interactions. The Coulomb potential, however, is a long-range interaction and it is only the presence of the many-body system that, due to screening, reduces the length scale of this interaction. Indeed, as already mentioned in Sec. III.H, at sufficiently low densities there are experiments that require density matrices involving at least six operators for a proper description (Bolton *et al.*, 2000).

The assumption is even less fulfilled in quasi-zero-dimensional nanostructures, the so-called quantum dots or semiconductor macroatoms (Jacak, Hawrylak, and

Wójs, 1998). Due to their discrete or atomiclike energy spectrum, they are intrinsically few-electron systems. Such macroatoms typically exhibit few-carrier effects both in transport (Schmidt *et al.*, 1995; Tarucha *et al.*, 1996; Rontani *et al.*, 1998) and in optics (Dekel *et al.*, 1998; Motohisa *et al.*, 1998; Hohenester, Rossi, and Molinari, 1999), due to the limited number of confined electrons and/or holes in the nanostructure: the energy needed to add an extra electron or electron-hole pair to the system depends on the current number of electrons and/or holes. In order to describe such few-carrier effects, correlations have to be properly taken into account; in particular, the mean-field or Hartree-Fock description, commonly employed as a first step in systems of higher dimensionality, cannot be used to describe single semiconductor macroatoms, for which the detailed knowledge of the microscopic few-electron wave function is required. Therefore the introduction of quasi-zero-dimensional systems requires on the theoretical side a careful consideration of the relevant correlations between the particles.

We are therefore led to conclude that ultrafast optical spectroscopy of semiconductors in the last three decades has allowed us to improve our understanding of nonequilibrium carrier dynamics significantly, from macroscopic or phenomenologic models to kinetic and quantum-kinetic treatments, to partially microscopic approaches.

We stress that a partially microscopic treatment of the carrier dynamics in few-electron systems, apart from practical difficulties, on the one hand leads to a reformulation of the concept of dephasing, and on the other hand raises once again the measurement problem. Indeed, semiconductor macroatoms are currently considered as potential candidates for quantum computation/information[12] processing devices. To this end, a recent study (Zanardi and Rossi, 1998) has shown that a proper tailoring of few-electron states may lead to a strong suppression of phonon-induced decoherence processes in quantum dot arrays. The key point is that in a quantum-correlated few-electron system, each electron does not interact individually with environmental degrees of freedom, in clear contrast to any single-particle kinetic formulation.

Finally, a crucial point for a proper modeling of ultrafast experiments on few-electron systems is the description of the measurement process. Since quantum correlation, i.e., entanglement effects, may play a significant role in such systems, it is vital to describe at the same microscopic level (i) the initial-state preparation, (ii) its quantum-mechanical evolution, and (iii) the measurement process. On the theoretical side this is the only way to account properly for the increasingly sophisticated experiments in ultrafast optics, for which the separation between "measured system" and "detector" becomes ill defined.

[12]See, for example, Molotkov (1996), Loss and DiVincenzo (1998), Zanardi and Rossi (1998), and Biolatti *et al.* (2000); for a review on quantum computation, see, Steane (1998) and DiVincenzo and Bennet (2000).

ACKNOWLEDGMENTS

We wish to thank V. M. Axt for many fruitful discussions and for carefully reading the manuscript. We also thank the many co-workers from our own groups as well as from several other places with whom we had the pleasure of collaborating over the past few years on the study of ultrafast dynamics in semiconductors. Their work as well as many discussions with other colleagues active in the field have strongly contributed to this review. This work was supported by the Commission of the European Union in the framework of the Training and Mobility of Researchers (TMR) network *Ultrafast Quantum Optoelectronics* and by the Deutsche Forschungsgemeinschaft within the *Schwerpunktprogramm Quantenkohärenz in Halbleitern*.

REFERENCES

Abella, I. D., N. A. Kurnit, and S. R. Hartmann, 1966, Phys. Rev. **141**, 391.
Allen, L., and J. H. Eberly, 1987, *Optical Resonance and Two-Level Atoms* (Dover, New York).
Altevogt, T., H. Puff, and R. Zimmermann, 1997, Phys. Rev. A **56**, 1592.
Argyres, P. N., 1962, Phys. Rev. **126**, 1386.
Assion, A., T. Baumert, J. Helbing, V. Seyfried, and G. Gerber, 1996, Chem. Phys. Lett. **259**, 488.
Atanasov, R., A. Haché, J. L. P. Hughes, H. M. van Driel, and J. E. Sipe, 1996, Phys. Rev. Lett. **76**, 1703.
Axt, V. M., G. Bartels, and A. Stahl, 1996, Phys. Rev. Lett. **76**, 2543.
Axt, V. M., M. Herbst, and T. Kuhn, 1999, Superlattices Microstruct. **26**, 117.
Axt, V. M., and S. Mukamel, 1998, Rev. Mod. Phys. **70**, 145.
Axt, V. M., and A. Stahl, 1994a, Z. Phys. B: Condens. Matter **93**, 195.
Axt, V. M., and A. Stahl, 1994b, Z. Phys. B: Condens. Matter **93**, 205.
Axt, V. M., A. Stahl, E. J. Mayer, P. Haring Bolivar, S. Nüsse, K. Ploog, and K. Köhler, 1995, Phys. Status Solidi B **188**, 447.
Axt, V. M., K. Victor, and T. Kuhn, 1998, Phys. Status Solidi B **206**, 189.
Axt, V. M., K. Victor, and A. Stahl, 1996, Phys. Rev. B **53**, 7244.
Balescu, R., 1961, Phys. Fluids **4**, 94.
Balslev, I., and A. Stahl, 1988, Solid State Commun. **67**, 85.
Balslev, I., R. Zimmermann, and A. Stahl, 1989, Phys. Rev. B **40**, 4095.
Bányai, L., D. B. Tran Thoai, E. Reitsamer, H. Haug, D. Steinbach, M. U. Wehner, M. Wegener, T. Marschner, and W. Stolz, 1995, Phys. Rev. Lett. **75**, 2188.
Bányai, L., D. B. Tran Thoai, C. Remling, and H. Haug, 1992, Phys. Status Solidi B **173**, 149.
Bányai, L., Q. T. Vu, and H. Haug, 1998, Phys. Rev. B **58**, R13 341.
Bányai, L., Q. T. Vu, M. Mieck, and H. Haug, 1998, Phys. Rev. Lett. **81**, 882.
Bar-Ad, S., and I. Bar-Joseph, 1991, Phys. Rev. Lett. **66**, 2491.

Bartels, G., V. M. Axt, K. Victor, A. Stahl, P. Leisching, and K. Köhler, 1995, Phys. Rev. B **51**, 11 217.
Bartels, G., G. C. Cho, T. Dekorsy, H. Kurz, A. Stahl, and K. Köhler, 1997, Phys. Rev. B **55**, 16 404.
Bartels, G., A. Stahl, V. M. Axt, B. Haase, U. Neukirch, and J. Gutowski, 1998, Phys. Rev. Lett. **81**, 5880.
Bastard, G., 1989, *Wave Mechanics Applied to Semiconductor Heterostructures* (Les Editions de Physique, Les Ulis).
Baumert, T., T. Brixner, V. Seyfried, M. Strehle, and G. Gerber, 1997, Appl. Phys. B: Lasers Opt. **B65**, 779.
Becker, P. C., H. L. Fragnito, C. H. Brito Cruz, R. L. Fork, J. E. Cunningham, J. E. Henry, and C. V. Shank, 1988, Phys. Rev. Lett. **61**, 1647.
Betzig, E., J. K. Trautmann, T. D. Harris, J. S. Weiner, and R. L. Kostelak, 1991, Science **251**, 1468.
Binder, E., 1997, *Kohärenzzerfall in optisch angeregten Halbleitern* (Neue Wissenschaft, Frankfurt am Main).
Binder, E., T. Kuhn, and G. Mahler, 1994, Phys. Rev. B **50**, 18 319.
Binder, E., D. Preisser, and T. Kuhn, 1997, Phys. Status Solidi B **204**, 87.
Binder, E., J. Schilp, and T. Kuhn, 1998, Phys. Status Solidi B **206**, 227.
Binder, R., D. Scott, A. E. Paul, M. Lindberg, K. Henneberger, and S. W. Koch, 1992, Phys. Rev. B **45**, 1107.
Biolatti, E., R. C. Iotti, P. Zanardi, and F. Rossi, 2000, Phys. Rev. Lett. **85**, 5647.
Birkedal, D., and J. Shah, 1998, Phys. Rev. Lett. **81**, 2372.
Bloch, F., 1928, Z. Phys. **52**, 555.
Bogoliubov, N. N., 1967, *Lectures on Quantum Statistics* (Gordon and Breach, New York), Vol. 1.
Bolton, S. R., U. Neukirch, L. J. Sham, D. S. Chemla, and V. M. Axt, 2000, Phys. Rev. Lett. **85**, 2002.
Bonitz, M., 1998, *Quantum Kinetic Theory* (Teubner, Stuttgart).
Bonitz, M., D. Semkat, and H. Haug, 1999, Eur. Phys. J. B **9**, 309.
Brumer, P., and M. Shapiro, 1995, Sci. Am. (Int. Ed.) **272** (3), 34.
Brunetti, R., C. Jacoboni, and F. Rossi, 1989, Phys. Rev. B **39**, 10 781.
Camescasse, F. X., A. Alexandrou, D. Hulin, L. Bányai, D. B. Tran Thoai, and H. Haug, 1996, Phys. Rev. Lett. **77**, 5429.
Capasso, F., 1990, *Physics of Quantum Electron Devices* (Springer, Berlin).
Carruthers, P., and F. Zachariasen, 1983, Rev. Mod. Phys. **55**, 245.
Castella, H., and R. Zimmermann, 1999, Phys. Rev. B **59**, R7801.
Chachisvilis, M., H. Fidder, and V. Sundström, 1995, Chem. Phys. Lett. **234**, 141.
Chen, C., Y.-Y. Yin, and D. S. Elliot, 1990, Phys. Rev. Lett. **64**, 507.
Cho, G. C., T. Dekorsy, H. J. Bakker, R. Hvel, and H. Kurz, 1996, Phys. Rev. Lett. **77**, 4062.
Cho, G. C., W. Kütt, and H. Kurz, 1990, Phys. Rev. Lett. **65**, 764.
Cohen-Tannoudji, C., J. Dupont-Roc, and G. Grynberg, 1989, *Photons and Atoms* (Wiley, New York).
Combescot, M., and R. Combescot, 1989, Phys. Rev. B **40**, 3788.
Dabbicco, M., A. M. Fox, G. von Plessen, and J. F. Ryan, 1996, Phys. Rev. B **53**, 4479.
Dekel, E., D. Gershoni, E. Ehrenfreund, D. Spektor, J. M. Garcia, and P. M. Petroff, 1998, Phys. Rev. Lett. **80**, 4991.
Dekorsy, T., H. Auer, C. Waschke, H. J. Bakker, H. G. Roskos, H. Kurz, V. Wagner, and P. Grosse, 1995, Phys. Rev. Lett. **74**, 738.
Dekorsy, T., G. C. Cho, and H. Kurz, 2000, in *Light Scattering in Solids VIII: Fullerenes, Semiconductor Surfaces, Coherent Phonons*, edited by M. Cardona and G. Güntherodt, Topics in Applied Physics Vol. 76 (Springer, Berlin), p. 169.
Dekorsy, T., A. M. T. Kim, G. C. Cho, K. Köhler, and H. Kurz, 1996, in *Ultrafast Phenomena X*, edited by P. F. Barbara, J. G. Fujimoto, W. H. Knox, and W. Zinth, Springer Series in Chemical Physics Vol. 62 (Springer, Berlin), p. 382.
Dekorsy, T., A. M. T. Kim, G. C. Cho, H. Kurz, A. V. Kuznetsov, and A. Förster, 1996, Phys. Rev. B **53**, 1531.
Dekorsy, T., P. Leisching, K. Köhler, and H. Kurz, 1994, Phys. Rev. B **50**, 8106.
Dekorsy, T., R. Ott, H. Kurz, and K. Köhler, 1995, Phys. Rev. B **51**, 17 275.
DiVincenzo, D. P., and C. Bennet, 2000, Nature (London) **404**, 247.
Dupont, E., P. B. Corkum, H. C. Liu, M. Buchanan, and Z. R. Wasilewski, 1995, Phys. Rev. Lett. **74**, 3596.
Egri, I., 1985, Phys. Rep. **119**, 363.
El Sayed, K., L. Bányai, and H. Haug, 1994, Phys. Rev. B **50**, 1541.
El Sayed, K., S. Schuster, H. Haug, F. Herzel, and K. Henneberger, 1994, Phys. Rev. B **49**, 7337.
Feldmann, J., K. Leo, J. Shah, D. A. B. Miller, J. E. Cunningham, T. Meier, G. von Plessen, A. Schulze, P. Thomas, and S. Schmitt-Rink, 1992, Phys. Rev. B **46**, 7252.
Fluegel, B., N. Peyghambarian, G. Olbright, M. Lindberg, S. W. Koch, M. Joffre, D. Hulin, A. Migus, and A. Antonetti, 1987, Phys. Rev. Lett. **59**, 2588.
Fox, A. M., J. J. Baumberg, M. Dabbicco, B. Huttner, and J. F. Ryan, 1995, Phys. Rev. Lett. **74**, 1728.
Franz, W., 1958, Z. Naturforsch. A **13A**, 484.
Frensley, W. R., 1990, Rev. Mod. Phys. **62**, 745.
Fröhlich, D., A. Kulik, B. Uebbing, A. Mysyrowicz, V. Langer, H. Stolz, and W. von der Osten, 1991, Phys. Rev. Lett. **67**, 2343.
Fürst, C., A. Leitenstorfer, A. Laubereau, and R. Zimmermann, 1997, Phys. Rev. Lett. **78**, 3733.
Fürst, C., A. Leitenstorfer, A. Nutsch, G. Tränkle, and A. Zrenner, 1997, Phys. Status Solidi B **204**, 20.
Gammon, D., E. S. Snoke, B. V. Shanabrook, D. S. Katzer, and D. Park, 1996, Phys. Rev. Lett. **76**, 3005.
Garro, N., M. J. Snelling, S. P. Kennedy, R. T. Phillips, and K. H. Ploog, 1999, Phys. Rev. B **60**, 4497.
Giessen, H., A. Knorr, S. Haas, S. W. Koch, S. Linden, J. Kuhl, M. Hetterich, M. Grün, and C. Klingshirn, 1998, Phys. Rev. Lett. **81**, 4260.
Glutsch, S., U. Siegner, and D. S. Chemla, 1995, Phys. Rev. B **52**, 4941.
Göbel, E. O., K. Leo, T. C. Damen, J. Shah, S. Schmitt-Rink, W. Schäfer, J. F. Müller, and K. Köhler, 1990, Phys. Rev. Lett. **64**, 1801.
Goodnick, S. M., and P. Lugli, 1988, Phys. Rev. B **38**, 10 135.
Guenther, T., V. Emiliani, F. Intonti, C. Lienau, and T. Elsaesser, 1999, Appl. Phys. Lett. **75**, 3500.
Guernsey, R., 1962, Phys. Rev. **127**, 1446.
Haacke, S., S. Schaer, B. Deveaud, and V. Savona, 2000, Phys. Rev. B **61**, R5109.

Haacke, S., R. A. Taylor, R. Zimmermann, I. Bar-Joseph, and B. Deveaud, 1997, Phys. Rev. Lett. **78**, 2228.
Haas, S., F. Rossi, and T. Kuhn, 1996, Phys. Rev. B **53**, 12 855.
Haase, B., U. Neukirch, J. Gutowski, J. Nürnberger, W. Faschinger, M. Behringer, D. Hommel, V. M. Axt, G. Bartels, and A. Stahl, 2000, J. Cryst. Growth **214**, 856.
Haché, A., Y. Kostoulas, R. Atanasov, J. L. P. Hughes, J. E. Sipe, and H. M. van Driel, 1997, Phys. Rev. Lett. **78**, 306.
Hader, J., T. Meier, S. Koch, F. Rossi, and N. Linder, 1997, Phys. Rev. B **55**, 13 799.
Hahn, E. L., 1950, Phys. Rev. **80**, 580.
Hanewinkel, B., A. Knorr, P. Thomas, and S. Koch, 1999, Phys. Rev. B **60**, 8975.
Hanke, L., D. Fröhlich, A. L. Ivanov, P. B. Littlewood, and H. Stolz, 1999, Phys. Rev. Lett. **83**, 4365.
Haring Bolivar, P., F. Wolter, A. Müller, H. Roskos, H. Kurz, and K. Köhler, 1997, Phys. Rev. Lett. **78**, 2232.
Haug, H., 1988, in *Optical Nonlinearities and Instabilities in Semiconductors*, edited by H. Haug (Academic, San Diego), p. 53.
Haug, H., 1992, Phys. Status Solidi B **173**, 139.
Haug, H., 2001, in *Ultrafast Physical Processes in Semiconductors*, edited by K. T. Tsen, Semiconductors and Semimetals No. 67 (Academic, San Diego), p. 205.
Haug, H., and L. Bányai, 1996, Solid State Commun. **100**, 303.
Haug, H., and A.-P. Jauho, 1996, *Quantum Kinetics in Transport and Optics of Semiconductors* (Springer, Berlin).
Haug, H., and S. W. Koch, 1993, *Quantum Theory of the Optical and Electronic Properties of Semiconductors* (World Scientific, Singapore).
Heberle, A. P., J. J. Baumberg, E. Binder, T. Kuhn, K. Köhler, and K. H. Ploog, 1996, IEEE J. Sel. Top. Quantum Electron. **2**, 769.
Heberle, A. P., J. J. Baumberg, and K. Köhler, 1995, Phys. Rev. Lett. **75**, 2598.
Herbst, M., V. M. Axt, and T. Kuhn, 2000, Phys. Status Solidi B **221**, 419.
Hess, H. F., E. Betzig, T. D. Harris, L. N. Pfeiffer, and K. W. West, 1994, Science **264**, 1740.
Hess, O., and T. Kuhn, 1996, Phys. Rev. A **54**, 3347.
Hillmer, H., S. Hansmann, A. Forchel, M. Morohashi, E. Lopez, H. P. Meier, and K. Ploog, 1988, Appl. Phys. Lett. **53**, 1937.
Hohenester, U., and W. Pötz, 1997, Phys. Rev. B **56**, 13 177.
Hohenester, U., F. Rossi, and E. Molinari, 1999, Solid State Commun. **111**, 187.
Hohenester, U., P. Supancic, P. Kocevar, X. Q. Zhou, W. Kütt, and H. Kurz, 1993, Phys. Rev. B **47**, 13 233.
Houston, W. V., 1940, Phys. Rev. **57**, 184.
Hu, Y., R. Binder, S. Koch, S. Cundiff, H. Wang, and D. Steel, 1994, Phys. Rev. B **49**, 14 382.
Hübner, M., J. Kuhl, T. Stroucken, A. Knorr, S. W. Koch, R. Hey, and K. Ploog, 1996, Phys. Rev. Lett. **76**, 4199.
Hügel, W. A., M. F. Heinrich, M. Wegener, Q. T. Vu, L. Bányai, and H. Haug, 1999, Phys. Rev. Lett. **83**, 3313.
Huhn, W., and A. Stahl, 1984, Phys. Status Solidi B **124**, 167.
Jack, L., P. Hawrylak, and A. Wójs, 1998, *Quantum Dots* (Springer, Berlin).
Jacoboni, C., and P. Lugli, 1989, *The Monte Carlo Method for Semiconductor Device Simulations* (Springer, Vienna).
Jacoboni, C., and L. Reggiani, 1983, Rev. Mod. Phys. **55**, 645.
Jahnke, F., and S. W. Koch, 1995, Appl. Phys. Lett. **67**, 2278.
Jahnke, F., M. Koch, T. Meier, J. Feldmann, W. Schäfer, P. Thomas, S. W. Koch, E. O. Göbel, and H. Nickel, 1994, Phys. Rev. B **50**, 8114.
Jahnke, F., *et al.*, 1996, Phys. Rev. Lett. **77**, 5257.
Jauho, A. P., and K. Johnsen, 1996, Phys. Rev. Lett. **76**, 4576.
Je, K.-C., T. Meier, F. Rossi, and S. Koch, 1995, Appl. Phys. Lett. **67**, 2978.
Joffre, M., D. Hulin, A. Migus, and M. Combescot, 1989, Phys. Rev. Lett. **62**, 74.
Joschko, M., M. Woerner, T. Elsaesser, E. Binder, T. Kuhn, R. Hey, H. Kostial, and K. Ploog, 1997, Phys. Rev. Lett. **78**, 737.
Joschko, M., M. Woerner, T. Elsaesser, E. Binder, T. Kuhn, R. Hey, H. Kostial, and K. Ploog, 1998, OSA Trends Opt. Photonics Ser. **18**, 80.
Kadanoff, L. P., and G. Baym, 1962, *Quantum Statistical Mechanics* (Benjamin, New York).
Kane, E. O., 1959, J. Phys. Chem. Solids **12**, 184.
Kash, J. A., and J. C. Tsang, 1989, in *Light Scattering in Solids IV: Electron Scattering, Spin Effects, SERS and Morphic Effects*, edited by M. Cardona and G. Güntherodt, Topics in Applied Physics Vol. 54 (Springer, Berlin), p. 423.
Kash, J. A., J. C. Tsang, and J. M. Hvam, 1985, Phys. Rev. Lett. **54**, 2151.
Keldysh, L. V., 1958, Sov. Phys. JETP **34**, 788.
Keldysh, L. V., 1965, Sov. Phys. JETP **20**, 1018.
Khitrova, G., H. M. Gibbs, F. Jahnke, M. Kira, and S. W. Koch, 1999, Rev. Mod. Phys. **71**, 1591.
Kim, D.-S., J. Shah, J. E. Cunningham, T. C. Damen, W. Schäfer, M. Hartmann, and S. Schmitt-Rink, 1992, Phys. Rev. Lett. **68**, 1006.
Kim, D.-S., J. Shah, T. C. Damen, W. Schäfer, F. Jahnke, S. Schmitt-Rink, and K. Köhler, 1992, Phys. Rev. Lett. **69**, 2725.
Kira, M., F. Jahnke, W. Hoyer, and S. W. Koch, 1999, Prog. Quantum Electron. **23**, 189.
Kira, M., F. Jahnke, and S. Koch, 1998, Phys. Rev. Lett. **81**, 3263.
Kittel, C., 1963, *Quantum Theory of Solids* (Wiley, New York).
Kner, P., W. Schäfer, R. Lövenich, and D. S. Chemla, 1998, Phys. Rev. Lett. **81**, 5386.
Knorr, A., F. Steininger, B. Hanewinkel, S. Kuckenburg, P. Thomas, and S. W. Koch, 1998, Phys. Status Solidi B **206**, 139.
Kocevar, P., 1985, Physica B & C **134B**, 155.
Koch, S., T. Meier, T. Stroucken, A. Knorr, J. Hader, F. Rossi, and P. Thomas, 1995, in *Microscopic Theory of Semiconductors: Quantum Kinetics, Confinement and Lasers*, edited by S. W. Koch (World Scientific, Singapore), p. 81.
Krieger, J. B., and G. J. Iafrate, 1986, Phys. Rev. B **33**, 5494.
Kuhn, T., 1998, in *Theory of Transport Properties of Semiconductor Nanostructures*, edited by E. Schöll (Chapman and Hall, London), p. 173.
Kuhn, T., V. M. Axt, M. Herbst, and E. Binder, 1999, in *Coherent Control in Atoms, Molecules, and Semiconductors*, edited by W. Pötz and W. A. Schroeder (Kluwer Academic, Dordrecht), p. 113.
Kuhn, T., E. Binder, F. Rossi, A. Lohner, K. Rick, P. Leisching, A. Leitenstorfer, T. Elsaesser, and W. Stolz, 1994, in *Coherent Optical Interactions in Semiconductors*, Vol. 330 of *NATO Advanced Study Institutes Series B: Physics*, edited by R. T. Phillips (Plenum, New York), p. 33.
Kuhn, T., and F. Rossi, 1992a, Phys. Rev. Lett. **69**, 977.
Kuhn, T., and F. Rossi, 1992b, Phys. Rev. B **46**, 7496.
Kuhn, T., F. Rossi, A. Leitenstorfer, A. Lohner, T. Elsaesser, W. Klein, G. Boehm, G. Traenkle, and G. Weimann, 1996, in *Hot*

Carriers in Semiconductors, edited by K. Hess, J.-P. Leburton, and U. Ravaioli (Plenum, New York), p. 199.
Kurnit, N. A., I. D. Abella, and S. R. Hartmann, 1964, Phys. Rev. Lett. **13**, 567.
Kuznetsov, A. V., 1991, Phys. Rev. B **44**, 13 381.
Kuznetsov, A. V., and C. J. Stanton, 1994, Phys. Rev. Lett. **73**, 3243.
Kwong, N.-H., and M. Bonitz, 2000, Phys. Rev. Lett. **84**, 1768.
Leisching, P., P. Haring Bolivar, W. Beck, Y. Dhaibi, F. Brüggemann, R. Schwedler, H. Kurz, K. Leo, and K. Köhler, 1994, Phys. Rev. B **50**, 14 389.
Leitenstorfer, A., T. Elsaesser, F. Rossi, T. Kuhn, W. Klein, G. Boehm, G. Traenkle, and G. Weimann, 1996, Phys. Rev. B **53**, 9876.
Leitenstorfer, A., S. Hunsche, J. Shah, M. Nuss, and W. Knox, 1999, Phys. Rev. Lett. **82**, 5140.
Leitenstorfer, A., A. Lohner, T. Elsaesser, S. Haas, F. Rossi, T. Kuhn, W. Klein, G. Boehm, G. Traenkle, and G. Weimann, 1994, Phys. Rev. Lett. **73**, 1687.
Leitenstorfer, A., A. Lohner, K. Rick, P. Leisching, T. Elsaesser, T. Kuhn, F. Rossi, W. Stolz, and K. Ploog, 1994, Phys. Rev. B **49**, 16 372.
Lenard, A., 1960, Ann. Phys. (N.Y.) **10**, 390.
Leo, K., T. C. Damen, J. Shah, E. O. Göbel, and K. Köhler, 1990, Appl. Phys. Lett. **57**, 19.
Leo, K., E. O. Göbel, T. C. Damen, J. Shah, S. Schmitt-Rink, W. Schäfer, J. F. Müller, K. Köhler, and P. Ganser, 1991, Phys. Rev. B **44**, 5726.
Leo, K., P. Haring Bolivar, F. Brüggemann, and R. Schwedler, 1992, Solid State Commun. **84**, 943.
Leo, K., J. Shah, T. C. Damen, A. Schulze, T. Meier, S. Schmitt-Rink, P. Thomas, E. Göbel, S. Chuang, M. S. C. Luo, W. Schäfer, K. Köhler, and P. Ganser, 1992, IEEE J. Quantum Electron. **28**, 2498.
Leo, K., J. Shah, E. O. Göbel, T. C. Damen, S. Schmitt-Rink, W. Schäfer, and K. Köhler, 1991, Phys. Rev. Lett. **66**, 201.
Leo, K., M. Wegener, J. Shah, D. S. Chemla, E. O. Göbel, T. C. Damen, S. Schmitt-Rink, and W. Schäfer, 1990, Phys. Rev. Lett. **65**, 1340.
Likforman, J.-P., M. Joffre, G. Chériaux, and D. Hulin, 1995, Opt. Lett. **20**, 2006.
Lindberg, M., R. Binder, and S. W. Koch, 1992, Phys. Rev. A **45**, 1865.
Lindberg, M., and S. W. Koch, 1988a, Phys. Rev. B **38**, 3342.
Lindberg, M., and S. W. Koch, 1988b, J. Opt. Soc. Am. B **5**, 139.
Lindberg, M., and S. W. Koch, 1988c, Phys. Rev. B **38**, 7607.
Lipavský, P., V. Špička, and B. Velický, 1986, Phys. Rev. B **34**, 6933.
Lohner, A., K. Rick, P. Leisching, A. Leitenstorfer, T. Elsaesser, T. Kuhn, F. Rossi, and W. Stolz, 1993, Phys. Rev. Lett. **71**, 77.
Loss, D., and D. P. DiVincenzo, 1998, Phys. Rev. A **57**, 120.
Lugli, P., P. Bordone, L. Reggiani, M. Rieger, P. Kocevar, and S. M. Goodnick, 1989, Phys. Rev. B **39**, 7852.
Luo, M. S. C., S. L. Chuang, P. C. M. Planken, I. Brener, and M. C. Nuss, 1993, Phys. Rev. B **48**, 11 043.
Lyssenko, V. G., G. Valušis, F. Löser, K. Leo, M. M. Dignam, and K. Köhler, 1997, Phys. Rev. Lett. **79**, 301.
Madelung, O., 1978, *Introduction to Solid-State Theory* (Springer, Berlin).
Mahan, G., 1990, *Many-Particle Physics* (Plenum, New York).
Mayer, E. J., *et al.*, 1994, Phys. Rev. B **50**, 14 730.
Mayer, E. J., *et al.*, 1995, Phys. Rev. B **51**, 10 909.
McQuarrie, D. A., 1976, *Statistical Mechanics* (Harper and Row, New York).
Meden, V., J. Fricke, C. Wöhler, and K. Schönhammer, 1996, Z. Phys. B: Condens. Matter **99**, 357.
Meden, V., C. Wöhler, J. Fricke, and K. Schönhammer, 1995, Phys. Rev. B **52**, 5624.
Meier, T., S. W. Koch, M. Phillips, and H. Wang, 2000, Phys. Rev. B **62**, 12 605.
Meier, T., F. Rossi, P. Thomas, and S. Koch, 1995, Phys. Rev. Lett. **75**, 2558.
Mendez, E., F. Agullo-Rueda, and J. Hong, 1988, Phys. Rev. Lett. **60**, 2426.
Mieck, B., and H. Haug, 1999, Phys. Status Solidi B **213**, 397.
Molinari, E., 1994, in *Confined Electrons and Photons: New Physics and Applications*, edited by E. Burstein and C. Weisbuch (Plenum, New York).
Molotkov, S. N., 1996, JETP Lett. **64**, 237.
Motohisa, J., J. J. Baumberg, A. P. Heberle, and J. Allam, 1998, Solid-State Electron. **42**, 1335.
Mycek, M.-A., S. Weiss, J.-Y. Bigot, S. Schmitt-Rink, D. S. Chemla, and W. Schaefer, 1992, Appl. Phys. Lett. **60**, 2666.
Mysyrowicz, A., D. Hulin, A. Antonetti, A. Migus, W. T. Masselink, and H. Morkoç, 1986, Phys. Rev. Lett. **56**, 2748.
Nenciu, G., 1991, Rev. Mod. Phys. **63**, 91.
Noll, G., U. Siegner, S. G. Shevel, and E. O. Göbel, 1990, Phys. Rev. Lett. **64**, 792.
Nuss, M. C., P. C. M. Planken, I. Brener, H. G. Roskos, M. S. C. Luo, and S. L. Chuang, 1994, Appl. Phys. B: Lasers Opt. **B58**, 249.
Oberli, D. Y., J. Shah, and T. C. Damen, 1989, Phys. Rev. B **40**, 1323.
Osman, M. A., and D. K. Ferry, 1987, Phys. Rev. B **36**, 6018.
Östreich, T., K. Schönhammer, and L. J. Sham, 1995, Phys. Rev. Lett. **74**, 4698.
Otremba, R., S. Grosse, M. Koch, J. Feldmann, V. M. Axt, T. Kuhn, and W. Stolz, 1999, Solid State Commun. **109**, 317.
Pantke, K.-H., D. Oberhauser, V. G. Lyssenko, J. M. Hvam, and G. Weimann, 1993, Phys. Rev. B **47**, 2413.
Phillips, M., and H. Wang, 1999, Solid State Commun. **111**, 317.
Phillips, R. T., 1994, Ed., *Coherent Optical Processes in Semiconductors* (Plenum, New York).
Planken, P. C. M., I. Brener, M. C. Nuss, M. S. C. Luo, and S. L. Chuang, 1993, Phys. Rev. B **48**, 4903.
Planken, P. C. M., M. C. Nuss, I. Brener, K. W. Goossen, M. S. C. Luo, S. L. Chuang, and L. Pfeiffer, 1992, Phys. Rev. Lett. **69**, 3800.
Pötz, W., 1996a, Appl. Phys. Lett. **68**, 2553.
Pötz, W., 1996b, Phys. Rev. B **54**, 5647.
Pötz, W., 1997a, Phys. Rev. Lett. **79**, 3262.
Pötz, W., 1997b, Appl. Phys. Lett. **71**, 395.
Pötz, W., 1998, Appl. Phys. Lett. **72**, 3002.
Pötz, W., and P. Kocevar, 1983, Phys. Rev. B **28**, 7040.
Pötz, W., and W. A. Schroeder, 1999, Eds., *Coherent Control in Atoms, Molecules, and Semiconductors* (Kluwer, Dordrecht).
Pötz, W., M. Žiger, and P. Kocevar, 1995, Phys. Rev. B **52**, 1959.
Prengel, F., and E. Schöll, 1999a, Phys. Rev. B **59**, 5806.
Prengel, F., and E. Schöll, 1999b, Semicond. Sci. Technol. **14**, 379.
Prengel, F., E. Schöll, and T. Kuhn, 1997, Phys. Status Solidi B **204**, 322.

Quade, W., E. Schöll, F. Rossi, and C. Jacoboni, 1994, Phys. Rev. B **50**, 7398.
Rappen, T., U.-G. Peter, and M. Wegener, 1994, Phys. Rev. B **49**, 10 774.
Rappen, T., U.-G. Peter, M. Wegener, and W. Schäfer, 1993, Phys. Rev. B **48**, 4879.
Redmer, R., J. R. Madureira, N. Fitzer, S. M. Goodnick, W. Schattke, and E. Schöll, 2000, J. Appl. Phys. **87**, 781.
Richter, A., G. Behme, M. Süpitz, C. Lienau, T. Elsaesser, M. Ramsteiner, R. Nötzel, and K. H. Ploog, 1997, Phys. Rev. Lett. **79**, 2145.
Rieger, M., P. Kocevar, P. Lugli, P. Bordone, L. Reggiani, and S. M. Goodnick, 1989, Phys. Rev. B **39**, 7866.
Rontani, M., F. Rossi, F. Manghi, and E. Molinari, 1998, Appl. Phys. Lett. **72**, 957.
Roskos, H. G., M. C. Nuss, J. Shah, K. Leo, D. A. B. Miller, A. M. Fox, S. Schmitt-Rink, and K. Köhler, 1992, Phys. Rev. Lett. **68**, 2216.
Roskos, H., C. Waschke, R. Schwedler, P. Leisching, Y. Dhaibi, H. Kurz, and K. Köhler, 1994, Superlattices Microstruct. **15**, 281.
Rossi, F., 1998, in *Theory of Transport Properties of Semiconductor Nanostructures*, edited by E. Schöll (Chapman and Hall, London), p. 283.
Rossi, F., A. di Carlo, and P. Lugli, 1998, Phys. Rev. Lett. **80**, 3348.
Rossi, F., M. Gulia, P. Selbmann, E. Molinari, T. Meier, P. Thomas, and S. Koch, 1996, in *The Physics of Semiconductors*, edited by M. Scheffler and R. Zimmermann (World Scientific, Singapore), p. 1775.
Rossi, F., S. Haas, and T. Kuhn, 1994, Phys. Rev. Lett. **72**, 152.
Rossi, F., T. Meier, P. Thomas, S. W. Koch, P. E. Selbmann, and E. Molinari, 1995, Phys. Rev. B **51**, 16 943.
Rossi, F., T. Meier, P. Thomas, S. W. Koch, P. E. Selbmann, and E. Molinari, 1996, in *Hot Carriers in Semiconductors*, edited by K. Hess, J.-P. Leburton, and U. Ravaioli (Plenum, New York), p. 157.
Rota, L., P. Lugli, T. Elsaesser, and J. Shah, 1993, Phys. Rev. B **47**, 4226.
Rota, L., F. Rossi, P. Lugli, and E. Molinari, 1995, Phys. Rev. B **52**, 5183.
Rücker, H., E. Molinari, and P. Lugli, 1992, Phys. Rev. B **45**, 6747.
Ryan, J. F., and M. C. Tatham, 1992, in *Hot Carriers in Semiconductor Nanostructures: Physics and Applications*, edited by J. Shah (Academic, Boston), p. 345.
Savasta, S., and R. Girlanda, 1999, Phys. Rev. B **59**, 15 409.
Schäfer, W., 1996, J. Opt. Soc. Am. B **13**, 1291.
Schäfer, W., D. S. Kim, J. Shah, T. C. Damen, J. E. Cunningham, K. W. Goosen, L. N. Pfeiffer, and K. Köhler, 1996, Phys. Rev. B **53**, 16 429.
Schilp, J., T. Kuhn, and G. Mahler, 1994a, Phys. Rev. B **50**, 5435.
Schilp, J., T. Kuhn, and G. Mahler, 1994b, Semicond. Sci. Technol. **9**, 439.
Schilp, J., T. Kuhn, and G. Mahler, 1994c, in *Proceedings of the 22nd International Conference on the Physics of Semiconductors*, Vancouver, edited by D. J. Lockwood (World Scientific, Singapore), p. 341.
Schilp, J., T. Kuhn, and G. Mahler, 1995, Phys. Status Solidi B **188**, 417.
Schmenkel, A., L. Bányai, and H. Haug, 1998, J. Lumin. **76-77**, 134.
Schmidt, T., M. Tewordt, R. H. Blick, R. J. Haug, D. Pfannkuche, K. von Klitzing, A. Förster, and H. Lüth, 1995, Phys. Rev. B **51**, 5570.
Schmitt-Rink, S., and D. S. Chemla, 1986, Phys. Rev. Lett. **57**, 2752.
Schmitt-Rink, S., D. S. Chemla, and H. Haug, 1988, Phys. Rev. B **37**, 941.
Schmitt-Rink, S., J. Löwenau, and H. Haug, 1982, Z. Phys. B: Condens. Matter **47**, 13.
Schmitt-Rink, S., *et al.*, 1992, Phys. Rev. B **46**, 10 460.
Schoenlein, R. W., D. M. Mittelman, J. J. Shiang, A. P. Alivisatos, and C. V. Shank, 1993, Phys. Rev. Lett. **70**, 1014.
Scholz, R., T. Pfeifer, and H. Kurz, 1993, Phys. Rev. B **47**, 16 229.
Schönhammer, K., 1998, Phys. Rev. B **58**, 3518.
Schönhammer, K., and C. Wöhler, 1997, Phys. Rev. B **55**, 13 564.
Schultheis, L., J. Kuhl, A. Honold, and C. W. Tu, 1986, Phys. Rev. Lett. **57**, 1797.
Schultheis, L., M. D. Sturge, and J. Hegarty, 1985, Appl. Phys. Lett. **47**, 995.
Schülzgen, A., R. Binder, M. E. Donovan, M. Lindberg, K. Wundke, H. M. Gibbs, G. Khitrova, and N. Peyghambarian, 1999, Phys. Rev. B **82**, 2346.
Shah, J., 1992, Ed., *Hot Carriers in Semiconductor Nanostructures: Physics and Applications* (Academic, Boston).
Shah, J., 1999, *Ultrafast Spectroscopy of Semiconductors and Semiconductor Nanostructures* (Springer, Berlin).
Shah, J., B. Deveaud, T. C. Damen, W. T. Tsang, A. C. Gossard, and P. Lugli, 1987, Phys. Rev. Lett. **59**, 2222.
Shah, J., and R. C. C. Leite, 1969, Phys. Rev. Lett. **22**, 1304.
Shank, C. V., R. L. Fork, R. F. Leheny, and J. Shah, 1979, Phys. Rev. Lett. **42**, 112.
Shapiro, M., and P. Brumer, 1986, J. Chem. Phys. **84**, 4103.
Shapiro, M., and P. Brumer, 1997, J. Chem. Soc., Faraday Trans. **93**, 1263.
Sieh, C., T. Meier, F. Jahnke, A. Knorr, and S. Koch, 1999, Phys. Rev. Lett. **82**, 3112.
Smirl, A. L., M. J. Stevens, X. Chen, and O. Buccafusca, 1999, Phys. Rev. B **60**, 8267.
Smith, G. O., E. J. Mayer, J. Kuhl, and K. Ploog, 1994, Solid State Commun. **92**, 325.
Sönnichsen, C., A. C. Duch, G. Steininger, M. Koch, G. von Plessen, and J. Feldmann, 2000, Appl. Phys. Lett. **76**, 140.
Stanton, C. J., D. W. Bailey, and K. Hess, 1988, IEEE J. Quantum Electron. **24**, 1614.
Steane, A., 1998, Rep. Prog. Phys. **61**, 117.
Steinbach, D., G. Kocherscheidt, M. U. Wehner, H. Kalt, M. Wegener, K. Ohkawa, D. Hommel, and V. M. Axt, 1999, Phys. Rev. B **60**, 12 079.
Steininger, F., A. Knorr, T. Stroucken, P. Thomas, and S. W. Koch, 1996, Phys. Rev. Lett. **77**, 550.
Steininger, F., A. Knorr, P. Thomas, and S. W. Koch, 1997, Z. Phys. B: Condens. Matter **103**, 45.
Supancic, P., U. Hohenester, P. Kocevar, D. Snoke, R. M. Hannak, and W. W. Rühle, 1996, Phys. Rev. B **53**, 7785.
Tarucha, S., D. G. Austing, T. Honda, R. J. van der Hage, and L. P. Kouwenhoven, 1996, Phys. Rev. Lett. **77**, 3613.
Tran Thoai, D. B., and H. Haug, 1993, Phys. Rev. B **47**, 3574.
Ulbrich, R., 1977, Solid-State Electron. **21**, 51.
Ulbrich, R. G., 1988, in *Optical Nonlinearities and Instabilities in Semiconductors*, edited by H. Haug (Academic, San Diego), p. 121.

van Driel, H. M., 1979, Phys. Rev. B **19**, 5928.
Voisin, P., J. Bleuse, C. Bouche, S. Gaillard, C. Alibert, and A. Regreny, 1988, Phys. Rev. Lett. **61**, 1639.
Vollmer, M., H. Giessen, W. Stolz, W. W. Rühle, L. Ghislain, and V. Elings, 1999, Appl. Phys. Lett. **74**, 1791.
von der Linde, D., J. Kuhl, and H. Klingenberg, 1980, Phys. Rev. Lett. **44**, 1505.
von Plessen, G., T. Meier, J. Feldmann, E. O. Göbel, P. Thomas, K. W. Goossen, J. M. Kuo, and R. F. Kopf, 1994, Phys. Rev. B **49**, 14 058.
von Plessen, G., and P. Thomas, 1992, Phys. Rev. B **45**, 9185.
Vu, Q., L. Bányai, H. Haug, F. Camescasse, J.-P. Likforman, and A. Alexandrou, 1999, Phys. Rev. B **59**, 2760.
Vu, Q., L. Bányai, P. Tamborenea, and H. Haug, 1997, Europhys. Lett. **40**, 323.
Wang, H., K. Ferrio, D. Steel, Y. Z. Hu, R. Binder, and S. W. Koch, 1993, Phys. Rev. Lett. **71**, 1261.
Wang, H., J. Shah, T. C. Damen, and L. N. Pfeiffer, 1995, Phys. Rev. Lett. **74**, 3065.
Wannier, G. H., 1960, Phys. Rev. **117**, 432.
Warren, W. S., H. Rabitz, and M. Dahleh, 1993, Science **259**, 1581.
Waschke, C., H. G. Roskos, R. Schwedler, K. Leo, H. Kurz, and K. Köhler, 1993, Phys. Rev. Lett. **70**, 3319.
Wegener, M., D. S. Chemla, S. Schmitt-Rink, and W. Schäfer, 1990, Phys. Rev. A **42**, 5675.
Wehner, M. U., M. H. Ulm, D. S. Chemla, and M. Wegener, 1998, Phys. Rev. Lett. **80**, 1992.
Weiner, A., D. Leaird, J. Patel, and J. Wullert, 1990, Opt. Lett. **15**, 326.
Weiss, S., M.-A. Mycek, J.-Y. Bigot, S. Schmitt-Rink, and D. S. Chemla, 1992, Phys. Rev. Lett. **69**, 2685.
Wigner, E., 1932, Phys. Rev. **40**, 749.
Woerner, M., and J. Shah, 1998, Phys. Rev. Lett. **81**, 4208.
Wolter, F., H. G. Roskos, P. Haring Bolivar, G. Bartels, H. Kurz, H. T. Grahn, and R. Hey, 1997, Phys. Status Solidi B **204**, 83.
Wyld, H. W., and B. D. Fried, 1963, Ann. Phys. (N.Y.) **23**, 374.
Yoon, H. W., D. R. Wake, and J. P. Wolfe, 1992, Phys. Rev. B **92**, 13 461.
Zak, J., 1968, Phys. Rev. Lett. **20**, 1477.
Zanardi, P., and F. Rossi, 1998, Phys. Rev. Lett. **81**, 4752.
Zener, C., 1934, Proc. R. Soc. London, Ser. A **145**, 523.
Zimmermann, R., 1990, Phys. Status Solidi B **159**, 317.
Zimmermann, R., and J. Wauer, 1994, J. Lumin. **58**, 271.
Zimmermann, R., J. Wauer, A. Leitenstorfer, and C. Fürst, 1998, J. Lumin. **76-78**, 34.